CryoSat-2 precise orbit determination using DORIS phase measurements

Ramanathan Gurumoorthy

Master of Science Thesis Report

TU Delft

CryoSat-2 precise orbit determination using DORIS phase measurements

by

Ramanathan Gurumoorthy

to obtain the degree of Master of Science
at the Delft University of Technology,
to be defended publicly on Thursday February 28, 2019 at 9:00 AM.

Student number: 4516591

Thesis committee:	Dr. ir. Ernst J.O. Schrama,	TU Delft, Supervisor
	Prof. Dr. ir. P.N.A.M Visser,	TU Delft, Committee Chair
	Ir. B.C. Root,	TU Delft, Lecturer
	Ir. J. Bouwmeester,	TU Delft, Researcher

TU Delft

Preface

I would like to express my gratitude to my dear parents for their exceptional support and unconditional love. I feel lucky and blessed beyond measure. Words go undoubtedly inexpressible for all that they have done. If there is any glory for this work, I would bestow all the glory to them.

I am glad Dr. Ernst Schrama accepted to supervise my thesis research. The depth of knowledge shared during meetings was immense and was a good learning experience. Solving this problem with him has opened up fascinating world of orbit determination that previously went unnoticed. I would like to thank Dr. ir. Wouter van der wal in the Astrodynamics and Space missions department for appointing me as a teaching assistant. The opportunity was certainly well timed.

To all my friends in Delft who were my strength and support during thesis journey - Thank you ! The friendship and moments with - Amanthla, Corne, Datta, Frederic, Hanneke, Leon, Maaike, Max, Rosalie, Rutger, Sunayna, Tom and Wouter in the room 9.06 and in flex space are invaluable and will be cherished ! To the other important bunch of pals at DARE - Lars, Mark, Esmee, Noah, Matteo, Thomas, Bram and many others in the Stratos III and PRG - the journey has been amazing and unforgettable, thanks for keeping me motivated and busy. To the boys Bharath and Anantha, I don't think the whole MSc. journey would have been easier without your company. My unforeseen meetings and coffee discussion with my *Fellowship* pal Lupi has always been enjoyable.

Ramanathan Gurumoorthy
Delft, February 2019

Abstract

CryoSat-2 is a European Space Agency (ESA) altimeter mission with an objective to study the connection between cryosphere melting and global sea level rise. The satellite carries a Doppler navigation system (DORIS) and a Satellite Laser Ranging system (SLR) to aid the precise computation of orbits down to centimetre level.

CNES/IDS releases DORIS tracking data in two formats for CryoSat-2. One is the raw format called RINEX and other is the pre-processed Doppler format called version 2.2. V2.2 data contains all information necessary for straightforward usage in orbit determination - measurements time-tagged in TAI, range-rate measurements, ionospheric correction, tropospheric correction, antenna corrections and flags that indicate unusable measurements. RINEX does not contain any corrections and has the phase and pseudo range measurements at short latency allowing users to have flexibility in processing. Additionally, data required for formulating the corrections are present in RINEX. For missions in and after 2016, CNES/IDS supplies tracking data only in RINEX and not in V2.2. Analysis centres using DORIS data now have to independently develop processing strategies to process RINEX data. This problem is the main objective of this research.

In this thesis, a pre-processor called *RX2RR* (RINEX to Range-Rate) has been built in Fortran in an attempt to process the raw data and compute all the necessary corrections. *RX2RR* converts RINEX format to a format exactly similar to V2.2 such that RINEX can now be used in any orbit determination tool that has been previously using V2.2. In this processor, clock synchronisation of on-board clock to International Atomic Time is performed. A new approach of utilizing Meteorological data in RINEX for troposphere delay corrections is implemented. Use of real time data from numerical weather models is also presented for tropospheric correction. Ionospheric delay and antenna phase centre corrections are performed using iono-free phase centre. An editing strategy to remove outliers in Doppler data is implemented and tested.

To demonstrate the performance of the tool, we perform orbit determination using NASA Goddard Space Flight Center's orbit computation software GEODYN-II. We use *RX2RR* processed RINEX data and CNES processed V2.2 data of CryoSat-2 for year 2016. Tracking residuals from both POD runs are compared and average difference in R.M.S residual is found to be approximately 0.011 mm/s over a year. This validates that the corrections are formulated and implemented correctly. The result proves our capability to process the RINEX measurements independently and the tool developed has extended the capability of GEODYN-II to process RINEX observations from DORIS system.

Keywords: Precise orbit determination (POD), DORIS, IDS, GEODYN-II

Contents

Chapter 1

Introduction

1.1 Problem Background

DORIS, which stands for Doppler Orbitography and Radiopositioning Integrated by Satellite, is a French satellite tracking system jointly developed by CNES, IGN and GRGS for precise orbit determination of satellites. The system is based on the principle of Doppler effect on the radio signals that are emitted from terrestrial ground beacons and received on a satellite. Unlike other navigation systems, DORIS is an uplink device. The signal transmitters are fixed to the ground while the receivers are present on-board the satellites. The Doppler observations performed by the satellite are sent to the ground station for further processing and analysis. Once processed, these observations enable one to estimate the satellite positions to centimetre level precision in the radial component of the orbit, which is an important criteria for altimeter missions and for studying various geophysical processes.

The DORIS tracking system consists of two segments - ground segment (consisting of signal emitter beacon and ground processing station) and space segment (i.e. satellites with receiver). CNES is responsible for the operation of this DORIS tracking system and distributing the data to the users in a certain format. Presently, observation data are distributed to users in two different formats - 2.2 format and RINEX format.

A data distribution format called DORIS version 2.2 or simply V2.2 is the classical Doppler exchange format currently used for all the missions involved in the DORIS tracking system till 2015. In addition to the time-tagged range-rate measurements of satellite with respect to the receivers, it consists of delay corrections, geometry corrections and processing indicators for each observation. The time-tagging and correction processing is entirely performed by CNES. These corrections can be applied on the range rate during observation processing.

A widely known format called RINEX was adapted for the DORIS system and was introduced for missions carrying DORIS in and after 2008. The RINEX format has been originally developed for GPS data exchange (Gurtner, 1994) and later became widely accepted for GNSS data. Since it makes little assumption about the data and only constraints the formatting, it could be used for data from navigation systems other than GNSS such as DORIS (cite DORIS RINEX 3.0). In addition, missions following in and after 2008 carry third generation DORIS instrument named DGXX receiver. Conveniently, these receivers can generate DORIS data compatible with RINEX format. Due to the these reasons, RINEX for DORIS data was established. The difference between the DORIS/RINEX and usual GNSS/RINEX is that the former is station based and latter is satellite based. Data from four missions in DORIS network - Jason-2 (launch - 2008) CryoSat-2 (2010), HY-2A (2011), SARAL (2013) have been made available in both RINEX format and 2.2 format. So in this case, CNES releases the raw measurements

as RINEX and also releases the pre-processed measurements as V2.2 data. But for missions launched in and after 2016, only RINEX data are available.

RINEX format contains raw measurements at short latency. Despite its flexibility, it is challenging to work with such data since editing is challenging compared to V2.2 and does not contain any corrections for the measurements. Instead of range-rate, phase data are available which are not incompatible with most orbit determination tools. Delay corrections such as ionosphere and troposphere corrections have to computed by the users. Satellite attitude must be employed to compute the antenna geometry corrections. Most importantly, timetagging of the measurements must be done by the users to realize the measurements in TAI. Since the measurements are raw, additional editing processor must be established to successfully remove the outliers present in the data and a converter to adapt the data so that orbit computation software can use this.

Various analysis centres use V2.2 data up until now, however, for future altimeter missions carrying DORIS system, CNES will terminate distributing data in V2.2. Users now have to depend only on RINEX data and develop their own processing strategy/solution. This has already started taking into effect. Distribution of V2.2 format has been terminated for Sentinel 3A and Jason 3 missions. The data for these missions are only available in RINEX format. This data transition problem is the main objective of this thesis work.

This problem is applicable to all missions in the DORIS network. For this thesis research, Cryosat-2 mission has been chosen for two reasons:

1. The Astrodynamics and Space missions department at TU Delft has well developed in-house tools that uses for precise orbit solution of CryoSat-2.

2. The availability of both DORIS 2.2 and RINEX 3.0 during the mission time-frame conveniently allows validation of the computed orbit.

In order to produce precise orbits using RINEX format, the user has to perform following tasks:

1. Perform On-board clock synchronisation for time-tagging of measurements and computation of on-board frequency offset. User can also use the clock solution provided in the RINEX format, but this has certain inconsistencies.

2. Implement a tropospheric model to compute the tropospheric delay.

3. Compute ionospheric correction and implement iono-free phase center geometry correction.

4. Implement antenna phase center to center of mass correction from attitude of satellite.

5. Implement editing strategy to remove large outliers in the range rate measurements

6. Implement a converter to process RINEX phase data in GEODYNII orbit computation software.

The outcome of this research would improve the capability of the A&S capability to process the RINEX format data for computation of precise orbits. With tasks identified, the main research question is put forth.

1.2 Research question

The main research question put forth for the thesis research is:

Can we construct a preprocessor that enables centimetre level radial orbit accuracy for CryoSat-2 mission using DORIS/RINEX 3.0 data ?

The sub-research questions identified are:

1. Can we build a time-tagging solution with the same precision as achieved in DORIS 2.2 format and RINEX PANDOR version ?
2. Does including all reference/master beacons during the clock synchronisation process improve the time-tagging accuracy ?
3. Can the time-tagging be improved by successive iteration of orbits from GEODYNII in the clock synchronisation process ?
4. Does the a priori orbit have effect on the time tagging solution ?
5. Does the implementation of antenna phase correction using nominal attitude mode for CryoSat-2 achieve the precision required ?
6. Do the ionosphere and troposphere corrections implemented achieve the same level as V2.2 ?
7. Does the RINEX data need additional editing criteria to improve the quality of the measurements ?
8. Is it possible to build a processor that accepts RINEX phase data and convert it to a format such that it can be used in GEODYNII software ?

The first four sub-research questions correspond to time-tagging of measurements using the RINEX data. The fifth, sixth questions correspond to corrections that needs to be performed for observations and last question corresponds adaptability to GEODYNII software. Answering these sub-research questions would lead us to an answer for the main research question.

1.3 Thesis outline

The starting chapter will lay down the foundations of precise orbit determination process and strategy implemented in A&S department of TU Delft for computing precise orbits of CryoSat-2 mission. With Chapter 3, the main part of thesis begins explaining about the DORIS/RINEX format. In chapter 4, time tagging problem is explained that will help in answering first two research questions. Chapter 5 explains how the RINEX data will be processed. It also explains how other corrections such as troposphere, ionosphere and antenna phase centre corrections are implemented. In chapter 5, main results are presented.

1.4 Research plan

The research was initiated by first knowing about the DORIS system. Two data formats from DORIS were then studied in detail. The orbit determination performed at A&S department of TU Delft was then familiarized. A processor was built (*RX2ST*) to convert the RINEX data to

station files. In this process, individual station files were created containing all the information pertaining to a station. First the clock synchronization procedure was built and implemented in the processor. Following this all other corrections were built and tested. In the final stage of processor, the corrections available were formatted in the same style as V2.2 and data was produced. Using GBF converter, the processed results were converted to GBF format. Using the GBF format of the processed data, GEODYN-II was run for orbit determination. Finally the residuals were studied and conclusions were made about the performance of the pre-processor.

Chapter 2

Orbit determination

2.1 DORIS processing strategy at TU Delft

This section is briefly about the POD process already performed at TU Delft by Schrama (2018). Further, the study to adapt the RINEX 3.0 data will be based on steps and models as presented in Schrama (2018). The performance of the orbit determination for CryoSat-2 is currently based on the Doppler 2.2 range rate data and SLR data.

The parameter estimation is done using a iterative Bayesian least squares. This method is implemented in the GEODYN II orbit determination software developed by NASA's Goddard Space Flight Center (Rowlands et al., 1993). Least squares technique is the adjustment of the orbit models to best fit the observations. This is achieved by minimizing the sum of the squares of observation residuals. Batch LS refers to processing all the data at once in a single step. For this reason, it is suitable for post-processing because the observation data over whole time-span must be available. The batch least squares is explained in section 2.1.1.

The ITRF2014 reference system is used for SLR tracking stations and DORIS beacon positions. EIGEN5c gravity model is used currently for the DORIS study. Recently, the temporal gravity model has been updated. An updated version of ocean tide model FES2014 is used to specify the dynamical forces on the satellite by ocean tides. The Solar Radiation Pressure (SRP) model for CryoSat-2 is based on the CNES model and model scaling parameter is fixed at a constant value. The attitude model is specified from the star camera quaternion data.

POD is performed in arc that is about 144 hours long. An overlap of $\approx$ 24 hours is maintained to allow the verification of internal consistency. The initial state vector is usually from the DORIS navigator orbits. In case it is not available, either NORAD two-line elements is used or a previously computed trajectory is used. If the error is too large during the initial state vector, the POD convergence would fail. In reality, NORAD was never used at TU Delft.

The observation files are 10 second DORIS 2.2 format acquired from IDS and SLR data acquired from CDDIS maintained at GSFC. The empirical accelerations are estimated in order to absorb the un-modelled dynamics in the orbit determination. The imperfection in the force models can accumulate during the numerical integration process. It must be noted that these parameters do not represent any physical effect. These are estimated every 6 hours currently (Schrama, 2018) and can be changed. The estimation of the accelerations is only performed for the along track and across track component. The radial component is not estimated since this can be modelled better by the measurements from DORIS. Much of the un-modelled forces occur at a frequency of one-cycle-per-orbital-revolution (1CPR) associated with orbital period of satellite. Mathematically, the 1CPR empirical acceleration model with periodic coefficients

are defined as

$$\vec{P}_{empirical} = \begin{bmatrix} a_R \\ a_T \\ a_N \end{bmatrix} = \begin{bmatrix} (C_R + R_c \cos\theta + R_s \sin\theta)\hat{u}_R \\ (C_T + T_c \cos\theta + T_s \sin\theta)\hat{u}_T \\ (C_N + N_c \cos\theta + N_s \sin\theta)\hat{u}_N \end{bmatrix} \tag{2.1}$$

Where

- a_R, a_T, a_N are the empirical acceleration components in Radial (R), Transverse (T) and Normal (N) direction. These are estimated along with the satellite state vectors in the least squares estimation process.
- θ is the argument of latitude of satellite, which is available during the POD.
- C_R, C_T, C_N are the constant acceleration in the radial, transverse and normal direction respectively
- R_s, R_c are sine and cosine parts of 1CPR radial acceleration
- T_s, T_c are sine and cosine parts of 1CPR transverse acceleration
- N_s, N_c are sine and cosine parts of 1CPR normal acceleration
- $\hat{u}_R, \hat{u}_T, \hat{u}_N$ are the unit vectors in R, T, N direction respectively.

The above equation is used to estimate the empirical acceleration at any point in the orbit. The accelerations are converted to geocentric inertial components using transformations. In the Bayesian least square adjustment, the accelerations are constrained between the consecutive arc terms.

Similarly, thermosphere drag model scaling parameter K_d is estimated. Solved K_d value is an approximation that depends on the atmospheric density model MSIS-86. This value is different from C_d of CryoSat-2 as C_d depends on the shape of satellite. Estimating such parameters helps to approximate the density of thermosphere to variations in solar flux and charged particle intensity. The ground beacon frequency offsets, pass parameters and tropospheric delay parameters are estimated during POD. For each pass, measurement bias, tropospheric scaling parameter and arc dependent receiver clock offset is solved. For DORIS and SLR, a certain degree elevation cut-off mask is also implemented.

2.1.1 Batch least squares

Let us consider that $\boldsymbol{x^0}$ is the vector containing the parameters. Then it can be defined as

$$\boldsymbol{x^0} = \boldsymbol{\beta} = \begin{bmatrix} x_0 \\ y_0 \\ z_0 \\ \dot{x_0} \\ \dot{x_0} \\ \dot{x_0} \\ \alpha_1 \\ \vdots \\ \alpha_j \end{bmatrix} \tag{2.2}$$

where $x_0, y_0, z_0, \dot{x_0}, \dot{y_0}, \dot{z_0}$ are the state vectors and α_j represents j solve-for parameters that are solved along with the state vectors (such as drag coefficient, solar radiation pressure coefficient, gravity harmonics etc.). The state vectors and the solve-for parameters are called as

the dynamic parameters. Collectively, let β represent the *dynamic parameters* and let us denote p for number of dynamic parameters. Let $\boldsymbol{y}$ be the vector containing the m observations at epochs say $1, 2, ..., m$ from systems such as DORIS or SLR or GPS.

$$\boldsymbol{y} = \begin{bmatrix} y_1 \\ y_2 \\ \vdots \\ y_m \end{bmatrix} \tag{2.3}$$

The observations $\boldsymbol{y}$ are related to the the following relation

$$\boldsymbol{y} = \boldsymbol{G} + \boldsymbol{\varepsilon} \tag{2.4}$$

The residual vector $\boldsymbol{\varepsilon}$ is given by

$$\boldsymbol{\varepsilon} = \boldsymbol{y} - \boldsymbol{G} \tag{2.5}$$

The system $\boldsymbol{G}$ is non-linear and needs to be linearized. For this purpose, we use Taylor series to arrive at a first order linearized approximation about the vector say, $\boldsymbol{x^0}$ which is the initial value or a-priori estimate.

$$G(\boldsymbol{x^0}) = f(\boldsymbol{x^0}) + \sum_{i=1}^{p} \frac{\partial f(\boldsymbol{x^0})}{\partial \boldsymbol{x_i}} \Delta \boldsymbol{x_i} \tag{2.6}$$

Now, the equation 2.5 becomes

$$\begin{aligned} \boldsymbol{\varepsilon} &= \boldsymbol{y} - f(\boldsymbol{x_0}) - \sum_{i=1}^{p} \frac{\partial f(\boldsymbol{x_0})}{\partial \boldsymbol{\beta_i}} \Delta \boldsymbol{\beta_i} \\ &= \boldsymbol{Y} - \boldsymbol{H}\boldsymbol{X} \end{aligned} \tag{2.7}$$

where $\boldsymbol{Y}$is the observation-computed (O-C) matrix containing the following terms

$$= \begin{bmatrix} y_1 - f_1(x^0) \\ y_2 - f_2(x^0) \\ \vdots \\ y_m - f_m(x^0) \end{bmatrix}_{m \times 1} \tag{2.8}$$

The H matrix also called as the design matrix can be elaborated as

$$H = \begin{bmatrix} \frac{\partial f_1}{\partial x} & \frac{\partial f_1}{\partial y} & \frac{\partial f_1}{\partial z} & \frac{\partial f_1}{\partial \dot{x}} & \frac{\partial f_1}{\partial \dot{y}} & \frac{\partial f_1}{\partial \dot{z}} & \frac{\partial f_1}{\partial \alpha_1} & \cdots & \frac{\partial f_1}{\partial \alpha_j} \\ \frac{\partial f_2}{\partial x} & \frac{\partial f_2}{\partial y} & \frac{\partial f_2}{\partial z} & \frac{\partial f_2}{\partial \dot{x}} & \frac{\partial f_2}{\partial \dot{y}} & \frac{\partial f_2}{\partial \dot{z}} & \frac{\partial f_2}{\partial \alpha_1} & \cdots & \frac{\partial f_2}{\partial \alpha_j} \\ \vdots & \vdots & \vdots & \vdots & \vdots & \vdots & \vdots & \ddots & \vdots \\ \frac{\partial f_m}{\partial x} & \frac{\partial f_m}{\partial y} & \frac{\partial f_m}{\partial z} & \frac{\partial f_m}{\partial \dot{x}} & \frac{\partial f_m}{\partial \dot{y}} & \frac{\partial f_m}{\partial \dot{z}} & \frac{\partial f_m}{\partial \alpha_1} & \cdots & \frac{\partial f_m}{\partial \alpha_j} \end{bmatrix}_{m \times p} \tag{2.9}$$

and X represents

$$\boldsymbol{X} = \begin{bmatrix} \Delta x_1 \\ \Delta x_2 \\ \vdots \\ \Delta x_p \end{bmatrix}_{p\times 1} \tag{2.10}$$

Now, with the residual expression $\boldsymbol{\varepsilon}$ elaborated, we need to find the best estimate $\hat{\boldsymbol{x}}$ minimizes equation . In order to do this, according to the least squares estimation, the following cost function must be minimized. In other words, the best estimate of state vector $\hat{\boldsymbol{x}}$ must minimize the sum of the square of residuals.

$$\begin{aligned} J &= \sum_{i=1}^{m} \varepsilon_i^2 \\ &= [\boldsymbol{Y} - \boldsymbol{H}\boldsymbol{X}]^T [\boldsymbol{Y} - \boldsymbol{H}\boldsymbol{X}] \end{aligned} \tag{2.11}$$

For weighted least-squares, the expression becomes

$$\begin{aligned} J &= \sum_{i=1}^{m} \boldsymbol{W}\varepsilon_i^2 \\ &= [\boldsymbol{Y} - \boldsymbol{H}\boldsymbol{X}]^T \boldsymbol{W} [\boldsymbol{Y} - \boldsymbol{H}\boldsymbol{X}] \end{aligned} \tag{2.12}$$

The conditions are that the (i) first derivative of J with respect to the solve-for parameters must be zero and (ii) second derivative of J with respect to solve-for parameters must be greater than zero. By the first condition and with some algebraic manipulation, we get

$$\Delta \boldsymbol{x} = (\boldsymbol{H}^T \boldsymbol{H})^{-1} \boldsymbol{H}^T \boldsymbol{Y} \tag{2.13}$$

The $\Delta \boldsymbol{x}$ is not the final solution. Since we linearise a non-linear system, the process is iterative and the process is stopped when the convergence is reached. In this case, it means the we continue the iteration until (O-C) values exceeds the defined tolerance.

$$\boldsymbol{x}^{k+1} = \boldsymbol{x}^k + \Delta \boldsymbol{x} \tag{2.14}$$

Once the convergence is reached at k^{th} iteration then the best estimate is $\hat{\boldsymbol{x}} = \boldsymbol{x}^k$ In practical situations, weights can be applied to measurements. This is given in the form of matrix with m elements. Then the least squares definition would be to find an best estimate that minimizes the sum of the square of weighted residuals.

$$\boldsymbol{W} = \begin{bmatrix} W_1 & \dots & 0 \\ \vdots & \ddots & \vdots \\ 0 & \dots & W_m \end{bmatrix} \tag{2.15}$$

Equation 2.13 becomes

$$\begin{aligned} \Delta \boldsymbol{x} &= (\boldsymbol{H}^T \boldsymbol{W} \boldsymbol{H})^{-1} \boldsymbol{H}^T \boldsymbol{W} \boldsymbol{Y} \\ &= \boldsymbol{N}^{-1} \boldsymbol{n} \end{aligned} \tag{2.16}$$

where $\boldsymbol{N} = \boldsymbol{H}^T \boldsymbol{W} \boldsymbol{H}$ is the normal matrix and $\boldsymbol{n} = \boldsymbol{H}^T \boldsymbol{W} \boldsymbol{Y}$ The assumption is made on the above system that number of measurements or observations (m) is greater than the parameters (p) estimated ($m > p$) For example, let us consider that we are estimating two parameters and

the weight matrix is identity matrix, then the equation 2.16 becomes

$$\begin{bmatrix} \frac{\partial f_1}{\partial \beta_1} & \frac{\partial f_2}{\partial \beta_1} & \cdots \\ \frac{\partial f_1}{\partial \beta_2} & \frac{\partial f_2}{\partial \beta_2} & \cdots \end{bmatrix}_{2\times m} \begin{bmatrix} \frac{\partial f_1}{\partial \beta_1} & \frac{\partial f_1}{\partial \beta_2} \\ \frac{\partial f_2}{\partial \beta_1} & \frac{\partial f_2}{\partial \beta_2} \\ \vdots & \vdots \end{bmatrix}_{m\times 2} = \begin{bmatrix} \frac{\partial f_1}{\partial \beta_1} & \frac{\partial f_2}{\partial \beta_1} & \cdots \\ \frac{\partial f_1}{\partial \beta_2} & \frac{\partial f_2}{\partial \beta_2} & \cdots \end{bmatrix}_{2\times m} \begin{bmatrix} \Delta y_1 \\ \Delta y_2 \\ \vdots \\ \Delta y_m \end{bmatrix}_{m\times 1} \tag{2.17}$$

Upon simplification, we get

$$\begin{bmatrix} \sum_{i=1}^{m} (\frac{\partial f_i}{\partial \beta_1})^2 & \sum_{i=1}^{m} (\frac{\partial f_i}{\partial \beta_1})(\frac{\partial f_i}{\partial \beta_2}) \\ \sum_{i=1}^{m} (\frac{\partial f_i}{\partial \beta_1})(\frac{\partial f_i}{\partial \beta_2}) & \sum_{i=1}^{m} (\frac{\partial f_i}{\partial \beta_2})^2 \end{bmatrix} = \begin{bmatrix} \sum_{i=1}^{m} (\frac{\partial f_i}{\partial \beta_1})(\Delta y_i) \\ \sum_{i=1}^{m} (\frac{\partial f_i}{\partial \beta_2})(\Delta y_i) \end{bmatrix} \tag{2.18}$$

The computed value of the observations f_i can be calculated from the state vectors and positions of DORIS stations at the time of measurement. In order to find the derivative of f_i with respect to the solve-for parameters $\boldsymbol{\beta}$, the following equation is used

$$\frac{\partial f}{\partial \beta} = \begin{bmatrix} \frac{\partial f}{\partial x} & \frac{\partial f}{\partial y} & \frac{\partial f}{\partial z} & \frac{\partial f}{\partial \dot{x}} & \frac{\partial f}{\partial \dot{y}} & \frac{\partial f}{\partial \dot{z}} \end{bmatrix} \begin{bmatrix} \frac{\partial x}{\partial \boldsymbol{\beta}} \\ \frac{\partial y}{\partial \boldsymbol{\beta}} \\ \frac{\partial z}{\partial \boldsymbol{\beta}} \\ \frac{\partial \dot{x}}{\partial \boldsymbol{\beta}} \\ \frac{\partial \dot{y}}{\partial \boldsymbol{\beta}} \\ \frac{\partial \dot{z}}{\partial \boldsymbol{\beta}} \end{bmatrix} \tag{2.19}$$

The coefficients, represented by left matrix in the R.H.S of the above equation are the partial derivatives of the computed observation with respect to the satellite state vectors, which can be computed analytically for any kind of observation. The terms on the right matrix on have to be computed from the numerical integration of the variational equations. The variational equation is given as

$$\ddot{\boldsymbol{X}}_{\boldsymbol{m}} = D_1 \boldsymbol{X}_{\boldsymbol{m}} + D_1 \dot{\boldsymbol{X}}_{\boldsymbol{m}} + A_f \tag{2.20}$$

Variational equations describe the variations in spacecraft state with respect to the solve-for parameters. These equations are linear and are solved simultaneously along with the equations of motion. The first-order equations are as follows

$$\begin{aligned} \dot{\boldsymbol{X}}_{\boldsymbol{m}} &= \boldsymbol{U}_{\boldsymbol{m}} \\ \dot{\boldsymbol{U}}_{\boldsymbol{m}} &= D_1 \boldsymbol{X}_{\boldsymbol{m}} + D_1 \dot{\boldsymbol{X}}_{\boldsymbol{m}} + A_f \end{aligned} \tag{2.21}$$

Integrating the equations above, we can determine the terms of the second matrix in the R.H.S of equation 2.19. GEODYN uses the Cowell's Sum method for integration of equations of motion and variational equations (Rowlands et al., 1993).

The position partial $\boldsymbol{X_m}$, velocity partial $\dot{\boldsymbol{X}}_{\boldsymbol{m}}$, acceleration partial $\ddot{\boldsymbol{X}}_{\boldsymbol{m}}$ are given as

$$\boldsymbol{X_m} = \begin{bmatrix} \frac{\partial x}{\partial x_0} & \frac{\partial x}{\partial y_0} & \frac{\partial x}{\partial z_0} & \frac{\partial x}{\partial \dot{x}_0} & \frac{\partial x}{\partial \dot{y}_0} & \frac{\partial x}{\partial \dot{z}_0} & \frac{\partial x}{\partial \alpha_1} & \cdots & \frac{\partial x}{\partial \alpha_j} \\ \frac{\partial y}{\partial x_0} & \frac{\partial y}{\partial y_0} & \frac{\partial y}{\partial z_0} & \frac{\partial y}{\partial \dot{x}_0} & \frac{\partial y}{\partial \dot{y}_0} & \frac{\partial y}{\partial \dot{z}_0} & \frac{\partial y}{\partial \alpha_1} & \cdots & \frac{\partial y}{\partial \alpha_j} \\ \frac{\partial z}{\partial x_0} & \frac{\partial z}{\partial y_0} & \frac{\partial z}{\partial z_0} & \frac{\partial z}{\partial \dot{x}_0} & \frac{\partial z}{\partial \dot{y}_0} & \frac{\partial z}{\partial \dot{z}_0} & \frac{\partial z}{\partial \alpha_1} & \cdots & \frac{\partial z}{\partial \alpha_j} \end{bmatrix} \tag{2.22}$$

$$\dot{\boldsymbol{X}}_{\boldsymbol{m}} = \begin{bmatrix} \frac{\partial \dot{x}}{\partial x_0} & \frac{\partial \dot{x}}{\partial y_0} & \frac{\partial \dot{x}}{\partial z_0} & \frac{\partial \dot{x}}{\partial \dot{x}_0} & \frac{\partial \dot{x}}{\partial \dot{y}_0} & \frac{\partial \dot{x}}{\partial \dot{z}_0} & \frac{\partial \dot{x}}{\partial \alpha_1} & \cdots & \frac{\partial \dot{x}}{\partial \alpha_j} \\ \frac{\partial \dot{y}}{\partial x_0} & \frac{\partial \dot{y}}{\partial y_0} & \frac{\partial \dot{y}}{\partial z_0} & \frac{\partial \dot{y}}{\partial \dot{x}_0} & \frac{\partial \dot{y}}{\partial \dot{y}_0} & \frac{\partial \dot{y}}{\partial \dot{z}_0} & \frac{\partial \dot{y}}{\partial \alpha_1} & \cdots & \frac{\partial \dot{y}}{\partial \alpha_j} \\ \frac{\partial \dot{z}}{\partial x_0} & \frac{\partial \dot{z}}{\partial y_0} & \frac{\partial \dot{z}}{\partial z_0} & \frac{\partial \dot{z}}{\partial \dot{x}_0} & \frac{\partial \dot{z}}{\partial \dot{y}_0} & \frac{\partial \dot{z}}{\partial \dot{z}_0} & \frac{\partial \dot{z}}{\partial \alpha_1} & \cdots & \frac{\partial \dot{z}}{\partial \alpha_j} \end{bmatrix} \tag{2.23}$$

$$\ddot{\boldsymbol{X}}_{\boldsymbol{m}} = \begin{bmatrix} \frac{\partial \ddot{x}}{\partial x_0} & \frac{\partial \ddot{x}}{\partial y_0} & \frac{\partial \ddot{x}}{\partial z_0} & \frac{\partial \ddot{x}}{\partial \dot{x}_0} & \frac{\partial \ddot{x}}{\partial \dot{y}_0} & \frac{\partial \ddot{x}}{\partial \dot{z}_0} & \frac{\partial \ddot{x}}{\partial \alpha_1} & \cdots & \frac{\partial \ddot{x}}{\partial \alpha_j} \\ \frac{\partial \ddot{y}}{\partial x_0} & \frac{\partial \ddot{y}}{\partial y_0} & \frac{\partial \ddot{y}}{\partial z_0} & \frac{\partial \ddot{y}}{\partial \dot{x}_0} & \frac{\partial \ddot{y}}{\partial \dot{y}_0} & \frac{\partial \ddot{y}}{\partial \dot{z}_0} & \frac{\partial \ddot{y}}{\partial \alpha_1} & \cdots & \frac{\partial \ddot{y}}{\partial \alpha_j} \\ \frac{\partial \ddot{z}}{\partial x_0} & \frac{\partial \ddot{z}}{\partial y_0} & \frac{\partial \ddot{z}}{\partial z_0} & \frac{\partial \ddot{z}}{\partial \dot{x}_0} & \frac{\partial \ddot{z}}{\partial \dot{y}_0} & \frac{\partial \ddot{z}}{\partial \dot{z}_0} & \frac{\partial \ddot{z}}{\partial \alpha_1} & \cdots & \frac{\partial \ddot{z}}{\partial \alpha_j} \end{bmatrix} \tag{2.24}$$

The coefficients of A_f are the direct derivatives of accelerations with respect to the solve for parameters.

$$\begin{bmatrix} 0 & 0 & 0 & 0 & 0 & 0 & \frac{\partial a_x}{\partial \alpha_1} & \cdots & \frac{\partial a_x}{\partial \alpha_l} \\ 0 & 0 & 0 & 0 & 0 & 0 & \frac{\partial a_y}{\partial \alpha_1} & \cdots & \frac{\partial a_y}{\partial \alpha_l} \\ 0 & 0 & 0 & 0 & 0 & 0 & \frac{\partial a_z}{\partial \alpha_1} & \cdots & \frac{\partial a_z}{\partial \alpha_l} \end{bmatrix} \tag{2.25}$$

The terms D_1 and D_2 which are the derivatives of accelerations with respect to satellite position and velocity are given by

$$\begin{bmatrix} \frac{\partial a_x}{\partial x} & \frac{\partial a_x}{\partial y} & \frac{\partial a_x}{\partial z} \\ \frac{\partial a_y}{\partial x} & \frac{\partial a_y}{\partial y} & \frac{\partial a_y}{\partial z} \\ \frac{\partial a_z}{\partial x} & \frac{\partial a_z}{\partial y} & \frac{\partial a_z}{\partial z} \end{bmatrix} \tag{2.26}$$

and

$$\begin{bmatrix} \frac{\partial a_x}{\partial \dot{x}} & \frac{\partial a_x}{\partial \dot{y}} & \frac{\partial a_x}{\partial \dot{z}} \\ \frac{\partial a_y}{\partial \dot{x}} & \frac{\partial a_y}{\partial \dot{y}} & \frac{\partial a_y}{\partial \dot{z}} \\ \frac{\partial a_z}{\partial \dot{x}} & \frac{\partial a_z}{\partial \dot{y}} & \frac{\partial a_z}{\partial \dot{z}} \end{bmatrix} \tag{2.27}$$

The initial conditions for the second order system (equation 2.20) is given as

$$\boldsymbol{X_m^0} = \begin{bmatrix} 1 & 0 & 0 & 0 & 0 & 0 & 0 & \ldots & 0 \\ 0 & 1 & 0 & 0 & 0 & 0 & 0 & \ldots & 0 \\ 0 & 0 & 1 & 0 & 0 & 0 & 0 & \ldots & 0 \end{bmatrix}_{3\times h} \tag{2.28}$$

and

$$\boldsymbol{V_m^0} = \begin{bmatrix} 0 & 0 & 0 & 1 & 0 & 0 & 0 & \dots & 0 \\ 0 & 0 & 0 & 0 & 1 & 0 & 0 & \dots & 0 \\ 0 & 0 & 0 & 0 & 0 & 1 & 0 & \dots & 0 \end{bmatrix}_{3\times h} \tag{2.29}$$

where $h = 6 + j$ is the number of dynamic parameters

The steps involved in the orbit determination process are

1. The initial conditions and planetary ephemerides are provided to the dynamical model.
2. The main equation of motion is integrated with the variational equations in order to calculate the state vectors and partial derivatives of the state vector with respect to the solve-for parameters.
3. Compute the theoretical observations f_i from the measurements.
4. Calculate the partial derivatives of theoretical observations with respect to the solve-for parameters.
5. Compute the normal matrix, iterate until convergence is reached.

It must be noted that some parameters don't depend on the variational equations such as the frequency offset of a DORIS beacon. The above explained procedure is set-up and organized in the GEODYN II (Rowlands et al., 1993).

2.1.2 Validation methods

In order to know whether the estimated orbit is accurate, it needs to be validated. This is done before the orbit solutions are used in other fields to deduce results such as ice thickness. The first validation method is by examining the residuals of range and range-rate measurements. These represent the model and measurement errors. In the least squares sense, the residuals represent how well the model fits the measurements. However, over-estimation and over-modelling also can reduce the residuals, but this cannot ensure that the calculated orbit is close to the true orbit.

Second method is to compare orbit arc from different estimations. The overlap analysis, however, can only indicate the internal consistency rather than accuracy. The overlapping is compared in all the three directions. Moreover, the focus is on the radial direction as it would influence the ocean altimeter results. The un-modelled errors such as the multipath error and observation noise are left in the observation equation.

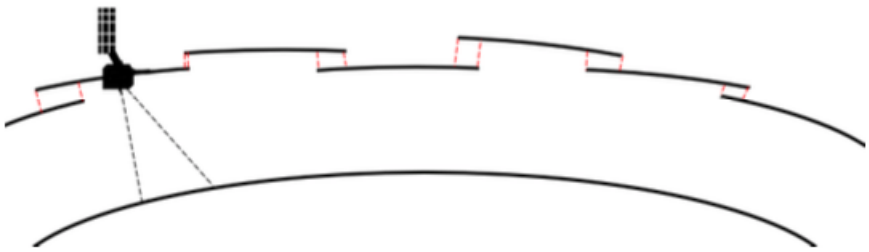

Figure 2.1: Validation using orbit arcs estimated in batch least squares. The red lines represent the overlap region of the arcs (Root, 2012).

The third method is to examine the differences in the overlapping arcs. For example, a single arc length of 6 days and a overlapping arc length of 3 days would mean that consecutive arcs overlap as shown in figure 6.15 (highlighted in red). Any uncertainty in the model and measurement errors would result in improper overlapping. For a POD, it is expected that the orbit arcs overlap perfectly, but a slight difference will exist due to errors. Such examination of orbit from different runs would help in orbit validation.

When all the three method satisfy the requirement of the orbit estimation, then it is certain that the estimated orbit is better.

2.2 Navigational mathematics

In this section reference frames used in this thesis will be explained along with any associated frame transformations.

2.2.1 Cartesian and geodetic coordinates

Before proceeding to the transformation between the Cartesian coordinates to Geodetic coordinates, it is appropriate here to highlight some important Geodesy concepts for understanding. Earth can neither be considered as a perfect sphere or a perfect ellipsoid. For convenience in calculations, it is approximated by an ellipsoid. There are two basic terms - Geoid and ellipsoid.

- Geoid - It is smooth figure having an irregular shape that best fits the mean sea level (MSL) in a least squares sense. This is a surface with constant gravity (equipotential surface).
- Ellipsoid - This is a surface that mathematically approximates the geoid by an ellipsoid. An ellipsoid is obtained by rotating ellipse about the minor axis coincident with the rotation axis of Earth. Centre of the ellipsoid coincides with the Centre of mass of Earth.

Since the ellipsoid approximates a geoid, this gives rise to different heights at certain regions. There are three heights that can be defined

- Geoid height (N) = Distance of surface of geoid from the surface of ellipsoid along the ellipsoidal normal. This is also referred to as Geoid undulation.
- Orthometric height (H) = Distance of the point of interest from the geoid.
- Geodetic height or altitude (h) = Sum of the geoid and orthometic height. ($h = H + N$)

The following clearly shows different heights

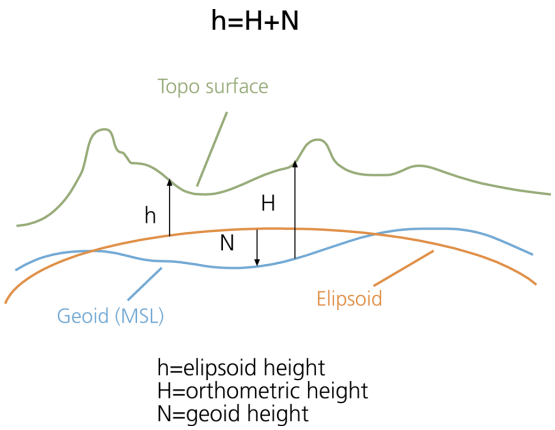

Figure 2.2: Height definitions in Geodesy Source: ESRI

These definitions are also addressed in tropospheric estimation section for defining the station position over the Geoid.

An ellipsoid is defined by two parameters a and b, which refer to semi-major axis a and semi-minor axis b. Other parameters referring to the ellipsoid can be derived from these two values such as

1. Flatness $f = \frac{a-b}{a}$
2. Eccentricity $e = \sqrt{\frac{a^2-b^2}{a^2}} = \sqrt{f(2-f)}$

Parameter set a and f are used to identify the kind of ellipsoid used to model the Earth. For example, World geodetic system (WGS84) and Geodetic Reference System (GRS80) ellipsoids have the following values:

- WGS84 a = 6378137 metres and $f = \frac{1}{298.257223563}$ (ICAO, 2002)
- GRS80 a = 6378137 metres and $f = \frac{1}{298.257222101}$ (Petit and Luzum, 2010)

Given the semi-major axis a and flatenning parameter f of an ellipsoid, one can realise the Cartesian coordinates in geodetic coordinates. A straightforward analytical solution for transformation from Cartesian coordinates to geodetic coordinates is not available, since the solution results in a fourth order equation. Although an approximate closed solution is available, an iterative approach is usually employed. An iterative subroutine has been built for this thesis based on the following formulation.

Let us consider the cartesian coordinates of a point on Earth as x, y, z. DORIS stations are provided in ITRF Cartesian coordinates. It is required to convert these coordinates to geodetic coordinates λ, φ, h where λ is latitude on ellipsoid, φ is longitude on ellipsoid and h is height above ellipsoid.

1. The altitude is initialized
$$h_0 = 0 \tag{2.30}$$
2. An arbitrary value of latitude is chosen by using the following approximation
$$\varphi_0 = \tan^{-1} \frac{z}{p(1-e^2)} \tag{2.31}$$
3. Geodetic longitude is computed as follows
$$\lambda = \tan^{-1} \left(\frac{y^e}{x^e} \right) \tag{2.32}$$

4. We iterate the following until convergence is reached in φ and h i.e. compare φ_i and φ_{i-1}, h_i and h_{i-1}

$$\begin{aligned} R_{N_i} &= \frac{a}{(1 - e^2 \sin^2 \varphi_{i-1})^{1/2}} \\ h_i &= \frac{\sqrt{x^2 + y^2}}{\cos \varphi_{i-1}} - R_{N_i} \\ \varphi_i &= \tan^{-1}\left(\frac{z}{\sqrt{x^2 + y^2}} \cdot \frac{(R_{N_i} + h_i)}{(R_{N_i}(1 - e^2) + h_i)}\right) \end{aligned} \tag{2.33}$$

   Here e is eccentricity, R_N is Normal Radius or radius of curvature of the prime vertical and the term p is defined as $\sqrt{x^2 + y^2}$

As recommended in IERS convention, GRS80 model is used for the transformation of ITRF solutions in Cartesian coordinates to geodetic coordinates. The transformation is available in the Fortran subroutine GCONV2.F provided by IERS. Although the iteration method has been set-up, the routine given by IERS is used in this thesis for transformation. The difference with respect to the iterative approach is that the later is based on Halley's method described in Fukushima (2006).

The geodetic coordinates can be converted to Cartesian coordinates by using the following transformation

$$\begin{bmatrix} x \\ y \\ z \end{bmatrix} = \begin{bmatrix} (R_N + h)\cos\varphi\cos\lambda \\ (R_N + h)\cos\varphi\sin\lambda \\ (R_N(1 - e^2) + h)\sin\varphi \end{bmatrix} \tag{2.34}$$

2.2.2 Azimuth and Elevation

For troposphere estimation, one requires the satellite elevation and azimuth with respect to the station. Other terms are used for elevation such as geodetic vertical angle or geodetic altitude. We also define zenith distance (ζ) which is equal to $90 - \varepsilon$. For this computation, a local frame called ENU reference frame attached to the DORIS station is used. ENU stands for East, North and Up which is defined as follows

- The x-axis point towards the East direction.
- The y-axis points to the North direction.
- The z-axis completed the right-handed coordinate system and points upwards perpendicular to the reference ellipsoid. ‘’

The origin of this frame coincides with antenna reference point. The DORIS station coordinates refer to the antenna reference point of the station antenna. To compute the satellite elevation and azimuth following method is used in this thesis.

1. Given the satellite coordinates in ECEF frame $\boldsymbol{r}^{sat}$ from the orbit solution and DORIS station ITRF coordinates $\boldsymbol{r}^{sta}$, the range between satellite and station is computed by

$$\boldsymbol{r}^{ecef}_{range} = \boldsymbol{r}_{sat} - \boldsymbol{r}_{sta} \tag{2.35}$$

2. For elevation and azimuth computation, the satellite-station range is required in the local geodetic coordinate system (ENU frame). Hence a transformation matrix is set-up to transform between local geodetic coordinate system (ENU frame) and geocentric

terrestrial reference frame (ECEF frame)

$$\begin{aligned} T_{enu}^{ecef} &= T_1\left(\frac{\pi}{2}-\varphi\right)T_3\left(\frac{\pi}{2}+\lambda\right) \\ &= \begin{bmatrix} -\sin\lambda & \cos\lambda & 0 \\ -\sin\phi\cos\lambda & -\sin\varphi\sin\lambda & \cos\varphi \\ \cos\varphi\cos\lambda & \cos\varphi\sin\lambda & \sin\varphi \end{bmatrix} \end{aligned} \tag{2.36}$$

3. Using T_{enu}^{ecef}, the range in geocentric coordinate system can be converted to the local coordinate system.

$$\boldsymbol{r}_{range}^{enu} = \boldsymbol{T}_{enu}^{ecef}\boldsymbol{r}_{range}^{ecef} \tag{2.37}$$

4. For convenience, we can use the following notations for vector components in r_{range}^{enu}

$$r_{range}^{enu} \equiv \begin{bmatrix} e \\ n \\ u \end{bmatrix} \tag{2.38}$$

5. Finally, elevation can be computed using the following relation

$$\varepsilon = \sin^{-1}\left(\frac{u}{|\boldsymbol{r}_{range}^{enu}|}\right) \tag{2.39}$$

6. Azimuth is computed using the following relation

$$\begin{aligned} \tan\alpha &= \frac{e}{n} \\ \alpha &= \operatorname{atan2}(n,e) \end{aligned} \tag{2.40}$$

If the computed azimuth is less than zero then 2π is added to the computed azimuth.

Chapter 3

RINEX structure and data processing

This chapter will explain in detail about the DORIS/RINEX format that will be used during the research. The format is based on the RINEX 3.0 that is also available for GPS data exchanges. For quick understanding, the RINEX data of CryoSat-2 containing the scientific measurements will be used to explain the observables.

3.1 Observables

As discussed before, RINEX format was initially designed for GNSS measurements. Further modifications were made to adapt it for DORIS application. DORIS/RINEX data contains the synchronous measurements from the DGXX receiver. These measurements are called as the observables which are (1) Time, (2) Phase and (3) Pseudo-Range. These observables are not corrected for any external effects such as ionospheric delay, tropospheric delay and relativity effects. Before moving on to the analysis of data, it is important to understand how the data is structured and where one can find the data necessary for this study. Following will describe the data structure of DORIS/RINEX 3.0
The RINEX files are divided into two sections: (1) Header and (2) Data as shown below in figure 3.1 and 3.2. For this purpose, DORIS measurement from CryoSat-2 was taken from the IDS `ftp` server and the fields present in them are explained below. Each field may not be present in the same line number in every RINEX file and may differ depending on the comments added or extra information. Let us first look at the header data.

3.1.1 Header

Line 1 - RINEX version and type

The first line of the header section conveys us three information:

- RINEX version - Version number of the RINEX data.
- File type - Letter **O** represents Observation data.
- Satellite system - Letter **D** represents DORIS. Other letters are also present but these are not in the scope of this study. **G**-GPS, **R**-GLONASS, **E**-Galileo, **S**-SBAS payload and **M**-Mixed

For purpose of this research we will be using 3.0 version.

```
     3.00           O                   D                   RINEX VERSION / TYPE
Expert              CNES                20171128 090021 UTC PGM / RUN BY / DATE
G = GPS R = GLONASS E = GALILEO S = GEO M = MIXED D = DORIS COMMENT
CRYOSAT-2                                                   SATELLITE NAME
2010-013A                                                   COSPAR NUMBER
SPA_BN1_4.7         CNES                                    OBSERVER / AGENCY
CHAIN1              DGXX                1.00                REC # / TYPE / VERS
DORIS               STAREC                                  ANT # / TYPE
        1.8480       -0.2000       -0.7510                  APPROX POSITION XYZ
        1.6312        0.0112        0.0137                  CENTER OF MASS: XYZ
D   10  L1  L2  C1  C2  W1  W2   F    P    T    H           SYS / # / OBS TYPES
  2017    11    27    00    00   28.8494178     DOR         TIME OF FIRST OBS
D  100   2  C1  C2                                          SYS / SCALE FACTOR
D           2.000                                           L2 / L1 DATE OFFSET
    52                                                      # OF STATIONS
D01  THUB THULE                         43001S005  3   0    STATION REFERENCE
D02  SPJB NY-ALESUND                    10317S005  3   0    STATION REFERENCE
D03  REZB REYKJAVIK                     10202S003  3   0    STATION REFERENCE
D04  MEUB METSAHOVI                     10503S016  3   0    STATION REFERENCE
D05  GR4B GRASSE                        10002S019  3 -15    STATION REFERENCE
D06  TLSB TOULOUSE                      10003S005  3   0    STATION REFERENCE
D07  WEUC WETTZELL                      14201S046  3  18    STATION REFERENCE
D08  PDOC PONTA DELGADA                 31906S004  3   0    STATION REFERENCE
D09  DIOB DIONYSOS                      12602S012  3   0    STATION REFERENCE
D10  SAQC SAL                           39601S004  3   0    STATION REFERENCE
D11  ASEB ASCENSION                     30602S005  3   0    STATION REFERENCE
D12  LICB LIBREVILLE                    32809S004  3   0    STATION REFERENCE
D13  HEMB ST HELENA                     30606S004  3   0    STATION REFERENCE
D14  TRJB TRISTAN DA CUNHA              30604S003  3   0    STATION REFERENCE
D15  BEMB BELGRANO                      66018S002  3   0    STATION REFERENCE
D16  SYQB SYOWA                         66006S005  3   0    STATION REFERENCE
D17  ADHC TERRE ADELIE                  91501S005  3   0    STATION REFERENCE
D18  OWFC OWENGA                        50253S002  3   0    STATION REFERENCE
D19  MSPB MOUNT STROMLO                 50119S004  3   0    STATION REFERENCE
D20  NOXB NOUMEA                        92701S004  3   0    STATION REFERENCE
D21  FUUB FUTUNA                        92902S003  3   0    STATION REFERENCE
D22  COBB COLD BAY                      49804S004  3   0    STATION REFERENCE
D23  STKB ST JOHN'S                     40101S003  3   0    STATION REFERENCE
D24  KRWB KOUROU                        97301S006  3   0    STATION REFERENCE
D25  CADB CACHOEIRA PAULISTA            41609S002  3   0    STATION REFERENCE
D26  RIRB RIO GRANDE                    41507S007  3   0    STATION REFERENCE
D27  YASB YARAGADEE                     50107S011  3   0    STATION REFERENCE
D28  MANB MANILLE                       22006S002  3   0    STATION REFERENCE
D29  JIWC JIUFENG                       21602S007  3   0    STATION REFERENCE
D30  BADB BADARY                        12338S002  3   0    STATION REFERENCE
D31  KRBB KRASNOYARSK                   12349S002  3   0    STATION REFERENCE
D32  YEMB YELLOWKNIFE                   40127S009  3   0    STATION REFERENCE
D33  GRFB GREENBELT                     40451S178  3   0    STATION REFERENCE
D34  MIAB MIAMI                         49914S003  3   0    STATION REFERENCE
D35  LAOB LE LAMENTIN                   97205S001  3   0    STATION REFERENCE
D36  ARFB AREQUIPA                      42202S007  3   0    STATION REFERENCE
D37  ROWC ROTHERA                       66007S005  3   0    STATION REFERENCE
D38  AMVB AMSTERDAM                     91401S005  3   0    STATION REFERENCE
D39  MNAC MANAGUA                       41201S002  3   0    STATION REFERENCE
D40  KEVC KERGUELEN                     91201S007  3   0    STATION REFERENCE
D41  CRQB CROZET                        91301S003  3   0    STATION REFERENCE
D42  MALB MALE                          22901S002  3   0    STATION REFERENCE
D43  EVEB EVEREST                       21501S001  3   0    STATION REFERENCE
D44  GONC GOLDSTONE                     40405S043  3   0    STATION REFERENCE
D45  SOFC SOCORRO                       40503S006  3   0    STATION REFERENCE
D46  RIMB RIKITEA                       92301S004  3   0    STATION REFERENCE
D47  MAUB MARION ISLAND                 30313S005  3   0    STATION REFERENCE
D48  REUB LA REUNION                    97401S002  3   0    STATION REFERENCE
D49  DJIB DJIBOUTI                      39901S003  3   0    STATION REFERENCE
D50  PAUB PAPEETE                       92201S010  3   0    STATION REFERENCE
D51  HBMB HARTEBEESTHOEK                30302S008  3   0    STATION REFERENCE
D52  KOLB KAUAI                         40424S009  3   0    STATION REFERENCE
     5                                                      # TIME REF STATIONS
D06          0.348          0.566                          TIME REF STATION
D17          3.979         13.734                          TIME REF STATION
D24          7.675         70.227                          TIME REF STATION
D50          7.904          4.221                          TIME REF STATION
D51          4.561         20.825                          TIME REF STATION
  2017    11    27    00    00    0.0000000                TIME REF STAT DATE
                                                            END OF HEADER
```

Figure 3.1: Header section of DORIS/RINEX 3.0 data format

```
> 2017 11 27 00 00 33.149947800  0  2       -4.300529947 0
D01  -2172556.181     -428106.646  -144907739.26111-144907372.01811      -128.500 7
        -116.950 7       135.526       1003.522 1       -15.245 1       83.332 1
D02  -3147537.550     -620226.612   135747367.25812 135747517.19412      -124.650 7
        -114.150 7       135.526       1003.000 0        -7.000 0       74.000 0
> 2017 11 27 00 00 36.149947800  0  2       -4.300529947 0
D01  -2258256.694     -444994.075  -144909001.00111-144908633.77011      -128.500 7
        -116.950 7       135.526       1003.522 1       -15.245 1       83.332 1
D02  -3282001.597     -646723.011   135745387.57812 135745537.49812      -124.650 7
        -114.150 7       135.526       1003.000 0        -7.000 0       74.000 0
```

Figure 3.2: Data section of DORIS/RINEX 3.0 data format

Figure 3.3: Line 1 of DORIS/RINEX 3.0 data format

Line 2 - PGM/RUN BY/DATE

The second line conveys three information:

- PGM - This represents the program creating the current file. (E.g. Expert)
- RUN BY - This is the agency creating the current file. (E.g. CNES - Centre national d'études spatiales)
- DATE - The date on which the file was created (E.g. 20171128 090021 in the format [YYYYMMDD HHMMSS ZONE]. The ZONE field is the time zone - either UTC or LCL will be specified representing Coordinated Universal Time and Local time with unknown local time system code respectively.)

```
Expert              CNES                20171128 090021 UTC PGM / RUN BY / DATE
```

Figure 3.4: Line 2 of DORIS/RINEX 3.0 data format

Line 3 - COMMENT

Comment line specifies the letters used in the satellite system in line 1 and its description. Not limited to the later, other information necessary for data interpretation shall also included in the comment.

```
G = GPS R = GLONASS E = GALILEO S = GEO M = MIXED D = DORIS COMMENT
```

Figure 3.5: Line 3 of DORIS/RINEX 3.0 data format

Line 4 - SATELLITE NAME

This line specifies the name of the satellite that performed the measurements using the DGXX receiver. The receiver was installed starting from the mission Jason-2 and has been made available to the missions launched after that. Available field definitions are **JASON-2, CRYOSAT-2, HY-2A, SARAL, JASON-3, SENTINEL-3**

```
CRYOSAT-2                                                   SATELLITE NAME
```

Figure 3.6: Line 4 of DORIS/RINEX 3.0 data format

Line 5 - COSPAR NUMBER

This line specifies the COSPAR (Committee on Space Research) number - an international naming convention for satellites. It contains the launch year followed by a 3 letter code representing the sequential identifier of that launch. For e.g. the COSPAR number 2010-013A

represents that the satellite was launched in 2010 and was the 13th successful launch made that year.

```
2010-013A                                                   COSPAR NUMBER
```

Figure 3.7: Line 5 of DORIS/RINEX 3.0 data format

MARKER TYPE

This represents the type of body to which the receiver is attached. E.g. A spacecraft, balloon, terrestrial vehicle etc. The field definitions are as follows:

```
GEODETIC          Earth-fixed, high-precision monumentation
NON_GEODETIC      Earth-fixed,  low-precision monumentation
SPACEBORNE        Orbiting space vehicle
AIRBORNE          Aircraft, balloon, etc.
WATER_CRAFT       Mobile water craft
GROUND_CRAFT      Mobile terrestrial vehicle
FIXED_BUOY        "Fixed" on water surface
FLOATING_BUOY     Floating on water surface
FLOATING_ICE      Floating ice sheet, etc.
GLACIER           "Fixed" on a glacier
BALLISTIC         Rockets, shells, etc
ANIMAL            Animal carrying a receiver
HUMAN             Human being
```

Figure 3.8: Marker keywords in RINEX 3.0 data format

For DORIS measurements, it is usually SPACEBORNE keyword since all the measurements are performed by the receiver on satellites.

Line 6 - OBSERVER/AGENCY

This refers to the processing unit and the agency providing the RINEX file. E.g. Here the SPACEBORNE is the processing unit and CNES is the agency.

```
SPA_BN1_4.7         CNES                                    OBSERVER / AGENCY
```

Figure 3.9: Line 6 of DORIS/RINEX 3.0 data format

Line 7 - REC#/TYPE/VERS

In this line, the symbols represent the following

- **REC** - Receiver chain used in DORIS. E.g. CHAIN1 or CHAIN
- **TYPE** - DORIS instrument (receiver) present in the satellite. E.g. DGXX receiver
- **VERS** - DORIS/DIODE Software version used onboard. DIODE is On-Board Orbit Determination software the computes orbit in real time with accuracy.

```
CHAIN1              DGXX                1.00                REC # / TYPE / VERS
```

Figure 3.10: Line 7 of DORIS/RINEX 3.0 data format

Line 8 - ANT#/TYPE

It represents the following

- **ANT#** - Antenna number if two or more antennas are present. E.g DORIS
- **TYPE** - Antenna type E.g STAREC

```
DORIS                 STAREC                                  ANT # / TYPE
```

Figure 3.11: Line 8 of DORIS/RINEX 3.0 data format

Line 9 - APPROX POSITION XYZ

The position of antenna reference point in the body-fixed coordinate system of satellite is provided in the X, Y, Z order

```
     1.8480        -0.2000        -0.7510                  APPROX POSITION XYZ
```

Figure 3.12: Line 9 of DORIS/RINEX 3.0 data format

Line 10 - CENTER OF MASS: XYZ

The position of center of mass of the satellite (defined at the launch) in the body-fixed coordinate system of satellite is provided in X, Y, Z order. The evolving inertia and center of mass of the satellite will be provided in a separate file.

```
     1.6312         0.0112         0.0137                  CENTER OF MASS: XYZ
```

Figure 3.13: Line 10 of DORIS/RINEX 3.0 data format

Line 11 - SYS#/OBS TYPES

These keywords act as legends for the DORIS measurements provided in the 'Data' section. It represents the following:

- **D** - D for DORIS. The corresponding value in 'Data' section will be the DORIS station number.
- **L1** - 2GHz phase measurement in full cycles
- **L2** - 400MHz phase measurement in full cycles
- **C1** - 2GHz pseudo range in km
- **C2** - 400MHz pseudo range in km
- **W1** - 2GHz power received in dBm
- **W2** - 400MHz power received in dBm
- **F** - Relative frequency offset in 1×10^{-11}
- **P** - Atmospheric pressure at the ground station (100 Pa or mBar)
- **T** - Temperature at the ground station in degree Celsius

- **H** - Humidity at the ground station in percent

```
D   10  L1  L2  C1  C2  W1  W2   F   P   T   H              SYS / # / OBS TYPES
```

Figure 3.14: Line 11 of DORIS/RINEX 3.0 data format

Line 12 - TIME OF FIRST OBS

This is the on-board receiver proper time of the first observation record in the file. In other words, this is the first measurement. The format is [YYYY MM DD hour minute seconds]. The time system used is specified next: **DOR** - DORIS system Time.

```
  2017    11    27    00    00   28.8494178     DOR          TIME OF FIRST OBS
```

Figure 3.15: Line 12 of DORIS/RINEX 3.0 data format

Line 13 - SYS / SCALE FACTOR

The following is represented

- **D** - Letter D specifies it is a DORIS measurement
- **100** - This is the scale factor that needs to applied only to **C1** and **C2** observations. In this case, the values have to be divided by 100.
- **2** - Number of observation types involved. In this case we have two types: **C1** and **C2**
- **C1 C2** - List of observation types. The types are mentioned.

```
D  100   2  C1  C2                                          SYS / SCALE FACTOR
```

Figure 3.16: Line 13 of DORIS/RINEX 3.0 data format

Line 14 - L2 / L1 DATE OFFSET

- **D** - This represents the satellite system. D for DORIS.
- **2.000** - This is the time delay between the L1 measurement date and L2 measurement date at the antenna phase center.

```
D          2.000                                          L2 / L1 DATE OFFSET
```

Figure 3.17: Line 14 of DORIS/RINEX 3.0 data format

Line 15 - # OF STATIONS

This represents the number of stations, for which observations are present in the file.

```
    52                                                    # OF STATIONS
```

Figure 3.18: Line 15 of DORIS/RINEX 3.0 data format

Line 16 - 67 STATION REFERENCE

The stations that are present in the observation record of the file is listed in chronologically based on **xx** numerical value in **Dxx** field. Each station is described with:

- **D01** - DORIS identifier; a internal number for each . E.g. DO1, DO2, DO3
- **Station acronym** - 4 character station acronym is given E.g. THUB
- **Station name** - Station name is given E.g. THULE
- **43001S005** - This is the DOMES number (Directory of MERIT Sites). This is unique for each station.
- **3** - Beacon type characterised by number
- **0** - Signed frequency shift factor (K)

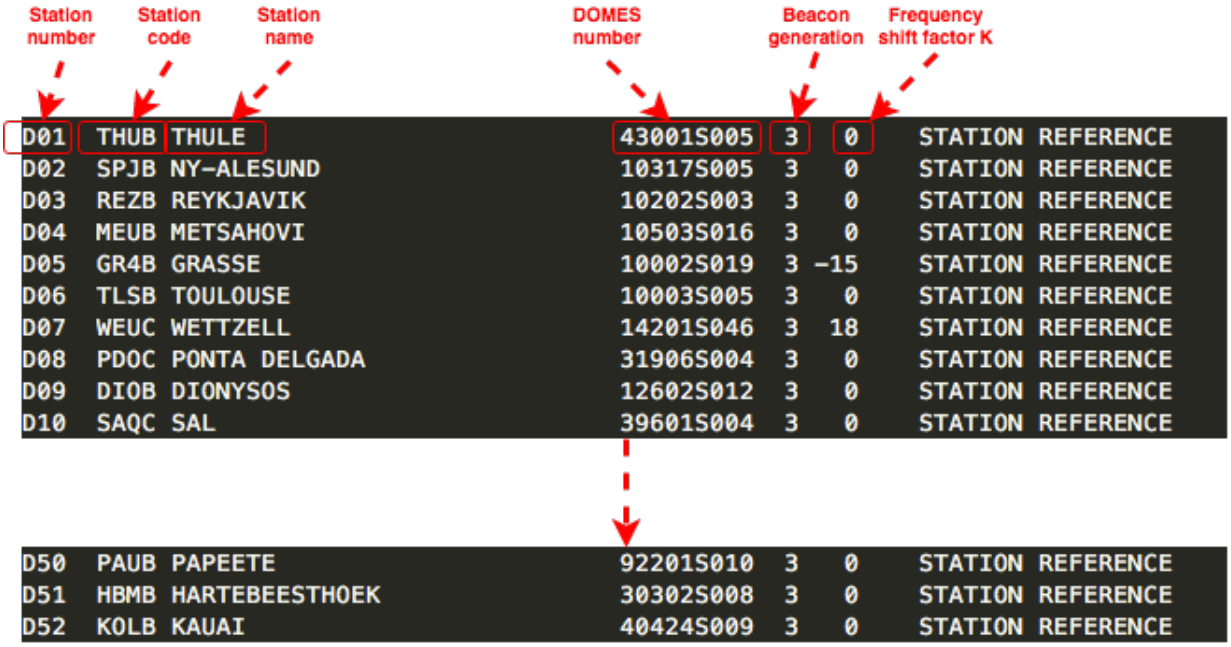

Figure 3.19: Line 16 of DORIS/RINEX 3.0 data format

Line 68 to 75 - # TIME REF STATIONS, TIME REF STATION, TIME REF STAT DATE, END OF HEADER

- **# TIME REF STATIONS** This represents the number of time reference stations (master beacons) in the file.
- **TIME REF STATION** Reference stations present in the file are tagged with this keyword. The parameters defined for each reference station are:
  - **D06** - This is the DORIS identifier. D for DORIS and a internal number for each station
  - **0.348** - Time offset of station reference time from TAI reference time at the date defined in TIME REF STAT DATE. The unit is in micro second.

– **0.566** - Shift of beacon reference time at the date defined in TIME REF STAT DATE. The unit is in 1×10^{-14} second.

- **TIME REF STAT DATE** - The date (at 00 hours 00 minutes 00seconds) on which the first measurement was performed on the first reference beacon in the file. E.g. The first reference beacon in the file is the **D06**. So, the date on which first measurement was performed on it is specified. This is used for time processing of Time offset and shift of beacon reference time mentioned above.

- **END OF HEADER** - This is the last record indicating the end of header section.

```
    5                                                   # TIME REF STATIONS
D06             0.348             0.566                 TIME REF STATION
D17             3.979            13.734                 TIME REF STATION
D24             7.675            70.227                 TIME REF STATION
D50             7.904             4.221                 TIME REF STATION
D51             4.561            20.825                 TIME REF STATION
  2017    11    27    00    00     0.0000000            TIME REF STAT DATE
                                                        END OF HEADER
```

Figure 3.20: Line 68 to 75 of DORIS/RINEX 3.0 data format

3.1.2 Data

Data section is the major part of a RINEX file containing the measurements necessary for this study. These are measurements performed by the on-board DGXX receiver at two frequencies during the satellite's pass over the beacon station. At a particular instant, number of stations present in the line of sight may differ and this is reflected in the number of measurements that will be available to us. Nevertheless, the 3rd generation DGXX recevier is capable of making 7 simultaneous measurements.
Overall data is divided in sequences, each available every 10 seconds. Each sequence consists of two measurements, first one at T_0 and second one at $T_0 + 3s$. The measurement at $T_0 + 10s$ is nothing but the one at T_1. The 10 second interval is called a sequence. A sequence consists of two record blocks (one at 0s and other at 3s) or observation record. A record block is a series of measurements and the amount of measurements depends on the number of stations over which the pass is made by the satellite. In other words, record block has measurements from different beacons.

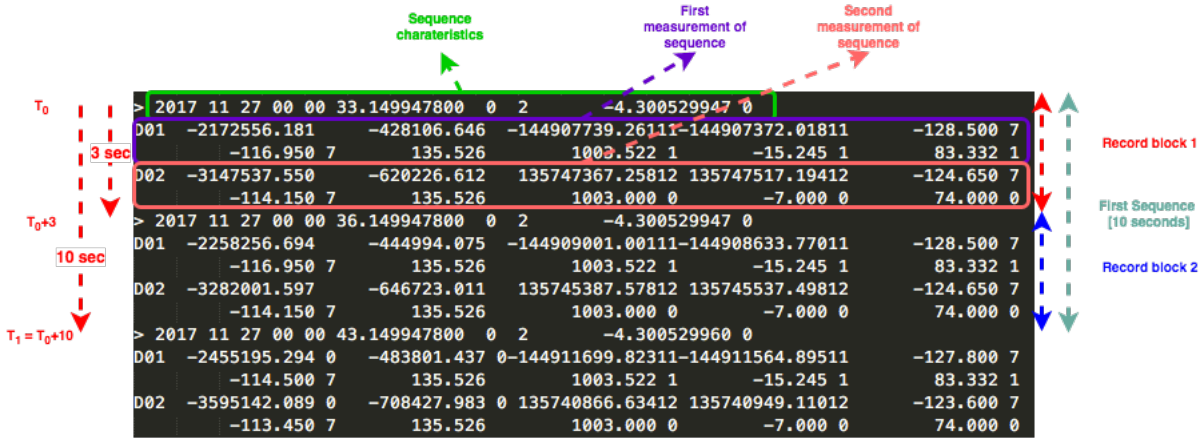

Figure 3.21: Data structure

Signal from a signal beacon station consists of 10 measurements made of:

- 2 phase measurements
- 2 pseudo measurements
- 2 power levels of the received signal
- A Ultra Stable Oscillator (USO) relative frequency offset
- 3 meteorological data (pressure, temperature, humidity).

These measurements are written in two lines with 5 measurements each. The keywords present in the header section represent these measurements in the data section as shown in figure (3.23).
Sometimes both the record blocks may not be present all the time causing the measurement at 0s of a sequence to be absent. This is because the receiver hasn't locked to the signal from the beacon and thus the sequence starts from the record block 2 (T_0 + 3s).
The flags in the figure (3.22) have to be taken care when using these information as it may indicate if the information is exploitable or not. The Epoch flag can be a 0 indicating that the measurement is exploitable. If it is 1, it conveys that there was a power failure between previous epoch and current epoch. A special event is marked by symbol >1. The receiver clock offset flag can either be a 1 or 0.

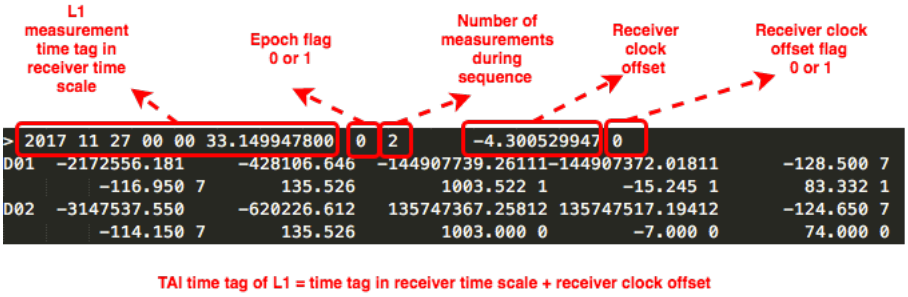

Figure 3.22: Information present in sequence characteristics

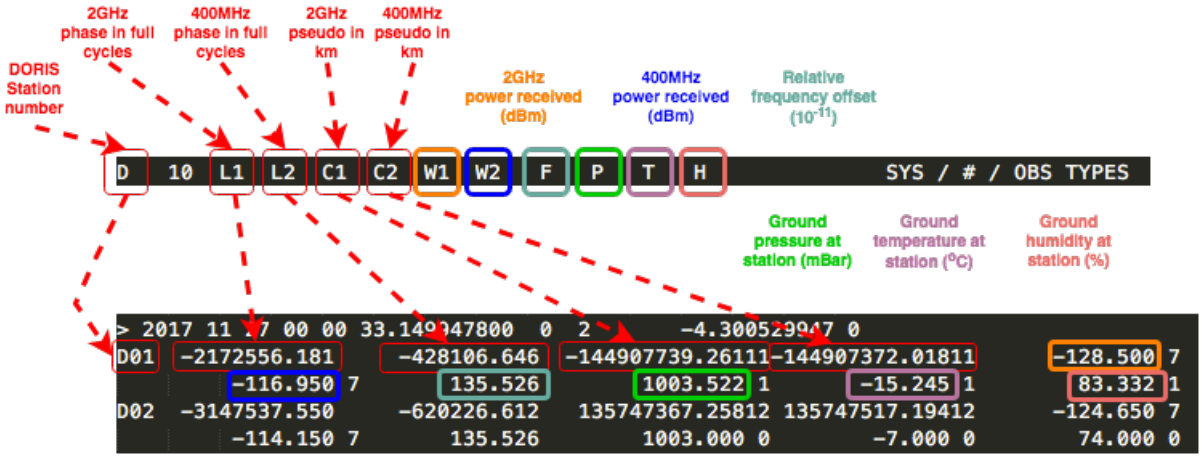

Figure 3.23: Line 11 of DORIS/RINEX 3.0 data format (top) and a single observation record (bottom). The data in the first measurement of sequence corresponding to each field is shown.

Chapter 4

Time tagging

In the following section we first describe the nature of the problem and propose how this can be solved. Explain what is a clock model. Following this, pseudo range modelling is explained.

4.1 Time-tagging/datation problem

The measurements in RINEX data are provided in the on-board proper time scale. The receiver clock is not attached to any particular time scale and is a free flowing clock. To make use of observations for orbit determination, it is necessary to tie the measurements to a coordinate time scale. This is called the time-tagging or datation or time synchronization. In DORIS, the coordinate time scale used is TAI (International Atomic Time). In this process, a clock solution is solved which gives the offset of the on-board clock with respect to consistent and well maintained time scale. In DORIS orbit determination, International Atomic Time (TAI) time scale will be used for time-tagging.

Users can use the solution provided in RINEX file for time-tagging. It is also possible for users to model the clock. In this research we try to model our own clock solution and do time-synchronisation.

Clock solution cannot be solved every epoch as in GPS since DORIS does not have sufficient number of satellites available at every epoch. Hence the solution is to build a clock model for on-board clock and retrieve offsets at every epoch. The issue with clock model is that they do not represent the true clock behaviour and is only an approximation. The remaining error in models are then translated to measurements. This can induce different effects depending on how the phase measurements are formulated i.e. whether a phase is used directly or phase increments are used. The following flow chart represents how the quality of clock model would affect the corrections considering that we use Doppler approach of processing the phase measurements.

It is clear how time-tagging can inject errors into multiple processing steps and is an important part of this research. The precision required for the time-tagging must be better than 10^{-7}. This can be considered as a requirement for our research. Later this will be compared PANDOR. In the following sections, we will first describe what is basically a clock and how can it be modelled

4.1.1 What can be done?

The only data that can aid the time-tagging in DORIS RINEX is the availability of pseudo range measurements. Pseudo range measurement is available for both frequencies in RINEX

data. The noise in these measurement are higher compared to the ones in GPS. 2GHz pseudo range measurement has noise in the order of magnitude of 5 km and 400 MHz has about 1 km. Pseudo range in DORIS RINEX is the distance between station antenna phase centre to satellite antenna phase centre including the ionospheric, tropospheric and clock errors of transmitter and receiver.

In DORIS system, not all stations are synchronized. Thus for these stations the pseudo range measurement represents the behaviour of free running station clock. However, there are few time reference/master stations which are monitored well accurately with respect to TAI. The stations maintain frequency according to standards to ensure low short term noise and long time variations. Thus, clock synchronization is available only for these particular stations in the DORIS station network.

Pseudo ranges over time reference stations can then be used to synchronize the on-board time with TAI. The synchronization here refers to the formulation of a clock model for satellite clock that gives relationship between on-board time and TAI.

These reference beacons clocks are well synchronized to TAI with well maintained offset and drift. Thus the transmitter clock error in the pseudo range measurement of time reference beacon. The only remaining large effect is the onboard clock offset which can be modelled using the pseudo range measurement (either C1 or C2). The noise in the pseudo range does not pose as an limitation to the correct synchronisation of the on-board clock.

4.2 Pseudo range modelling

Pseudo range equation is given by

$$\rho = c\big((\tau_r + h_r) - (\tau_e + h_e)\big) + \epsilon_c \tag{4.1}$$

where

- τ_r is the reception time (on-board proper time) This is the time at which phase and pseudo range measurements on two frequencies are acquired from stations in visibility. This time is present in the RINEX measurement file
- h_r is receiver clock offset. This is present in RINEX in the offset field. This can also be modelled by users using a clock model which will be done in this research.
- t_e is the ground beacon emission time measured by the beacon clock.
- h_e is beacon clock offset. The offset and drift are known for the time reference beacons and are unknown for normal beacons. [s]
- C is the pseudo range measurement in the RINEX [m]
- c is the speed of light [m/s]
- ϵ_c pseudo range measurement error. C1 (5km) and C2 (1km)

Proper time is the time of event observed when the observer is in the satellite reference frame. In thesis we use the above formulation to time tagging the measurements in TAI. However, the proper time and coordinate time cannot be assumed to have a linear evolution as this expression represents. Proper time τ_r is related to coordinate time t_r by relation

$$\begin{aligned} \tau_r &= t_r + \delta_r \\ \tau_e &= t_e + \delta_e \end{aligned} \tag{4.2}$$

where

- δ_r This term represents the receiver clock relativistic effect required to convert between proper time and coordinate time. This term has two components - a frequency bias and periodic variations.
- δ_e This term is represents the clock relativistic effect for the beacon clock.

Clock relativistic effect

The coordinate time scale used for computations related artificial satellites of the Earth is Geocentric Coordinate Time. For DORIS, International Atomic Time (TAI) is used for orbit computations. TAI is equivalent to TCG on the geoid by the relation

$$TAI = (1 - L_G)TCG \tag{4.3}$$

where $L_G = \frac{U_{GEO}}{c^2} = 6.969290134 \times 10^{-10}$. U_{GEO} refers to gravitational potential on Earth's Geoid. (Petit and Luzum, 2010) Relationship between coordinate time and proper time is given by

$$\frac{d\tau}{dt} = 1 - \frac{v^2}{2c^2} - \frac{U(x)}{c^2} \tag{4.4}$$

where

- τ is the proper time
- t is the coordinate time
- v is the velocity of satellite in inertial frame [m/s]
- $U(r)$ is the Gravitational potential at satellite location r.
- c is the speed of light [m/s]

The above expression applies to both receiver and beacon. Let us first look at the beacon clock term δ_e. For ground station it is just the frequency offset term. The second relativity correction term is zero. This is because on a geoid $\frac{d\tau}{dt} = 0$ and the reference clocks are corrected for altitude

For the receiver clock term δ_r, the equation is integrated along the orbit over the coordinate time and a relationship is obtained between proper time (τ) and coordinate time (t). The δ_r term has two parts - (i) First is the frequency offset (bias + drift) between the proper time and coordinate time and (ii) Periodic terms. If a linear evolution is assumed (as done in this thesis), the long term frequency drift component in δ_r gets absorbed in the polynomial model we adjust. However the periodic terms will not affect the time-tagging, but may affect the station position estimation. In the computation of periodic terms, one must consider the J_2 term of the Earth potential.

4.3 Modelling the clock

A mathematical formulation of how the time-offset of a clock with respect to a reference timescale evolves is given by a clock model. The reference timescale is simply a clock that is consistent and well maintained or in other words has accurate timekeeping. Reference timescale is chosen such that its quality and performance exceeds the performance of the clock

being modelled. In this thesis we chose the International Atomic Scale (TAI) as the reference timescale. We model our satellite clock with respect to TAI assuming that TAI as a approximation to true time, which in reality is a good approximation.

The first step in formulating a clock model is to express the time-offset using the following expression

$$h(t) = C(t)_{TAI} - C(t)_{sat} \tag{4.5}$$

where

- h is the time-offset of clock with respect to TAI.
- $C(t)_{TAI}$ Clock reading of TAI
- $C(t)_{sat}$ Clock reading of on-board clock at time
- t is the independent time variable based on TAI.

Using the time-offset h, the on-board clock can be synchronised with TAI by either adding or subtracting to the on-board clock. The sign of offset depends on whether the on-board clock is ahead or behind TAI. A sample clock offset diagram is shown below based on which certain concepts can be explained.

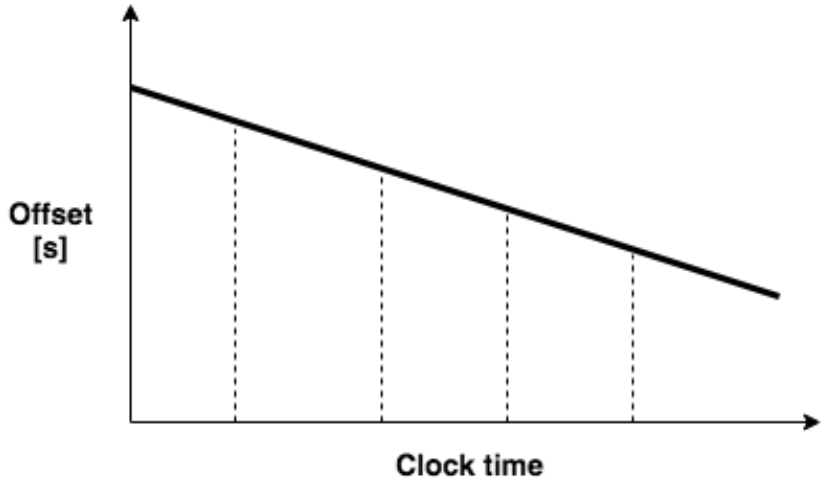

Figure 4.1: An example of offset-clock plot with x-axis refers to the clock time of the clock modelled and y-axis refers to the clock offset with respect to reference time scale.

An simplified example of offset plot is shown above. Here the dashed lines represent the points where the clock measurements are available allowing the computation of offset. The thick straight line represents to the behaviour of the interested clock with respect to TAI clock. The intercept represents the initial offset between TAI and the clock. The slope of the straight line represents the frequency stability of the clock. In reality clock behaviour is not a simple straight line as shown above, but is combination of deterministic and stochastic components.

Choice of reference time-scale or nominal frequency of the clock oscillator does not affect the performance of the that clock. The fractional frequency offset and its evolution determinate the timekeeping performance of that clock. Let $h(t)$ be the time-offset of the clock driven by an oscillator. Frequency of the oscillator $v(t)$ at instantaneous time t can be expressed as

$$f(t) = f_0 + \Delta f(t) \tag{4.6}$$

where

- $f(t)$ Actual frequency of the oscillator at time t [Hz]
- f_0 is the nominal frequency of the oscillator [Hz]
- $\Delta f(t)$ is frequency offset at time t from the nominal frequency [dimensionless]

Normalised frequency offset $f^{n,o}(t)$ of the oscillator can be expressed as derivative of the clock offset h with respect to time t

$$f^{n,o}(t) = \frac{dh}{dt} = \frac{f(t) - f_0}{f_0} \tag{4.7}$$

In the DORIS, clocks are present in the master beacon and in the satellite. With regards to notations, following will be used for receiver and transmitter

- h_e - Emitter clock offset
- h_r - Receiver clock offset
- $\frac{\Delta f_r}{f_{rn}}$ Normalised frequency offset of the receiver
- $\frac{\Delta f_e}{f_{en}}$ Normalised frequency offset of the transmitter

4.4 Standard clock model

A basic clock model can be expressed as a n-th order polynomial in the time interval $(t - t_0)$. For example, a second order polynomial can be expressed as

$$h(t) = a + b(t - t_0) + c(t - t_0)^2 \tag{4.8}$$

where

- a is the time-offset [s]
- b is the frequency offset i.e $f^{n,o}$ [s/s]
- c is the frequency drift parameter also sometimes known as clock ageing parameter. [s/s^2]

Depending on the requirement, a third order or fourth order polynomial could be fit to the offset data. The polynomial equation obtained is then clock model for that time interval. Frequency offset of the clock can be derived from the polynomial equation by taking its derivative as stated in equation 4.7. The model for clock offset and frequency offset would be then

$$\begin{aligned} h(t) &= a + b(t - t_0) + c(t - t_0)^2 + c(t - t_0)^3 \\ f^{n,o}(t) &= b + 2c(t - t_0) + 3c(t - t_0)^2 \end{aligned} \tag{4.9}$$

With our time-tagging solution with respect to International Atomic Time, we can now synchronise a free running clock to TAI time scale using the above equation. The frequency offset of the oscillator is taken into account using the second equation. However, it must be kept in mind that this is an approximation and depends mainly on the quality of master beacon used in the time synchronisation, since the largest error in psuedo range measurement is related to time offset.

Chapter 5

Measurement modelling

5.1 Phase modelling vs Doppler counts

The complete phase equation in L_1 and L_2 can be given as

$$\text{At epoch } t \text{ (OBT)} \begin{cases} \lambda_1 L_1 = d_0 + d_T + d_1 + \lambda_1 l_w - e + c\tau + k_1 \\ \lambda_2 L_2 = d_0 + d_T + d_1 + \lambda_2 l_w - e + c\tau + k_1 \end{cases} \tag{5.1}$$

The ionosphere combination is given by

$$\begin{aligned} \text{At epoch } t \text{ (OBT)} &\left\{ \lambda_c L_c = d_c + c\tau + a \right. \\ \text{At epoch } t + 10 \text{ (OBT)} &\left\{ \lambda_c L_c = d_c + c\tau + a \right. \end{aligned} \tag{5.2}$$

where:

- d_c is the signal propagation distance between the iono-free center on satellite and ground beacon.
$$d_c = d_0 + \frac{\gamma d_1 - d_2}{\gamma - 1} + h_{dry} + m_{wet} h_{z,wet} \tag{5.3}$$
Here d_1 and d_2 are the phase center correction for L_1 and L_2 frequency. Thus, iono-combination of these correction gives the iono-free phase center correction that is applied with distance d_0
- h_{dry} is the dry tropospheric delay
- m_{wet} is the wet mapping function
- $h_{z,wet}$ is the zenith wet tropospheric delay

For the reference beacon the clock model used is

$$\tau_e = a_0 + a_1 t + \delta a_0 + \delta a_1 t \tag{5.4}$$

In order to construct a doppler count we differentiate two successive measurements (i.e one at t and other at $t + 10$). This corresponds to doppler processing. The advantage of Doppler-like processing is that the ambiguity (a) in the phase can be eliminated. In addition this also removes the bias present in the beacon clock offset τ_e

In case of phase measurement modelling, there are intrinsic noises in the order of few mm that are uncorrelated between successive measurements. Doppler like processing would introduce the correlations between successive measurement which is an disadvantage.

However, the goal was to create data similar to DORIS 2.2 measurement format from RINEX 3.0 so that it can be supplied to the GEODYN with available data processing tools without any major alterations. Hence the Doppler like processing was chosen for this thesis study.

5.2 Range rate modelling

In RINEX, phase measurement is provided in two frequencies - 2036.25 MHz (L1) and 401.25 MHz (L2). The L1 frequency is used for range rate computation. L2 frequency is only used for computing ionospheric correction.

The basic range rate measurement ($v_{measured}$) or the relative velocity with respect to the station is expressed as follows:

$$v_{measured} = \frac{c}{f_{en}} \left(\frac{N}{\Delta \tau_r} - (f_{en} - f_{rt}) - f_{en} \right) \tag{5.5}$$

where

- $v_{measured}$ - relative velocity measured between ground beacon phase center and on-board antenna phase center.
- c - Speed of light (299792458 m/s)
- N - Doppler counts
- τ_r - Proper time interval
- f_{en} - Nominal beacon frequency
- f_{rt} - True frequency of the receiver

5.3 Tropospheric modelling

5.3.1 What is troposphere delay

Radio signals experience delay while propagating through the electrically neutral atmosphere. This is referred to as the Troposphere delay. The phenomenon behind the troposphere delay is due to the induced pole moment of the neutral atmosphere molecules and permanent dipole moment of the water vapour molecules. (Elgered, 1993)

The delay can be separated into two components on the basis of the contribution to error. First is the hydrostatic/dry component which contributes to around 80 percent or more of the delay depending on the time of the year and station location. Largest contribution to the hydrostatic delay can be traced back to dry air which is why it is often referred to as dry component. It can be determined with high precision using the surface pressure data available at the station because the surface pressure is representative of weight of all air layers. (VMF3 paper) Second is the wet component which contributes to less than 20 percent of the delay. The wet component is generally hard to determine due to high variability and uncertainties in atmospheric distribution. Surface measurements alone are not sufficient for the determination. Usual practice in orbit determination field is to adjust this parameter in

the parameter estimation procedure. In this thesis, it will be estimated in orbit computation software GEODYN along the frequency bias of the ground beacon.

The delay depends on the factors such as atmospheric condition along the signal path, satellite elevation above the station and station height above sea level. Empirical models take into account these factors and relate them to the overall delay. In addition, accurate models use the surface measurements at station such as pressure, temperature and relative humidity for the computation of delay. This means we cannot get the true value of tropospheric delay, but using the empirical models we can get close to the true value by taking into account the environment of signal travel.

To begin with, it is important to understand how these models are fundamentally built. A delay occurs when the geometrical distance travelled by the radio signal differs from the actual path. The delay experienced by a radio signal in the zenith direction (elevation = 90 deg) can be expressed mathematically (Petit and Luzum, 2010) (Schüler, 2001) as

$$d_{total,trop} = \int_{atm} n(s)ds - \int_{vac} ds \tag{5.6}$$

where

- S_{trop} - total/neutral slant path delay from on-ground antenna to satellite
- $n(s)$ - total refractive index as a function of distance s along the path.
- ds - differential increment in distance along the signal path in zenith direction.
- $_{atm}$ - represents the integration along the actual signal path from antenna to satellite through the atmosphere.
- $_{vac}$ - represents the integration along the virtual signal path from antenna to satellite through the vacuum.

The first integral represents the true curved path through the atmosphere and second integral represents the straight geometric path that the signal would travel under ideal conditions (vacuum). Thus, the difference between them is the delay/range error imparted by troposphere. The integration bounds for both integrals are between geocentric radius of station (r_s) and geocentric radius of the top of neutral atmosphere (r_a) where the water vapour concentration becomes minimal. So, the expression can further be written as

$$\begin{aligned} d_{total,trop} &= \int_{r_s}^{r_a} n(s)ds - \int_{r_s}^{r_a} ds \\ &= \int_{r_s}^{r_a} (n-1)ds \\ &= 10^{-6} \int_{r_s}^{r_a} N ds \end{aligned} \tag{5.7}$$

where

- N - total group refractivity of moist air. Relation between refractivity and index of refraction (n) can be expressed as $(N = (n-1) \times 10^6)$

The refractivity can be divided into hydrostatic (dry) and non-hydrostatic (wet) components of refractivity that contribute to the delay. So, the total delay d can also be expressed as sum

of dry delay and wet delay components.

$$\begin{aligned} d_{total,trop} &= 10^{-6} \int_{r_s}^{r_a} N ds \\ &= 10^{-6} \int_{r_s}^{r_a} N_{dry} ds + 10^{-6} \int_{r_s}^{r_a} N_{wet} ds \end{aligned} \tag{5.8}$$

$$\boxed{d_{total,trop} = d_{dry} + d_{wet}} \tag{5.9}$$

where

- N_{dry} - Dry component of refractivity
- N_{wet} - Wet component of refractivity
- d_{dry} - Zenith hydrostatic/dry delay (ZHD)
- d_{wet} - Zenith wet delay (ZWD)

Since, the fundamental equation is built based on delay in zenith direction, in troposphere delay studies, the term satellite zenith distance (z) is widely used instead of satellite elevation (η). Satellite zenith distance is related to satellite elevation by the expression $z = \frac{\pi}{2} - \eta$. The expression for $d_{total,trop}$ represents the vertical/zenith delay where the delay is considered along the zenith direction (elevation = 90 deg). So this expression, in general, does not apply for zenith other than 90 degrees and is considered simple. However, more accurate expression would be to take into account the exact satellite elevation. The reason is that the delay depends on the distance travelled by the radio signal through the troposphere, which is in turn is a function of satellite zenith distance (z). This is done by projecting the zenith delay along the direction of satellite using mapping functions (m) or obliquity factor. Mapping functions, thus, relate the delay at an arbitrary zenith distance (z) to the zenith delay. So, equations 5.9 can be rewritten as -

$$\boxed{d_{total,trop} = m_d(z) \cdot d_{dry} + m_w(z) \cdot d_{wet}} \tag{5.10}$$

where:

- m_d - dry component mapping function (function of zenith distance)
- m_w - wet component mapping function (function of zenith distance)

In order to more precisely determine the troposphere delay, additional terms called 'troposphere gradients' could be estimated. One of many reasons to estimate gradient parameters is to determine delay more precisely over stations near equator. This is to account for systematic component near equator in the North/South direction due to atmospheric bulge. (Petit and Luzum, 2010) However, one has to decide whether such a priori estimation strategy must be adopted based on the precision requirements. Similar to estimation of zenith delay parameters in orbit determination process, gradient components can also be estimated. Nevertheless, the concept of gradient will be explained here for later adaptation in RINEX processing.

The delay can be modelled further by distinguishing between the azimuthally symmetric and asymmetric delay. Here is the azimuth is measured east from North vector

$$d_{total,trop} = d_{dry,sym} + d_{dry,asym} + d_{wet,sym} + d_{wet,sym} \tag{5.11}$$

where:

- $d_{dry/wet,sym}$ - delay term taking symmetric effect in azimuth into account
- $d_{dry/wet,asym}$ - delay term taking asymmetric effect in azimuth into account

With the help of horizontal tropospheric gradient model, the asymmetric components can be determined The complete equation would be then the improvement of equation 5.10

$$\begin{aligned} d_{total,trop} = m_d(z) \cdot d_{dry} + m_w(z) \cdot d_{wet} + m_{azi,dry}(z) \cdot (G_{n,dry} \cdot \cos(\alpha) + G_{e,dry} \cdot \sin(\alpha)) \\ + m_{azi,wet}(z) \cdot (G_{n,wet} \cdot \cos(\alpha) + G_{e,wet} \cdot \sin(\alpha)) \end{aligned} \tag{5.12}$$

where:

- α - azimuth angle of the signal, measured east of north.
- $m_{azi,dry/wet}(z)$ - Azimuth mapping function for dry/wet component
- $G_{n,dry/wet}$ - North/South gradient for dry/wet component
- $G_{e,dry/wet}$ - East/West gradient for dry/wet component

The three equations 5.9, 5.10, 5.12 represent the tropospheric delay in three successively built models. First is modelled in zenith direction, second takes into account the satellite elevation effect and third takes into account asymmetries in the azimuth in addition to satellite elevation effect. The following sections will briefly explain empirical models that can used to estimate zenith delays and mapping functions present in these equations.

5.3.2 Zenith delay modelling

Hydrostatic delay part of three main equations must be chosen such that they provide most accurate estimate possible. Apriori model implemented in RINEX processing is

- Saastamoinen model (Saastamoinen, 1972)

Saastamoinen model

Saastamoinen Saastamoinen (1972) presented the equation to determine both dry and wet zenith delay. Modified equation by Davis et al. (1985) is given as

$$\begin{aligned} d_{dry} &= \frac{0.0022768 \pm 0.0000005 P_0}{f(\phi, H_s)} \\ f(\phi, H_s) &= 1 - 0.00266 \cos(2\phi) - 2.8 \times 10^{-7} H_s \end{aligned} \tag{5.13}$$

where:

- d_{dry} - Hydrostatic zenith delay (m)
- ϕ - Geodetic latitude of the station (rad)
- H_s - Station height above reference ellipsoid (Geodetic height) (m)
- P_0 - Total atmospheric pressure pressure at the antenna reference point (mbar or hPa) (1 mbar = 1 hPa)
- $f(\phi, H_s)$ - Gravity correction function

The wet zenith delay is given by

$$d_{wet} = 0.0022768\left(\frac{1255}{T_0} + 0.053\right)e_0 \tag{5.14}$$

where:

- e_0 - Partial pressure of water vapour at the ground beacon (mbar or hPa)
- T_0 - Surface temperature in Kelvin

This model is widely popular due to its high accuracy. It has been developed by assuming that dry atmosphere is in hydrostatic equilibrium. The equation for hydrostatic equilibrium follows from the ideal gas laws. Furthermore, gravity acceleration is considered as a function of height and requires only height of station and latitude for gravity correction. An equivalent model from Hopfield which was developed based on similar assumptions was considered in comparison. In this model, gravity was not modelled as a function of height and required surface temperature in addition to pressure for zenith hydrostatic delay estimation.

elgered et.al 1991 studied the RMS error budget and highlights that uncertainty in refractivity constant contributes to 2.4 mm, followed by uncertainities in parameters that were used in deriving the model such as gravity reduction (0.2 mm), universal gas constant (0.1 mm) and dry mean molar mass (0.1 mm). In addition to the above reasons, in Petit and Luzum (2010) hydrostatic delay has been recommended based on Saastamoinen (1972) model. Thus, based on the above discussion and due to superior accuracy, Saastamoinen model has been chosen for estimating the zenith hydrostatic delay during RINEX processing.

With respect to zenith wet delay, Saastamoinen (1972), Taply 1982 studied that error in the equation 5.14 may reach as high 10-20 cm in extreme atmospheric conditions. Furthermore, error in this estimation depends on uncertainty in temperature (T_0) (arising from measurement system) and partial pressure of water vapour (e_0) (arising from model that converts relative humidity to e). Due to these reasons, zenith wet delay estimation using Saastamonien model will not be considered for this thesis.

5.3.3 Empirical troposphere model in RINEX processing

In RINEX file, the pressure, temperature and relative humidity are given in mbar, Celsius and percent respectively. The three measurements are essential for troposphere modelling. However, these measurements are not available at all time due to malfunctioning of the instruments co-located with the beacons. In RINEX data, each of these values may be flagged individually with value 1, which indicates that they are not suitable for analysis. Thus, an approach was developed to consider only the good data from RINEX measurements and use empirical models for the missing information. For example, at some stations only pressure measurements can be used from RINEX, but the temperature and relative humidity may be unusable (flagged in RINEX). In such cases, temperature and relative humidity will be derived from empirical model (such as GPT3).

In the approach developed, three meteorological parameters are considered as one set i.e. P,T,H. Taking into account the missing/invalid cases, we would get 9 possible combinations of

the set. This is shown below.

$$\begin{matrix} \{P, T, H\} \\ \{P, T, H\} \\ \{P, T, H\} \\ \{P, T, H\} \\ \{P, T, H\} \\ \{P, T, H\} \\ \{P, T, H\} \\ \{P, T, H\} \\ \{P, T, H\} \end{matrix} \tag{5.15}$$

The blue colour represents that site measurements are available and red represents that they are unavailable. The different cases, how measurements are derived for each case and their correspondance to V2.2 measurement flag in the field 89 are discussed below

- **Case 1:** All the meteorological parameters are derived from GPT3 empirical model due unavailability of in-situ measurements. This corresponds to V2.2 measurement flag 9.
- **Case 2:** The valid pressure value from the RINEX data is used and the rest are used from GPT3 model. This corresponds to DORIS V2.2 meteorological flag 8.
- **Case 3:** Valid pressure and temperature are used from the RINEX data and humidity is used from GPT3 model. This corresponds to DORIS V2.2 measurement flag 5.
- **Case 4:** Valid temperature is used from RINEX data is used and rest are derived from GPT3 model. This corresponds to V2.2 measurement flag 6.
- **Case 5:** Valid temperature and relative humidity are used from RINEX and the pressure is derived from GPT3 model. This corresponds to the flag 1.
- **Case 6:** Valid relative humidity is used from RINEX and rest are derived from GPT3 model. This corresponds to flag 4.
- **Case 7:** Valid pressure and relative humidity are derived from RINEX and temperature is derived from GPT3 model. This corresponds to flag 3.
- **Case 8:** All the measurements are derived from in-situ measurements and no GPT3 model is used. This corresponds to flag 0.

It is certainly not a recommended choice to rely entirely on empirical model when the in-situ measurements are completely or partially available. This is because empirical models fail to capture the short term variations in the local weather. These variations may not follow the seasonal trend based on which a empirical model is build. In cases when the in-situ temperature and/or relative humidity measurements are available, the quality of empirical models can be improved by a method called site-augmentation. Landskron et al. (2016) shows that there are specific weighing coefficients that relate the empirical values to the in-situ measurements.

5.4 Ionospheric correction

Ionospheric correction needs to be taken into account when modelling the range-rate measurement since the ions have effect over the radio signals (both frequencies) when they travel

through the ionosphere part of the atmosphere. Before formulating the final equations that are used for range rate corrections, it is necessary to understand the

The first order effect of the ionosphere is eliminated by using the combination of phase measurements on the two frequencies (L1 and L2).

The ionospheric combination is given by

Ionospheric correction between two time-tags is computed as

$$\boxed{\dot{IC}_1 = \frac{1}{\Delta T_p}\left(\frac{\lambda_1 \Delta L_1 - \lambda_2 \Delta L_2}{(\gamma - 1)}\right)} \tag{5.16}$$

where

- ΔT_p is the proper time count interval (i.e. 10s in this case) [s]
- $\dot{IC}$ is the ionospheric correction rate formulated to be added to the range rate [m/s]
- λ_1 is the wavelength of frequency 1 [m]
- λ_2 is the wavelength of frequency 2 [m]
- $\Delta L_1 = L_1^{t_2} - L_1^{t_1}$ This is the phase increment in L_1 [cycles]
- $\Delta L_2 = L_2^{t_2} - L_2^{t_1}$ This is the phase increment in L_2 [cycles]
- $\gamma = (\frac{f_1}{f_2})^2$ is the square of the frequency ratio [-]

The above equation corresponds to ionospheric correction based on the combination alone. There is also a geometric correction that needs to be performed since the signals arrive at virtual point called iono-free phase center and not the 2GHz phase center. The geometric correction corresponding to the ionosphere comes from the antenna phase center geometry corrections. The Antenna correction for 2GHz phase center (on-board and ground) and 400 MHz phase center (on-board and ground) is computed as shown in previous section. The expression is given as

$$\dot{IC}_2 = \frac{1}{\Delta T_p}\left(\frac{\Delta d_1 - \Delta d_2}{\gamma - 1}\right) \tag{5.17}$$

where

- $\Delta d_1 = d_{L_1}^{t_2} - d_{L_1}^{t_1}$ is the geometry correction increment in 2GHz phase center [m]
- $\Delta d_2 = d_{L_2}^{t_2} - d_{L_2}^{t_1}$ is the geometry correction increment in 400MHz phase center [m]

Thus, ionospheric correction to the range rate can be formulated as

$$\dot{IC}_{net} = \dot{IC}_1 + \dot{IC}_2 \tag{5.18}$$

5.5 Antenna phase centre modelling

Precise coordinates of DORIS satellites and beacons depend on how accurately the signal path is modelled. Radio signals travel from the phase centre of ground antenna to the phase centre of satellite antenna. A phase centre is an electronic reference point (ERP) or a virtual point where the DORIS observations are acquired. These are not geometrically defined point and are defined virtually based on antenna manufacturer specification. In this thesis, the distance between ARP and Phase centre will be termed as Phase centre offset (PCO). In POD, orbits

must be referred to the centre of mass of satellite and not the phase centre of satellite antenna. Similarly, with respect to the ground segment, observations referring to phase centre cannot be used for geophysical studies and thus need to be referred to a geometrical point of the antenna called conventional reference point or Antenna Reference Point (ARP). Thus, for accurate measurement modelling, it is necessary to make corrections so that DORIS observations can refer to the motion of centre of mass with respect to a ground antenna reference point. This is shown in figure.

DORIS is dual frequency system that uses two frequencies L1 and L2 for observations. For a ground antenna, phase centres for these frequencies are defined at different locations from ARP in local coordinate frame i.e. radio signals arrive at different location from ARP for 2GHz compared to 400MHz. Similarly for on-board antenna, the phase centres of respective frequencies are defined at different locations in the satellite reference frame. These are documented in the technical sheets of the DORIS ground and space segments. In addition to this, in a dual frequency system such as DORIS, when using iono-free combination the signals arrive at a virtual point called iono-free phase centre and not at the 2GHz phase centre. This must be implemented in the RINEX processing or would induce a offset of 25 mm (both on-board and ground) (Lemoine et al., 2016). Contrary to RINEX, 2.2 measurement data contains antenna corrections and ionospheric geometric corrections are computed for 2GHz phase centres. (put reference) Given the phase centres of 2GHz and 400MHz, the user has to compute the iono-free phase centre and take this into account for antenna corrections.

If antenna corrections are neglected, this can induce significant effect in the measurement residuals especially when the satellite is making a high elevation pass over a station. The projection vector of antenna phase centre becomes larger when the elevation is higher causing an offset in the residuals. In addition, in Geodesy, tie vectors (TV) play a important role in the computation of ITRF as they allow to connect and constraint the estimation of geodetic coordinates of the co-location sites. (Tourain et al., 2016). Any mismodelling of PCO will result in anomaly in ITRF coordinate estimation using DORIS observations.

Since phase converted range rate observations are used in this research, antenna corrections in the form of range rate need to be formulated so that they can be conveniently added to range rate observations. For this, we build antenna corrections that is a sum of on-board and ground correction at an arbitrary time t and take increment at same intervals as the DORIS observations (similar to phase conversion of range rate). The final correction will be referred to as ARP-CoM correction in this thesis.

Getting most out of DORIS observations depends on a complete antenna modelling where Phase centre variations (PCV) must be considered that accounts for change in phase center depending on the signal incidence. A signal sent out and reaching the receiver has a specific azimuth and elevation angle with respect to the ground antenna. Hence for a antenna (ground or on-board), the net correction to be made would be PCO + PCV(α,η).

For the space antenna, CNES recommended to assume the PCV to be zero and constant over all azimuth and elevation angles. Concerning the ground antenna, although phase laws were provided in antenna modelling documentation, it was not taken into account in the DORIS contribution to ITRF 2008. After a new study in 2012 aimed to better characterize DORIS antenna, phase law has been recommended to be used in DORIS observations contributing to ITRF 2014 (Tourain et al., 2016). Antenna recommendations by CNES are followed in this thesis for modelling.

As explained in the first paragraph, it is clear that we need to make corrections for both on-board and ground antennas. So, at an arbitrary time t we define corrections at two levels:

1. Ground correction - This corresponds to projection of Antenna reference point to iono-free phase centre ($\boldsymbol{r}_{ARP-Iono}$) vector on the line of sight vector.

2. On-board correction - This corresponds to projection of the Centre of Mass to iono-free phase centre vector ($\boldsymbol{r}_{CoM-Iono}$) on the line of sight vector.

Following sections will explain about the correction at two levels separately followed by a section stating how the total correction is formulated at time t.

5.5.1 Ground correction

DORIS system has two types of ground antenna - (i) Alcatel (ii) Starec. The configuration of antenna are shown in figure 5.1. The type of antenna installed at any specific station can be identified by the fourth letter of beacon mnemonic/station code. The station code is a four letter unique given to a station with 4th letter representing the antenna type present in the station. "A" represents that a Alcatel antenna is installed, while "B" or "C" represents that a Starec antenna is installed. For example, the station code for Toulouse is TLSB which indicates that the antenna installed is a Starec antenna of type B. The difference between B and C Starec antenna is that the latter has less error on 2GHz phase centre position and has a improved manufacturing process (CNES and IDS, 2019). The phase centres and error budget are tabulated in table 5.1. The iono-free phase centre must be calculated by the user and is not provided in the technical documentation of the antennas.

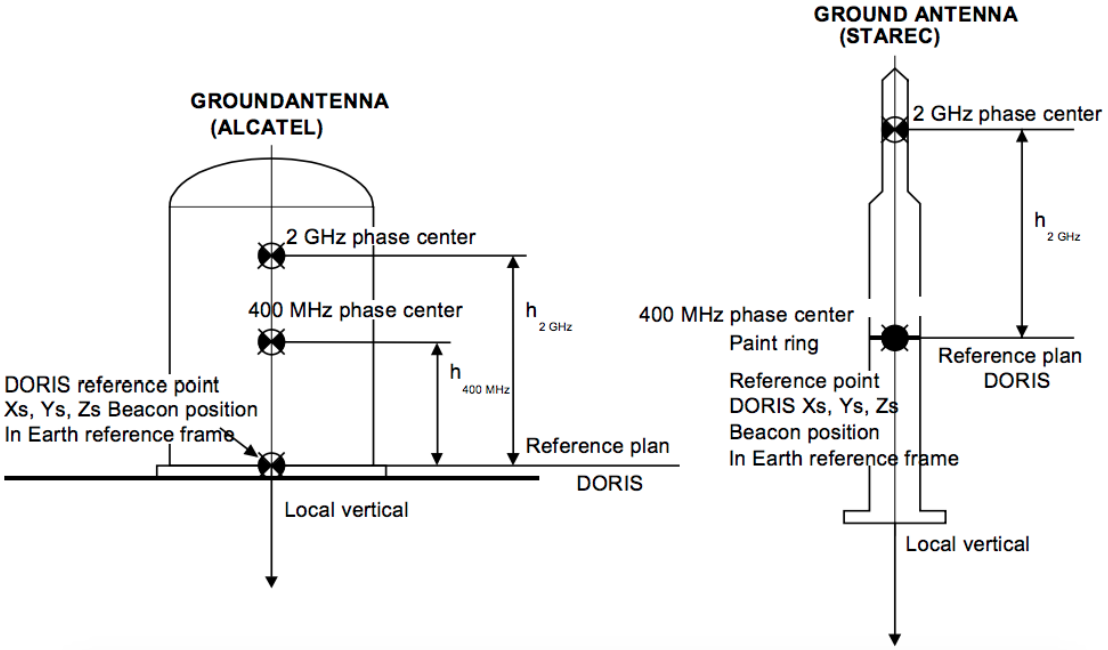

Figure 5.1: DORIS antenna types (IDS, 2019a)

Antenna type	Identification letter	400 MHz ($\boldsymbol{r}_{arp-400MHz}$)	2 GHz ($\boldsymbol{r}_{arp-2GHz}$)	Iono-free ($\boldsymbol{r}_{arp-iono}$)	Error (for 2GHz in up direction)
Alcatel	A	335	510	517	N/A
Starec	B	0	487	506	max +6/-8
Starec	C	0	487	506	max +/- 3

Table 5.1: Phase center and error budget for antenna. Iono-free phase centres are computed from L1 and L2 phase centre vectors. All units are in mm. (CNES and IDS, 2019)

We use 2GHz and 400 MHz phase centre for ionospheric geometry correction and iono-free phase centre for ARP-CoM correction. It is also important to take into account phase centre variation of the antenna.

Phase law for ground antenna

A phase centre is the centre of iso-phase surface of electromagnetic field expansion from an antenna. (Tourain et al., 2016) In ideal conditions, iso-phase surface is spherical surface. An actual surface, however, is not a sphere but a deformed spherical shape as shown in figure 5.2.

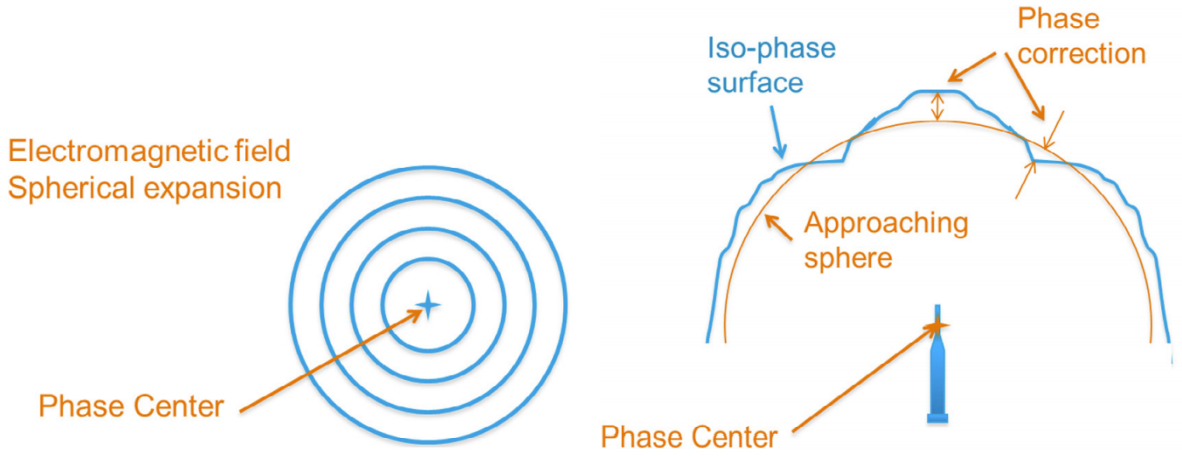

Figure 5.2: Left figure shows the ideal electromagnetic field expansion. Right figure shows the phase correction and its associated phase center (Tourain et al., 2016)

This deformed shape could be approximated by a sphere such that the surfaces of perfect sphere are close to surfaces of deformed sphere. Since a sphere is a 3D surface, this approximated surface is defined at elevations between 0 to 90 and for all azimuths. The centre of the approximated sphere is then the phase centre of an antenna and the gap between the approximated sphere and the deformed sphere in a particular direction (α,η) is the associated phase correction. In simple words, phase corrections are made to correct the deformed spherical surface fo spherical surface at a specific signal incident angle. For DORIS, phase correction/phase law was estimated for Starec and Alcatel antenna based on anechoic chamber experiments performed at the Compact Antenna Test Range (CATR) facility in the CNES. In the experiment a phase is measured for the specified phase centre position given by IDS. Phase corrections are then formulated to get to the theoretical iso-phase surface. In other words, corrections are added to the observations to get to the theoretical sphere and corrections are subtracted from the theoretical value to get the actual iso-phase sphere surface. Finally, a phase law model was computed by averaging different experimental phase law results obtained in CATR and has been provided in the ANTEX (ANTenna EXchange format) as a function of zenith angle. The phase correction is given at 5 degree interval from 0 to 90 degree zenith angle. To compute the net effect, the phase correction needs to be added to 2 GHz or 400 MHz phase centre. The phase law for both antennas are shown below. Linear and spline interpolation at random elevation angles are made to show the effect of interpolation.

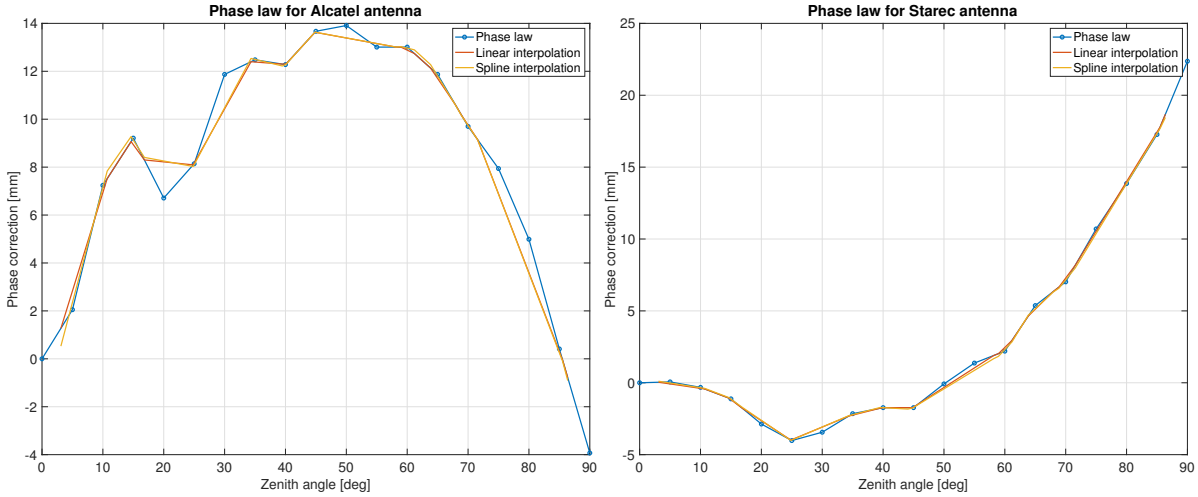

Figure 5.3: Phase laws for Alcatel and Starec DORIS antennas. X-axis represents the zenith angle in degrees and Y-axis represents the phase correction in up direction defined in local antenna frame. This value is to be added to the phase centre offset (PCO) (CNES and IDS, 2019)

In RINEX processing, linear interpolation is used to retrieve $\boldsymbol{r}^{pcv}_{arp-2GHz}$ and $\boldsymbol{r}^{pcv}_{arp-400MHz}$ at specified elevation angles. Following this, the net phase centre for L1 and L2 can then be written as

$$\begin{aligned} \boldsymbol{r}_{arp-2GHz} &= \boldsymbol{r}^{pco}_{arp-2GHz} + \boldsymbol{r}^{pcv}_{arp-2GHz} \\ \boldsymbol{r}_{arp-400MHz} &= \boldsymbol{r}^{pco}_{arp-400MHz} + \boldsymbol{r}^{pcv}_{arp-400MHz} \end{aligned} \tag{5.19}$$

For Iono-free phase centre computation, first we compute the vector $\boldsymbol{r}_{2GHz-iono}$

$$\boldsymbol{r}_{2GHz-iono} = \frac{\boldsymbol{r}_{400MHz-2GHz}}{\gamma - 1} \tag{5.20}$$

and add this to $\boldsymbol{r}_{arp-2GHz}$ to get the $\boldsymbol{r}_{arp-iono}$

$$\boldsymbol{r}_{arp-iono} = \boldsymbol{r}_{arp-2GHz} + \boldsymbol{r}_{2GHz-iono} \tag{5.21}$$

For convenience we present a new vector notation $\boldsymbol{r}^{enu}_{ant}$ that refers to either 2GHz (equation 5.22) or 400MHz (equation 5.23) or iono-free correction (equation 5.24) based on the context.

$$\boldsymbol{r}^{enu}_{ant} = \boldsymbol{r}_{arp-2GHz} \tag{5.22}$$

$$\boldsymbol{r}^{enu}_{ant} = \boldsymbol{r}_{arp-400MHz} \tag{5.23}$$

$$\boldsymbol{r}^{enu}_{ant} = \boldsymbol{r}_{arp-iono} \tag{5.24}$$

The above mentioned coordinates are specified in ENU frame which is a local geodetic coordinate system. The coordinates of the satellite or the line of sight vector is also represented in local coordinate system, but in x, y, z coordinates. A transformation of antenna vector in ENU frame to a vector in local Cartesian coordinate system is necessary in order to project the vector on the line of sight vector.

$$\boldsymbol{r}^{trt}_{ant} = (\boldsymbol{T}^{trt}_{enu})^T \cdot \boldsymbol{r}^{enu}_{ant} \tag{5.25}$$

The projection of $\boldsymbol{r}^{trt}_{ant}$ on $\boldsymbol{r}^{trt}_{los}$ is computed using dot product (see Figure 5.4). A dot product

between two vectors $\boldsymbol{a}$ and $\boldsymbol{b}$ can be written as

$$\boldsymbol{a} \cdot \boldsymbol{b} = |\boldsymbol{a}||\boldsymbol{b}| \cos(\theta) \tag{5.26}$$

The projection length of $\boldsymbol{b}$ on $\boldsymbol{a}$ can be written as

$$|\boldsymbol{a}| \cos(\theta) = \frac{\boldsymbol{a} \cdot \boldsymbol{b}}{|\boldsymbol{b}|} \tag{5.27}$$

Thus length of projection of 2GHz, 400MHz and iono-free phase centre vector on line of sight vector can be computed using the equation below provided $\boldsymbol{r}_{ant}^{enu}$ must refer to either 2GHz, 400MHz or iono-free phase centre based on the .

$$d_{L1} \equiv d_{L2} \equiv d_{iono} = \frac{\boldsymbol{r}_{ant}^{trt} \cdot \boldsymbol{r}_{los}^{trt}}{|\boldsymbol{r}_{los}^{trt}|} \tag{5.28}$$

where

- d_{L1}^{g} is the 2 GHz geometric phase centre correction for ground antenna
- d_{L2}^{g} is the 400 MHz geometric phase centre correction for ground antenna
- $d_{iono-free}^{g}$ is the iono-free geometric phase centre correction for ground antenna

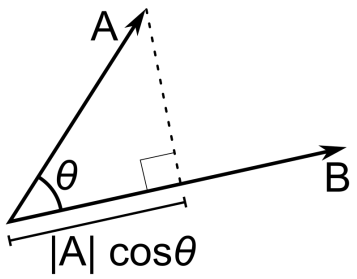

Figure 5.4: Vector dot product Source: Wikipedia

Now the objective is to compute the vector projection $\boldsymbol{r}_{ant}^{ecef}$

5.5.2 On-board correction

For CryoSat-2 the phase centre for 2GHz and 400MHz are

All units in m	X	Y	Z
Centre of Mass (Initial)	1.6312	0.0112	0.0137
L1 (2GHz)	1.848	-0.200	-0.751
L2 (400MHz)	1.832	-0.200	-0.598

Table 5.2: Coordinates given in satellite reference frame (IDS, 2015)

Using vector algebra, the phase centre coordinates with respect to centre of mass can be written as

$$\begin{aligned} \boldsymbol{r}_{CoM-2GHz} &= \boldsymbol{r}_{2GHz} - (\boldsymbol{r}_{CoM} + \Delta\boldsymbol{r}_{CoM}) \\ \boldsymbol{r}_{CoM-400MHz} &= \boldsymbol{r}_{400MHz} - (\boldsymbol{r}_{CoM} + \Delta\boldsymbol{r}_{CoM}) \end{aligned} \tag{5.29}$$

where

- $\boldsymbol{r}_{CoM-2GHz}$ is the boldsymboltor from Centre of mass to 2 GHz phase centre.
- $\boldsymbol{r}_{CoM-400MHz}$ is the vector from Centre of mass to 400 MHz phase centre.
- $\boldsymbol{r}_{CoM}$ is the vector form origin to centre of mass
- $\boldsymbol{r}_{2GHz}$ is the vector from origin to 2 GHz phase centre
- $\boldsymbol{r}_{400MHz}$ is the vector from origin to 400 MHz phase centre
- $\Delta\boldsymbol{r}_{CoM}$ Change in centre of mass from initial centre of mass (during launch)

Iono-free phase centre is computed as

$$\boldsymbol{r}_{2GHz-iono} = \frac{\boldsymbol{r}_{400MHz-2GHz}}{\gamma - 1} \tag{5.30}$$

where

- $\boldsymbol{r}_{2GHz-iono}$ is the vector from 2GHz to Iono-free phase centre.
- $\boldsymbol{r}_{400MHz-2GHz}$ is the vector from 400 MHz to 2 GHz phase centre

The $\boldsymbol{r}_{400MHz-2GHz}$ vector can be computed using the information in above table as

$$\boldsymbol{r}_{400MHz-2GHz} = \boldsymbol{r}_{2GHz} - \boldsymbol{r}_{400MHz} \tag{5.31}$$

The $\boldsymbol{r}_{CoM-iono}$ can then be computed as

$$\boldsymbol{r}_{CoM-iono} = \boldsymbol{r}_{2GHz} + \boldsymbol{r}_{2GHz-iono} \tag{5.32}$$

The evolution of centre of mass of CryoSat-2 with only a slight variation in x-axis of centre of mass. Due to this slow evolution, The values used in the RINEX processor are tabulated below.

All units in m	**X**	**Y**	**Z**	**Magnitude**
Centre of Mass	1.6322	0.0112	0.0137	1.6312
L1 (CoM-2GHz)	0.2158	-0.2112	-0.7647	2.0047
L2 (CoM-400MHz)	0.1998	-0.2112	-0.6117	1.9374
(400MHz-2GHz)	0.016	0	-0.153	0.1538
2GHz-iono	6.4637e-4	0	-0.0061	0.0062
CoM-iono	0.2164	-0.2112	-0.7708	0.8280

Table 5.3: Computed coordinates given in satellite reference frame.

The $\boldsymbol{r}_{CoM-2GHz}$, $\boldsymbol{r}_{CoM-400MHz}$ and $\boldsymbol{r}_{CoM-iono}$ are used in the data processing for the bringing the measurements from respective phase centers to the center of mass. Since the vectors are now defined in satellite reference frame, transformation to appropriate reference frame is required to realize the center of mass corrections to be added to the range-rate.

Two local orbit reference frames will be used for this purpose, one is PRY reference frame and RTN reference frame. Both of them are instantaneous reference frame i.e. they are time-varying. A local orbit frame (PRY) is defined by the unit vectors - Pitch $(\boldsymbol{e}_p)$, Roll $(\boldsymbol{e}_r)$ and Yaw $(\boldsymbol{e}_y)$ with origin in the centre of mass of the satellite. Another local orbit frame (RTN) is defined by the unit vectors given as follows

- $\boldsymbol{e}_r$ unit vector directed from geocenter to center of mass of satellite (Radial)

- $\boldsymbol{e}_t$ unit vector directed in the flight direction of the satellite (Along-track)
- $\boldsymbol{e}_n$ unit vector completes the right handed coordinate system (Cross-track)

Firstly, the vector $\boldsymbol{r}_{CoM-iono}$ defined in satellite reference frame is transformed to Pitch, Roll and Yaw (PRY) reference frame. CryoSat-2 satellite flies with a 6 deg pitch as the nominal mode i.e the body frame is inclined at 6 deg with respect to the flight frame. The transformation matrix is given as

$$\boldsymbol{T}_{pry}^{srf} = \begin{bmatrix} 0 & -1 & 0 \\ \cos(6) & 0 & \sin(6) \\ -\sin(6) & 0 & \cos(6) \end{bmatrix} \tag{5.33}$$

Secondly, we transform the above obtained vector in PRY frame to RTN frame. For CryoSat-2 the relation between PRY and RTN reference are given as

$$\begin{bmatrix} \boldsymbol{e}_p \\ \boldsymbol{e}_r \\ \boldsymbol{e}_y \end{bmatrix} = \begin{bmatrix} -\boldsymbol{e}_n \\ \boldsymbol{e}_t \\ \boldsymbol{e}_r \end{bmatrix} \tag{5.34}$$

Using the above relation, we can transform the $\boldsymbol{r}_{ant}^{pry}$ to $\boldsymbol{r}_{ant}^{rtn}$. Now, vector $\boldsymbol{r}_{ant}^{rtn}$ must be transformed to a reference frame in which the line of sight vector is defined so that we can project $\boldsymbol{r}_{ant}^{rtn}$ vector on the line of sight vector $\boldsymbol{r}_{los}^{rtn}$.

We set-up and compute a transformation matrix for transforming $\boldsymbol{r}_{ant}^{rtn}$ to $\boldsymbol{r}_{ant}^{ecef}$. Using the satellite position vector $\boldsymbol{r}$ and velocity vector $\boldsymbol{v}$, the unit vectors of RTN frame are formulated as

$$\boldsymbol{e}_r = \frac{\boldsymbol{r}}{|\boldsymbol{r}|} \tag{5.35}$$

$$\boldsymbol{e}_t = \frac{\boldsymbol{v}}{|\boldsymbol{v}|} \tag{5.36}$$

$$\boldsymbol{e}_n = \frac{\boldsymbol{r} \times \boldsymbol{v}}{|\boldsymbol{r} \times \boldsymbol{v}|} \tag{5.37}$$

The transformation matrix to transform from coordinates in RTN frame to the frame in which line of sight vector is defined is given as

$$\boldsymbol{T}_{ecef}^{rtn} = \begin{bmatrix} \boldsymbol{e}_r & \boldsymbol{e}_t & \boldsymbol{e}_n \end{bmatrix} \tag{5.38}$$

Following this, one can write

$$\boldsymbol{r}_{ant}^{ecef} = \boldsymbol{T}_{ecef}^{rtn} \boldsymbol{r}_{ant}^{rtn} \tag{5.39}$$

Using the transformed vector we compute the projection on the line of sight vector using scalar dot product. Shapiro delay has not been taken into account due to the fact that this has negligible effect on the antenna phase correction. Later it will be shown that quality of orbit only makes a minute difference The reason is simple enough to understand that Effect of projection of a antenna vector (order of less than a meter) on a vector that is thousand kilometres does not induce much error. Comparing TLE and NAV we observed a slight change in antenna correction over a pass with maximum value difference of 0.005 mm/s. This is the reason why the light time correction has been neglected for this correction.

5.5.3 Total antenna phase centre correction

With the ground correction and on-board correction formulated separately, we can now write the total correction for L1, L2 and iono-free phase centre at arbitrary time t as

$$d_{L1} = d^g_{L1} + d^s_{L1} \tag{5.40}$$

$$d_{L2} = d^g_{L2} + d^s_{L2} \tag{5.41}$$

$$d_{iono-free} = d^g_{iono-free} + d^s_{iono-free} \tag{5.42}$$

5.6 Measurement editing criteria

As the RINEX are not completely processed, they contain phase measurements as received by the receiver. These measurements cannot be used for range rate computation and would lead to a erroneous value. In order to remove such phase measurements, first level filtering consists of reading the measurement flags present in RINEX file. The measurement flags indicate whether it is suitable for further processing. There are different flag used for variety of measurements.

As explained previously, there are 10 measurements for every station -

1. 2GHz phase
2. 400 MHz phase
3. 2GHz pseudo range
4. 400 MHz pseudo range
5. 2 GHz received power level
6. 400 MHz received power level
7. Relative frequency offset of the on-board oscillator $\left(\frac{\Delta f_r}{f_{rN}}\right)$
8. Pressure
9. Temperature
10. Humidity

In RINEX format, a flag indicated close to the measurement value. The flags for every measurement is discussed below using a data from RINEX file.

L1 & L2 phase data

L1 and L2 data in RINEX are given as -

$$\boxed{\cdot\cdot -3983418.797 f_{11} f_{12}} \tag{5.43}$$

$$\boxed{\cdot\cdot -4152750.836 f_{21} f_{22}} \tag{5.44}$$

The first field $\cdot\cdot -3983418.797$ represents the L1 phase data, which is of format F14.3. The dots represent the spaces. L1 phase data is followed by 2 flags - f_{11} followed by f_{12} of 1 character

length each. This also applies to the L2 phase data whose flags are designated as f_{21} and f_{22} respectively.
The first flag on both phase data (f_{11} and f_{21}) can carry following values

1. Value is '1' if it is a central frequency measurement.
2. Value is blank if it okay for further processing.

The second flag on both phase data(f_{12} and f_{22}) can carry following values

1. Value is a (i) LL1 (Loss of lock indicator) or (ii) 0 if there is a continuity.
2. Value is blank if it okay for further processing.
3. Value is 1 if there is a discontinuity or cycle slip possible.

In RINEX processing implementation, we do not use the measurements that are indicated as central frequency measurements (indicated as 1 in f_{11} and f_{21}) and the measurements that can have discontinuity/cycle slip (indicated as 1 in f_{12} and f_{22}).

C1 & C2 pseudo range data

C1 and C2 data in RINEX are given as -

$$\boxed{29659030.977 f_{31} f_{32}} \tag{5.45}$$

$$\boxed{29659615.555 f_{41} f_{42}} \tag{5.46}$$

The first flag on both pseudo range (f_{31} and f_{41}) can carry following values

1. Value is '0' if the measurement is valid for time reference usage.
2. Value is '1' if it okay for further processing.

The second flag on both phase data(f_{32} and f_{42}) can carry following values

1. Any number in this field represents the processing unit (UT) number in which the measurement was carried out. The DGXX receiver is capable of measuring from seven stations simultaneously. So this number indicates which processing unit/channel was used for measuring.

In RINEX processing implementation, we consider only the pseudo range measurements that are valid for time synchronization calculation (indicated as 1 in f_{31} and f_{41}).

W1 & W2 power level data

W1 and W2 represent the power level received on the L1 and L2 frequency in dBm.

The power levels on two frequency in RINEX are given as -

$$\boxed{\cdots\cdots -116.250 f_{51} f_{52}} \tag{5.47}$$

$$\boxed{\cdots\cdots -108.200 f_{61} f_{62}} \tag{5.48}$$

The first flag on both power levels (f_{51} and f_{61}) can carry following values

1. Value is '1' if the station/beacon is on restart mode.
2. Value is blank if it is can be considered for further processing.

The second flag on both power levels (f_{52} and f_{62}) can carry following values

1. Values is in the range [0-7] if the station is in warming period.
2. Value is blank if it is can be considered for processing.

In RINEX processing implementation, we do not use the measurements that are measured when the station is on restart mode (indicated as 1 in f_{51} and f_{61}).

F Relative frequency data

An example data is shown below

$$\boxed{\cdots\cdots\cdot 79.217 f_{71} f_{72}} \tag{5.49}$$

Currently, the flags f_{71},f_{72} are not used for any purpose and are thus left blank. We don't use any information from these flags in our RINEX processing.

P, T & H meteorological data

These are meteorological measurements taken at station site and an example data is given below

$$\boxed{\cdots\cdots\cdot 985.000 f_{81} f_{82}} \tag{5.50}$$

$$\boxed{\cdots\cdots\cdot 5.945 f_{91} f_{92}} \tag{5.51}$$

$$\boxed{\cdots\cdots\cdot 78.110 f_{101} f_{102}} \tag{5.52}$$

The first flags (i.e. f_{81},f_{91} and f_{101}) are not used for any purpose and so they appear blank. The second flags on P,T,H (i.e. f_{82},f_{92} and f_{102}) can carry the following values

- Value is '1' if it is invalid measurement.
- Value is '0' if it is a valid measurement.

To summarize, the filtering of phase measurements and pseudo range measurements are done using the flags indicated in the RINEX data. The criteria for neglecting the measurement are as follows

- A Central frequency measurement
- Station on restart mode
- Discontinuity/cycle clip
- Valid meteorological information (individually on P,T,H)

5.6.1 Sigma clipping

Sigma clipping is defined as way to avoid the effect of outliers in the measurements. The method is simple iterative method, where outliers are removed in each iteration.

1. Calculate the standard deviation (σ) and median (m) of a distribution
2. Remove all points that are smaller or larger than $m \pm \alpha\sigma$. α is the number of iterations.
3. Go back to step 1, unless the selected exit criteria is reached

Exit criteria

1. When certain number of iterations has been completed (or)
2. When new measured σ_{new} is within a tolerance limit of the old one σ_{old}. The standard deviation is used because it is heavily influenced by the presence of outliers. Tolerance defined by:

$$\frac{\sigma_{old} - \sigma_{new}}{\sigma_{new}} \tag{5.53}$$

Sigma clipping median was used since it is a more robust statistical measure. Sigma clipping is implemented in two levels in the preprocessor. In the first level, the sigma clipping is first performed separately on negative range rate and positive range rate of an arbitrary pass. In the second level it is performed over a whole pass.

Chapter 6

Processing results

It is imperative to study the processing results and compare them with V2.2 in the form of observation residuals. Observation residuals/tracking residuals are main measure to assess the quality of the orbit determination process. With two observation data available - V2.2 and RINEX processed range-rate, we compute the tracking residuals individually and compare them. In this way, we can answer how far RINEX processing varies with V2.2.

For this study, V43 run performed by Schrama (2018) will be used as benchmark. V43 is a CryoSat-2 precise orbit solution that uses a certain configuration for dynamical models. The models used in this analysis are given below. For other POD solutions refer to Schrama (2018) We also need to study how variation in parameters (see Table 6.2) can affect the observation residuals and by how much. This allows the verification of preliminary conclusions we made. The RINEX processor has been built such that these parameters can be varied by the user at front-end. Thus we process the RINEX data for longer time series and vary the parameters to study the results. For this purpose a test set-up has been built with each test representing a variation. As we move forward in the line-up of tests, we conclude a best setting based on the outcome of previous test. Once we test all the variations we arrive at a stage with a best setting for data processing using RINEX. We start testing the variations in time tagging model first, since this is of utmost importance. The next stage in the order of importance (based on magnitude) is the troposphere models followed by data editing.

Setting	**Details**
Orbit	Navigator
Master beacon	Toulouse
Polynomial	10 days, 3 deg
Troposphere	Discrete, VMF3, Gradients
Phase law	Yes (for ground)
Iono free phase center	Yes

Table 6.2: Preliminary conclusions table. Based on literature and testing performed internally, we formulate a preliminary conclusion to start our processing tests.

6.1 Test-setup

The order in which we change the variations of parameter is based on the importance of the variation. The rationale behind the order in table 6.3 is that the effect of initial orbit is assumed to be important, however it is not entirely sure at this point if this true considering the fact that

	Details/Models	Remarks	
Software	GEODYN-II	Rowlands et al. (1993)	
Satellite	CryoSat-2		
Arc length	≈ 6 day with ≈ 1 day overlap		
Manoeuvres	Orbit and attitude manoeuvres not taken into account		
Reference system			
Precission & Nutation	IERS Convention 2010	Petit and Luzum (2010)	
Polar motion, Length of the day	EOP 14 C04 series	IERS (2017)	
Station coordinates & Velocity	ITRF2014	Willis et al. (2010)	
Displacement of reference			
Ocean tides	IERS Convention 2010	Petit and Luzum (2010)	
Ocean loading	FES2014	Chalmers (2017)	
Satellite reference			
Mass and centre of gravity	IDS 2017	Willis et al. (2010)	
Antenna vectors	IDS 2017	Willis et al. (2010)	
Attitude	Quaternions	ESA (2017)	
External orbits	Navigator orbits	ESA (2017)	
Gravity			
Static gravity field	EIGEN 5C	Förste et al. (2008)	
Temporal gravity	GSM + GAC	Schrama et al. (2014)	
Reference ellipsoid parameters	IERS Convention 2010	Petit and Luzum (2010)	
Planetary constants	IERS Convention 2010	Petit and Luzum (2010)	
Planetary ephermeris	DE200/LE200	Standish Jr (1982)	
Surface forces and empiricals			
SRP model (panel properties)	IDS 2017	Willis et al. (2010)	
Atmospheric density	MSIS	Hedin (1987)	
Albedo		Knocke et al. (1988)	
Solar flux	F10.7	NOAA (2017)	
Geomagnetic field constants	Ap and Kp	GFZ (2017)	
Measurements			
SLR	CRD	ILRS (2017)	
10s Doppler data	V2.2	Willis et al. (2010)	
Elevation cut off	10 degrees		
Weight	0.4 mm/s for DORIS 30 mm for SLR		
Reduced parameters/Adjustments	**Details**	**Frequency**	**Constraint**
Initial state vector	Postion & Velocity	per arc	No
Drag model	Scaling constant	3 hours	Yes
SRP model	Scaling constant	Once	Yes
Empirical acclerations	Along track & Cross track (Cosine and Sine terms)	6 hours	Yes
Beacon offset	Frequency offset of beacons	per pass	No
Zenith delay	Range delay	per pass	No
Station coordinates	Added and adjusted if missing in reference system	per arc	Yes

Table 6.1: Version 43 run configuration by Schrama (2018)

Relevance	Test	Details	Period of testing	Remark
Time tagging solution	T01	Initial orbit testing	Monthly	R.Q. (4)
	T02	Number of days for polynomial adjustment	Monthly	
	T03	Polynomial degree 2	Monthly	
	T04	Master beacons	Monthly	R.Q. (2)
	T05	GEODYN orbit iterative approach	Weekly	R.Q. (3)
	T06	Comparison of time-tagging solution with PANDOR and DIODE	Monthly	R.Q. (1)
Troposphere	T07	Comparison of Discrete and Empirical troposphere model with V2.2	Yearly	R.Q. (6)
Editing	T08	Data editing - Sigma clipping	Monthly	R.Q. (7)
	T09	Best setting	Yearly	M.R.Q

Table 6.3: Test setup table. Note: R.Q. stands for Research question and M.R.Q stands for Main research question

pseudo range contains high measurement noise. Despite the noise, accurate orbits may also get us to the true on-board clock offset. Not to forget, we also use orbits to build corrections for troposphere and antenna phase centre, which imparts importance on fixing a standard A-priori orbit before moving to next tests. Once we conclude on the initial orbit to be used, we test if number of days to fit in a polynomial in order to capture the long term drift for the on-board clock. We then proceed to make conclusion on whether a 2 deg or 3 deg polynomial is suitable. We test the iterative procedure of computing orbits and injecting them in our processor to see if the time tagging polynomial could be improved. Once the properties of the time-tagging model is fixed, we test our solution with PANDOR solution and DIODE solution and study the residuals.

A yearly period of testing has been chosen for troposphere in order study the comparative performance of empirical model and discrete models. 2016 has been chosen since both PANDOR and DIODE files are available during this period that will comparison of the clock model in *RX2RR* to the PANDOR and DIODE solutions. A yearly testing would also further reveal the following effects in the residuals and hence the performance of *RX2RR* processor to

- Effect of yaw steering mode or attitude manoeuvres of Cryosat-2 on the antenna phase center corrections
- Station beacon changes
- Seasonal variation translated as tropospheric delay
- Long term frequency drift of the oscillator (SAA effect)

Since these effects would be evident in a yearly observation residual and possibly repeat in the next subsequent year, only a year of analysis has been chosen for testing the performance of *RX2RR* processor.

6.1.1 Test T01 - Effect of preliminary orbit on observation residuals

In test 1, we study the effect of initial/apriori orbit used for clock model on the time synchronisation and subsequently on the tracking residuals.

With availability of precise orbits, it is certainly possible to take them into account in the time-synchronisation. But the purpose of this test is to check how far the orbit quality used for clock modelling has influence on the residuals and to distinguish clock modelling error. For clock modelling, we need to look at the quality of two elements - (i) Pseudo range and (ii) Orbit quality. Pseudo range measurements C1 and C2 from DORIS have noise of ∼5km and ∼1km respectively (IDS, 2019b). Accuracy of 1 mm in phase modelling corresponds to $10^{-7}s$ in time-tagging (Mercier et al., 2010). Although we don't perform phase modelling, this can be considered applicable for Doppler like processing. In order to reach a precision better than 10^{-7}s one needs to have orbits of at least 30 metres accuracy in addition to the pseudo range noise (∼1km) contributing to $3 \times 10^{-6}s$. Following this discussion, we fix the precision required in clock offset as 10^{-7}s for this test. The test is performed using C1 pseudo range data (noise ∼5km) that are flagged suitable for time synchronisation. The test span is for period of three months from January to March 2016. Other parameters in table 6.2 except orbit are maintained constant.

In order to see the effect of orbit quality on tracking residuals, three POD runs are performed - (i) V2.2 (benchmark) (ii) RINEX using TLE orbit and (iii) RINEX using Navigator orbits. First POD run uses V2.2 data (time-tag present in the data), second POD run uses the RINEX measurements processed with TLE time solution and the third POD run uses RINEX measurements processed with Navigator time solution. Figure 6.4 shows the residuals from three POD runs. Clearly, no significant change is observed in the residuals between TLE and Navigator orbits. A very small increase in residuals is observed for measurements processed using TLE orbit, but this has insignificant effect in the POD problem. The observed difference between V2.2 and RINEX (Navigator) is a net effect of multiple factors, which will be discussed later in detail.

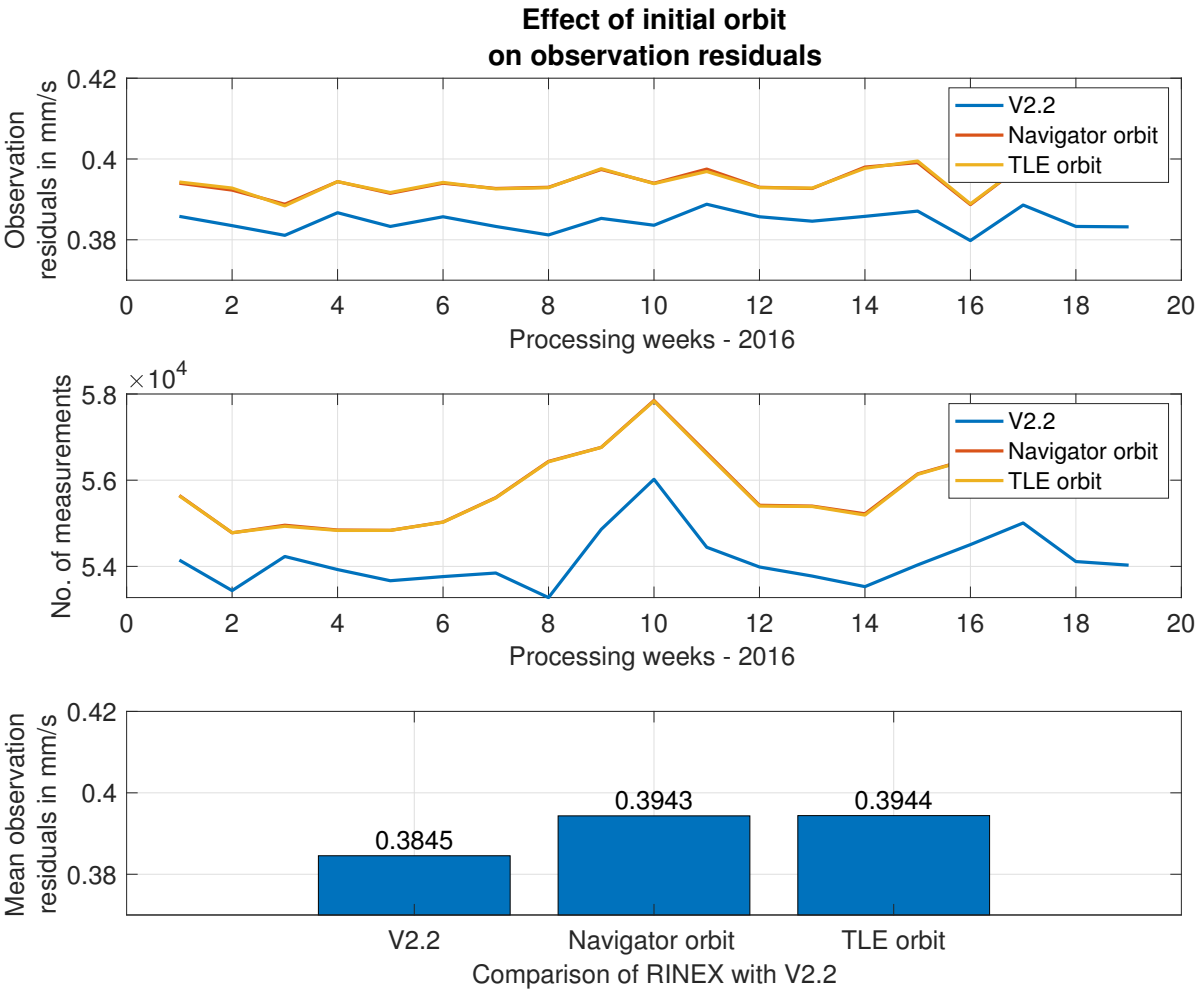

Figure 6.1

In order to see effect of orbit error on clock model, we compute the difference between the time-tagging solution obtained by using Navigator orbit and TLE orbit. This is shown in figure 6.2. An arc represents a 10 day time-interval over which a new clock model is estimated. If the time interval does not match with period specified *RX2RR* estimates a new clock model for the remaining number of days. The trend that is seen is due to the propagation errors Oscillations observed are a direct translation of propagation errors in the time solutions. With figure 6.4 and 6.2, we can conclude that the error imparted by the orbit in time solution is not significant enough to change the tracking residuals. Thus orbit quality is not an issue for clock as long as the error in orbit is of the order of TLE orbits. It is possible that orbit induces minor error in the computation of troposphere elevation and antenna correction during RINEX processing, thus we need to distinguish time error.

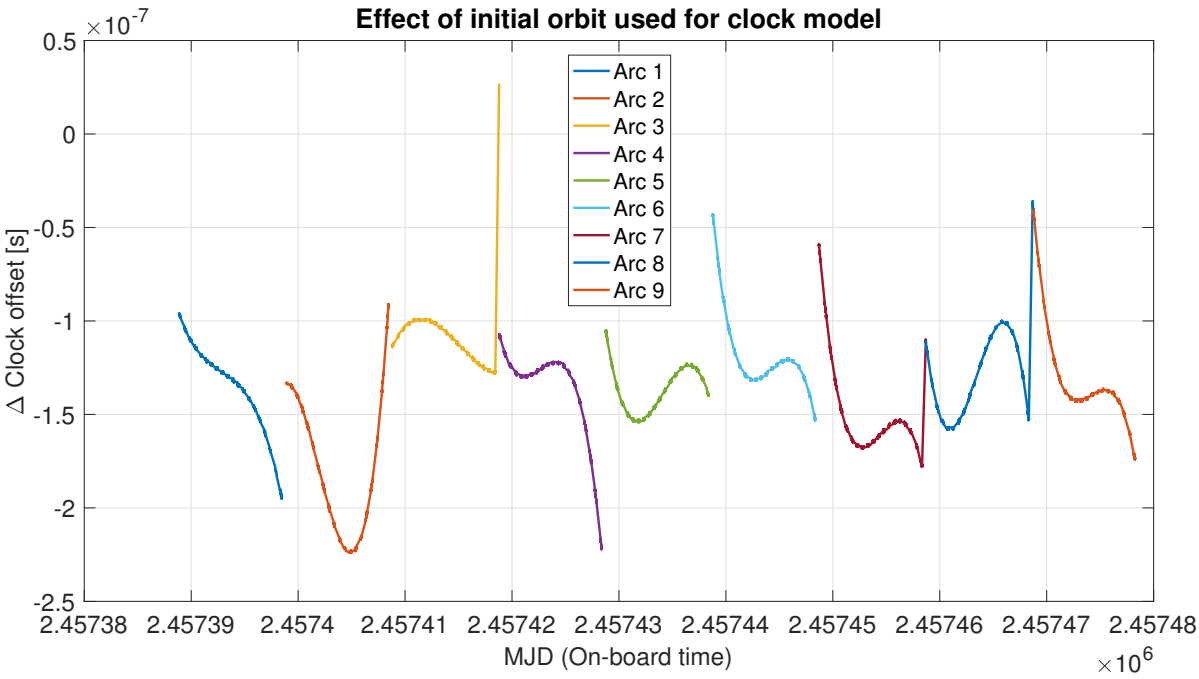

Figure 6.2: The plot shows the difference between clock offsets estimated from TLE orbits and Navigator orbits over a period of three months from January to Match 2016. This plot shows the effect of orbit error on the clock modelling.

In order to distinguish the time-tagging error from other error sources such as from troposphere and antenna corrections, we look at the uncertainty in the estimated clock model. This also determines the quality of our clock model. This is shown in figure 6.3. As discussed earlier, we need at least a precision of 10^{-7}s in the time-tags, which is achieved. in order to achieve 1mm precision in the phase. Assuming negligible error in Toulouse master beacon, the error observed in figure 6.3 is a combination of (i) C1 pseudo range measurement noise (ii) Orbit modelling error (iii) relativistic offset in clock drift (iv) relativistic periodic terms (v) possible SAA induced effect on oscillator. The C1 pseudo range measurement noise is not modelled here and so cannot be improved. Keeping C1 noise constant, the orbit quality doesn't seem to improve the clock model as shown earlier. So, precision shown in figure 6.3 is affected by combination of (iii), (iv) and (v). These 3 effects are absorbed in the polynomial estimated. In this thesis, we do not model the relativistic frequency drift component. This is not negligible and should be included. Effects (iv) and (v) represent short-period effects affecting the oscillator. These effects are also not taken into account during clock modelling since (iv) is negligible for POD and reception time tagging and (v) due to modelling challenges. The periodic relativistic effect is negligible compared to the microsecond accuracy provided by pseudo range. They are however important when station positions are estimated. But this is out of scope of this thesis. It is suspected that effect (v) is visible in the arc 3 in figure 6.3 indicated by increase in uncertainty. This has been verified with error in clock polynomial drift term and and clearly shows an increase as shown in table 6.4. Our model fails to capture local clock drift induced by frequency changes over SAA and thus there is a increase in uncertainty in clock drift component. To conclude, it is necessary to keep in mind that theses three effects are neglected and must be taken into account for more accurate clock modelling.

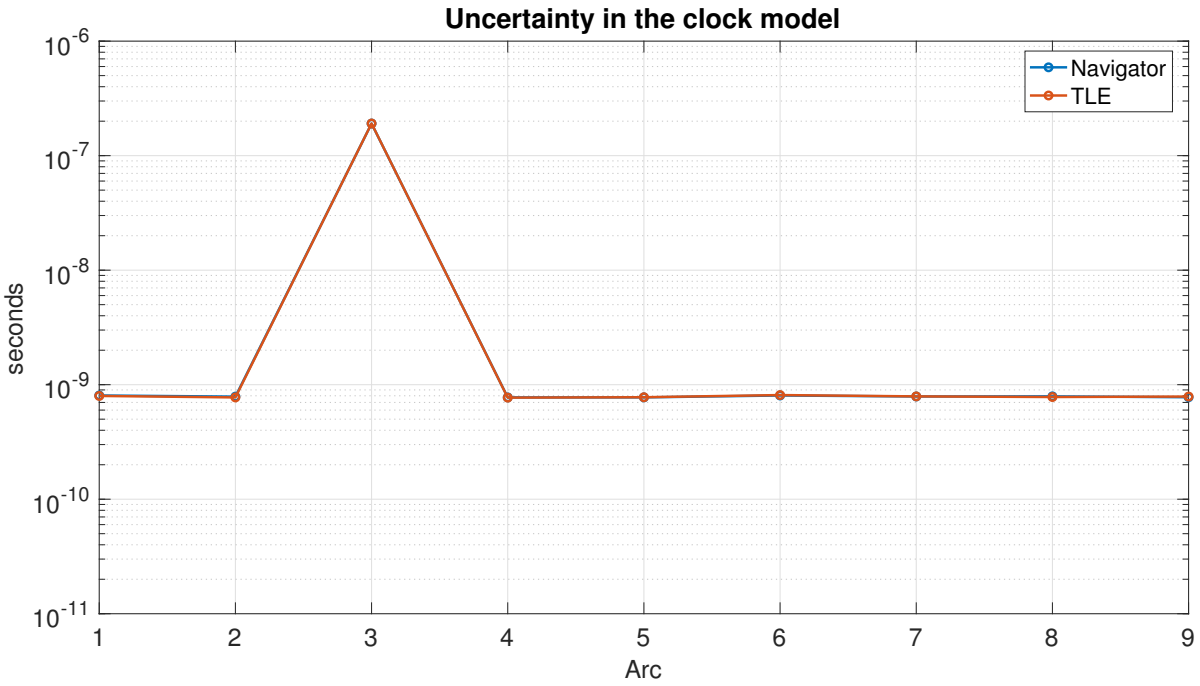

Figure 6.3: This plot shows the uncertainty in the clock model estimated for test T01 for time period from January to March 2016. X-axis represents the arc number (a 10 day time interval over which a new clock model is estimated). Y-axis represents the uncertainty in seconds.

Uncertainty	Bias	Drift	Drift rate	Acceleration rate
Arc 1	1.8726e-11	1.1737e-14	1.9619e-18	9.2072e-23
Arc 2	1.8054e-11	1.1371e-14	1.9174e-18	9.058e-23
Arc 3	1.9076e-07	1.2128e-10	2.0573e-14	9.7594e-19

Table 6.4: Uncertainty in clock polynomial components for the month January 2016 (3 arcs)

From this test we conclude two points:

1. Time solution difference obtained from TLE orbit and Navigator is not significant enough to affect the tracking residuals. Orbit precision is not an issue in time-tagging as long as they are of the order of TLE orbits confirming to this test. Despite the pseudo range measurement noise in RINEX, we are able to achieve the clock precision required. Thus pseudo range measurement noise is not a limitation to achieve the time solution.

2. The quality of time-tagging was studied based on the uncertainty in the clock model. This shows that the time solution with sufficient precision is achieved although there are three effects not taken into account - relativistic frequency bias, relativistic periodic terms and local clock drift due to SAA effect. This lets us distinguish the time-error and confirm that the difference in the residuals might be marginally due to time-tagging but not predominately compared to other systematics.

Following this, we proceed to further tests with Navigator orbits chosen as initial orbit during RINEX processing.

6.1.2 Test T02 - Effect of time interval for time-tagging polynomial

In this test, the effect of polynomial time-interval on the time synchronisation and subsequently on the tracking residuals is studied.

The purpose of this test is to shed light on possible presence of short term instability in DORIS clock of CryoSat-2. Any instability less than 10 day will be shown in the estimated polynomial error terms. Number of days in the time interval depends on the on-board oscillator characteristics and their characteristics depend on the orbit of the satellite (altitude). ENVISAT carries DORIS and flew at 800 km close to the operational altitude of Cryosat-2. Study indicates that for DORIS solution strategy in GSFC, time bias per 7 day arc is estimated for ENVISAT used 7 days (Zelensky et al., 2006). Based on this, we choose 5 days for the time interval. In order to see the effect of orbit quality on tracking residuals, three POD runs are performed - (i) V2.2 (benchmark) (ii) RINEX using 10 day time interval clock solution and (iii) RINEX using 5 day time interval clock solution.

Examining the residuals in figure 6.4, we do not observe any significant change between the 10 day and 5 day adjustments in period tested. However there is a slight increase in residuals for 5 day time interval. This is due to degradation in the quality of clock model as shown in figure 6.6. The pattern seen in figure 6.5 is due to the reason that a five day polynomial become stringent compared to 10 days because of which the anomalous behaviour in the arc 3 is absorbed for five day time interval. From this we can conclude that a 10 day polynomial can be chosen since no significant change or improvement is observed in the residuals. A 10 day time interval would also provide a better average estimate of long-term drift of oscillator than a 5 day interval.

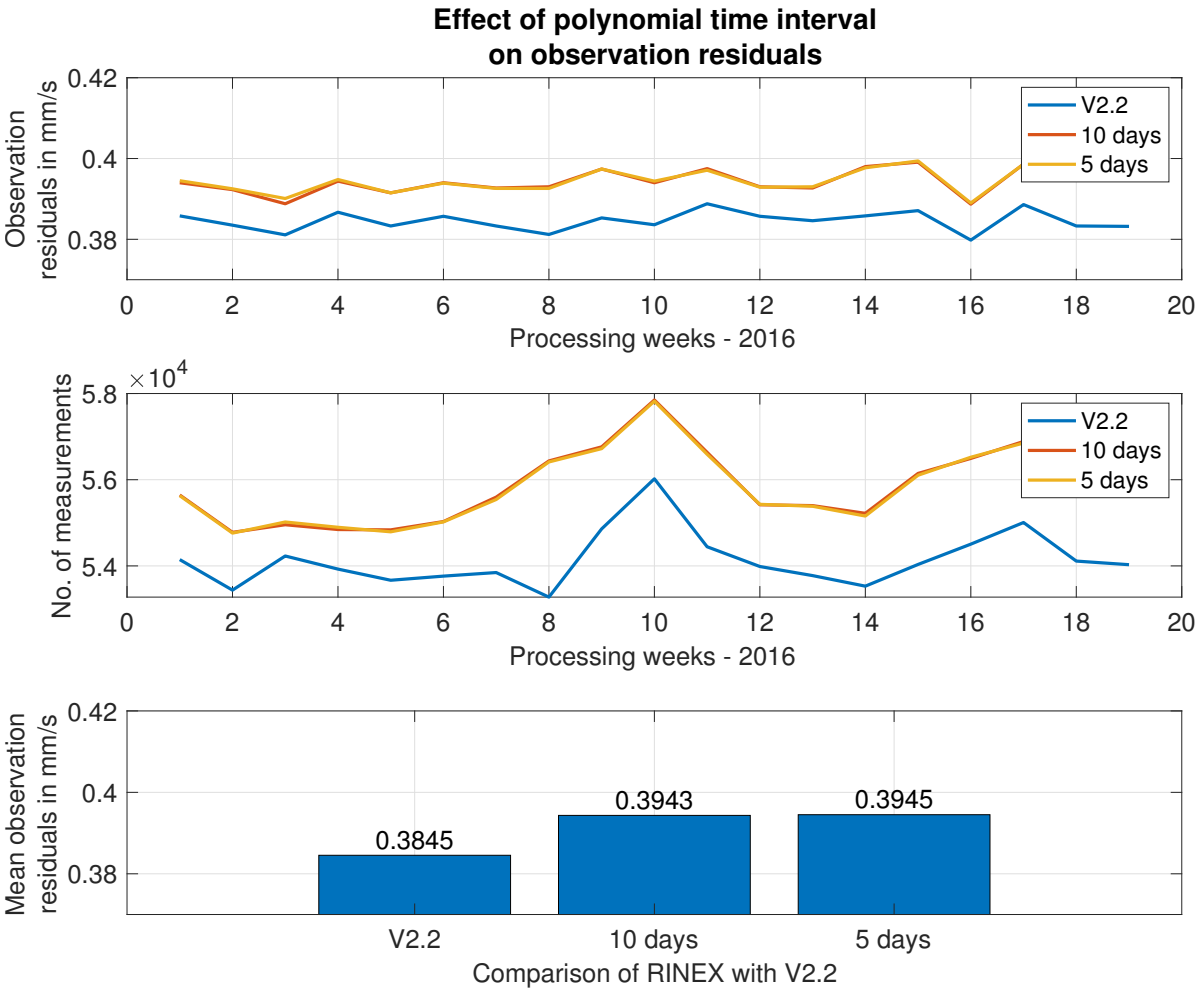

Figure 6.4

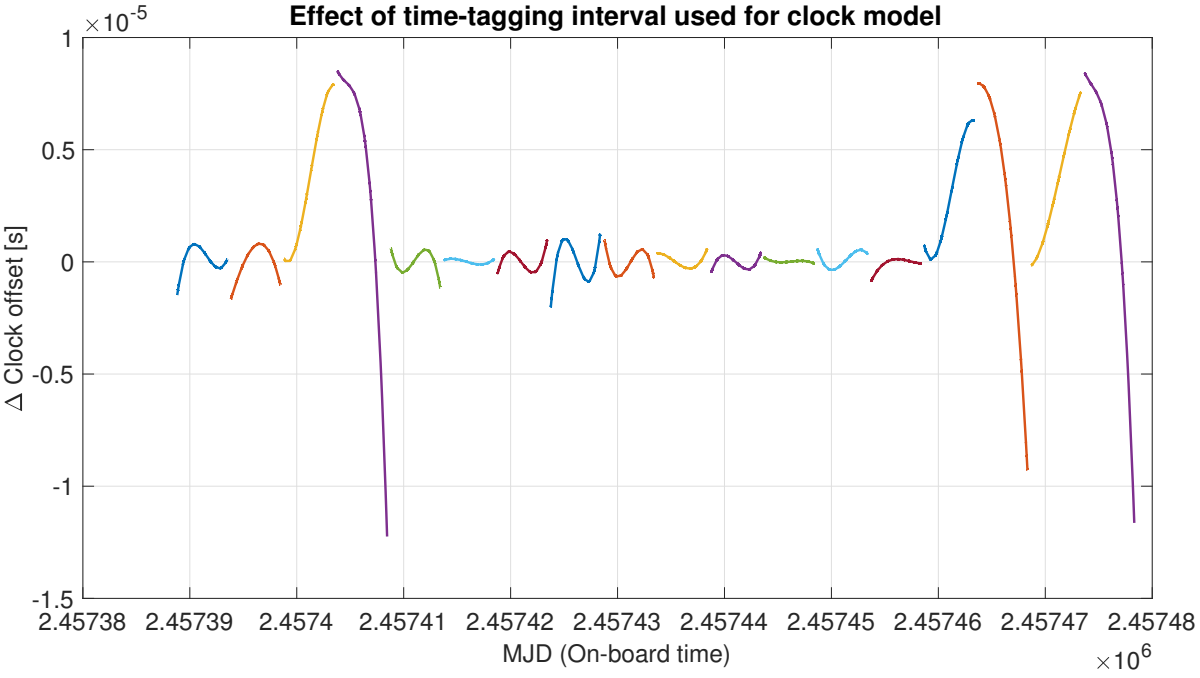

Figure 6.5

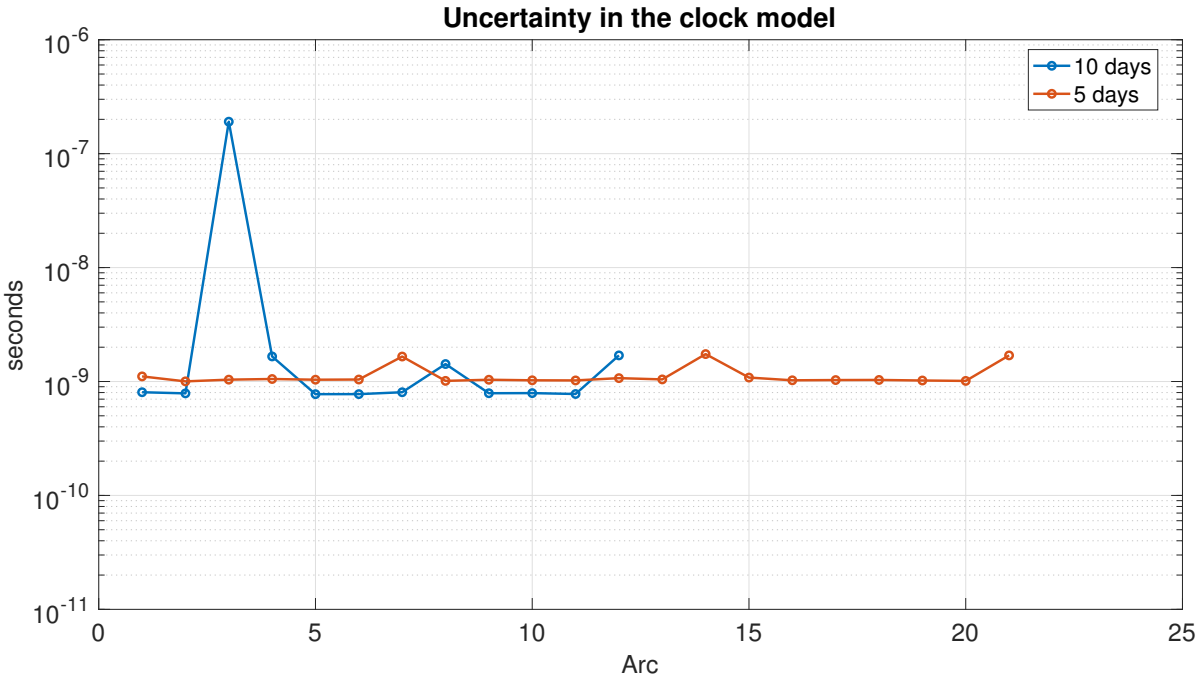

Figure 6.6

6.1.3 Test T03 - Effect of order of time-tagging polynomial

In this test we study the effect of polynomial order used for clock model on the quality of time-tagging and tracking residuals. Three POD runs were performed - (i) V2.2 (ii) RINEX using 2nd order clock polynomial (iii) RINEX using 3rd order clock polynomial. A 2nd order clock polynomial is compared with 3rd order clock polynomial, both adjusted over same test period. It was seen that in the period of testing, the 2nd order polynomial showed no significant effect

on time tagging and hence the observation residuals remained almost equal. This might be because a frequency bias is estimated per pass over the station and this recovers any short term on-board behaviour. Additionally, when adjusting a 3rd order polynomial, we estimate an additional term in clock model called satellite clock acceleration-rate component compared to 2nd order polynomial. This might lead to over fitting causing an error in the clock model. This also points that the CryoSat-2 satellite clock has negligible acceleration rate term and thus the 2nd order polynomial capturing it remains unaffected.

Since no major improvements in residuals was observed for 2nd order polynomial, we proceed to maintain our preliminary conclusion of having a 3rd order clock polynomial.

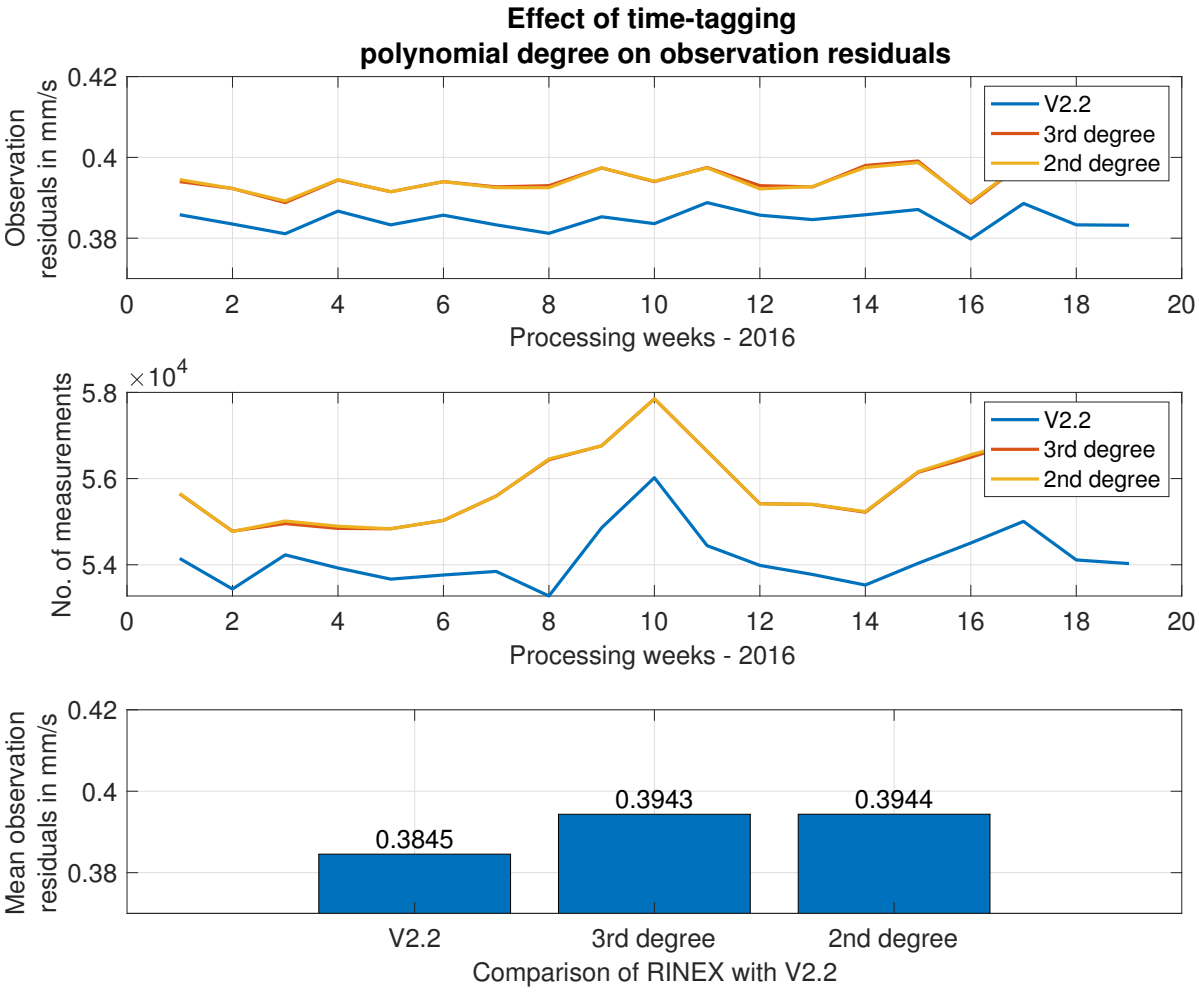

Figure 6.7

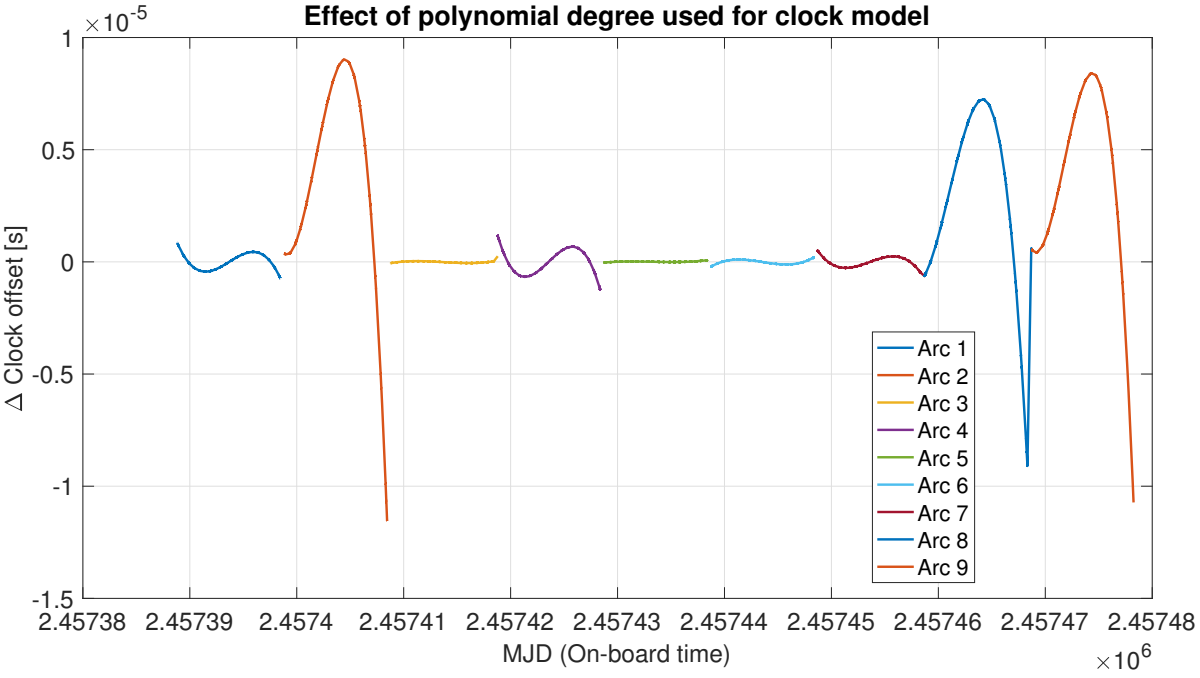

Figure 6.8

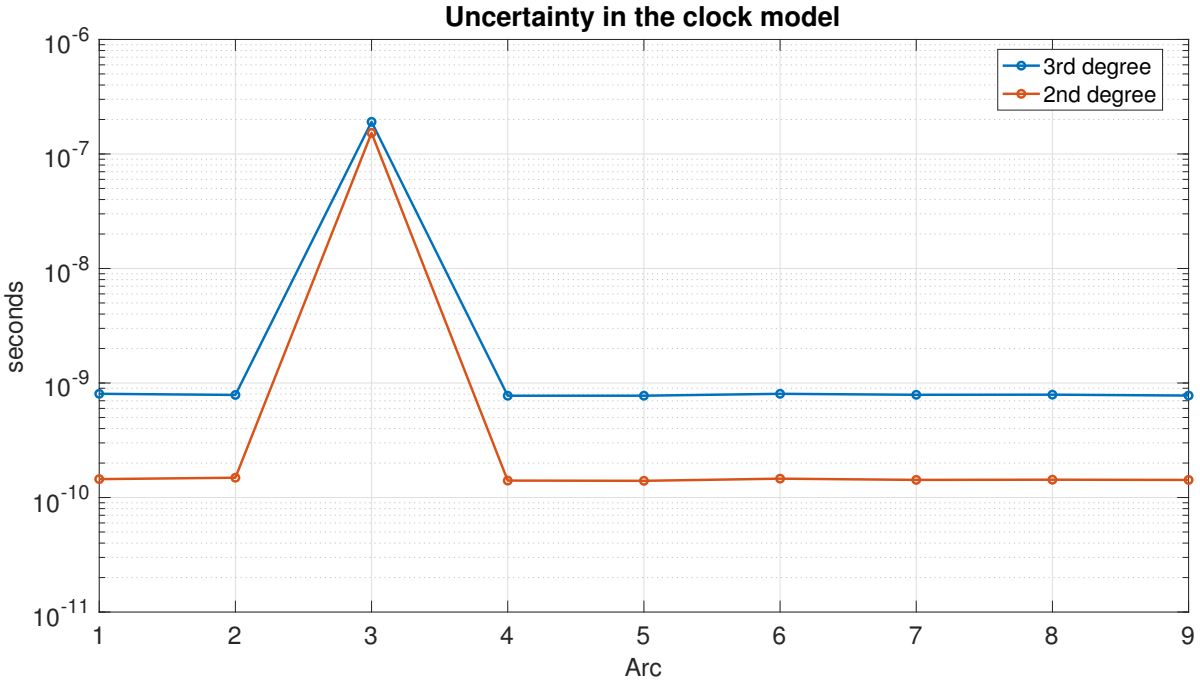

Figure 6.9

6.1.4 Test T04 - Quality of master beacons in the time-tagging

In this test, time synchronization quality of all master beacons are compared. Five POD runs are performed - (i) V2.2 (ii),(iii),(iv) and (v) indicates RINEX processing using time solution derived using Toulouse, Terre Adelie, Kourou, Papeette respectively. During the period of testing, five master beacons were operational namely - Toulouse, Terre Adelie, Papeette, Kourou and Hartebeesthoek. The Hartebeesthoek station could not included in processing due to in-

consistency in the availability of pseudo range data and hence no clock solution was produced by *RX2RR* processor. Other stations were used for time-tagging and their effect on residuals is shown in figure 6.10. It is clear that Toulouse master beacon has the lowest residual. The reason may be attributed to the fact that clock is well monitored with TAI and is updated frequently to avoid large drifts. The pseudo range data is also consistently available that are flagged valid for time-tagging purposes. In additional, presence of pseudo range data for longer duration (multiple passes) also ensures adequate average estimate of clock solution, which in case of Toulouse, is achieved. Other stations however shed higher residuals, Kourou lies in the SAA region and its impact on clock solution is seen here as residuals. This region induces short period fluctuations in the frequency the CryoSat-2 and becomes more challenging to model such anomalous behaviour. Terre Adelie and Papeette experience higher clock drift and bias. Although time keeping corrections are made to bring back drift to lesser values, these were observed not to be made regularly. Such procedures may impart breaks in the pseudo-range modelling affecting the clock polynomial model we use.

Thus, based on this study, we conclude that Toulouse master beacon shall be used for clock synchronisation and including all the master beacons for clock synchronisation would degrade the clock solution.

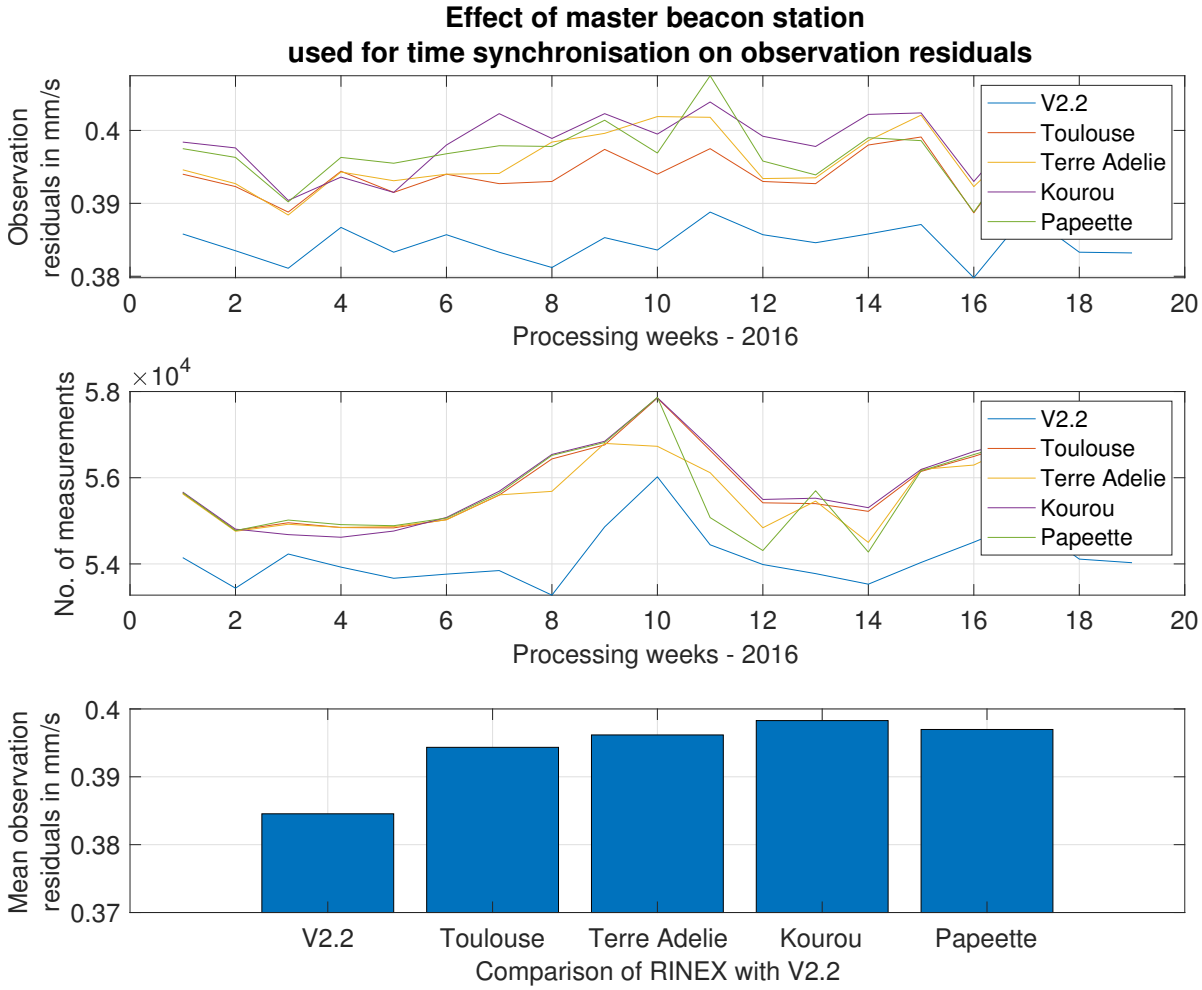

Figure 6.10

	run1	run2	run3	run4
Tracking residuals	0.4055	0.4054	0.4054	0.4054

Table 6.5: GEODYN-II iterative run in *RX2RR* processor

6.1.5 Test T05 - GEODYN-II iterative orbit approach

This test is performed to examine the suggestion given by CNES (CNES, 2018), with expectation that successive injection of GEODYN-II produced orbits in *RX2RR* processor would improve clock solution and subsequently improve the residuals. RINEX measurements are processed with setting as specified in preliminary conclusions. Runs were performed for 1 week between 21 July 2017 and 26 July 2017. Once a first run is performed, we use the GEODYN-II orbit from run 1 to estimate a new clock solution for run 2 RINEX processing. From run 1, improved orbits were obtained from GEODYN-II (better than the navigator orbits (initial orbits) used in run 1). This was then used for building clock solution for run 2. In this way we iterate and look for change in residuals. Only a small reduction in the residuals was observed in run 2, which is not significant enough to make any substantial conclusion. After run 2, no change was observed. The values are tabulated in table 6.5. The reason is again the same as discussed in Test T01 which describes the effect of orbit on clock solution.

6.1.6 Test T06 - Comparison of own time solution with PANDOR and DIODE solution in RINEX

The purpose of this test is to compare the clock model developed in this thesis with the clock solution provided in RINEX data by CNES/IDS. There are two versions of RINEX data available - (i) DIODE and (ii) PANDOR. The DIODE version of time-tagging is not smooth and irregular patterns were observed in the clock solution and frequency offsets. The instability might be because DIODE uses Kalman filter to estimate the frequency drift of the USO (Jayles et al., 2015). We use least squares method to arrive at a clock model. It is interesting to note that we use the same Navigator orbits from DIODE software and achieve better results. This validates how we perform our iterative clock synchronisation process involving multiple steps at each iteration such as interpolation of orbits at measurement epochs, time scale conversion, geometric modelling of satellite-station distance. Between January 2015 and January 2017, PANDOR tool was provided by CNES with an aim to improve the time-tagging issue present in DIODE. The concept was to process the time-tagging solution on-ground and replace the clock offset field in RINEX data with this solution. The new solution is estimated as combination of on-ground and on-board clock USO. However, short term high frequency noise was noticed in the time-tags. This time solution is a result of processing multiple satellite and multiple beacons. The frequency offset was maintained same as DIODE version. Due to no improvements in PANDOR, the IDS decided to fall back to DIODE time-tagging to be provided in RINEX (IDS, 2016). From this we can conclude that both DIODE and PANDOR versions of RINEX data don't improve the time-tagging. It is thus necessary to build own clock solution while using DORIS/RINEX data.

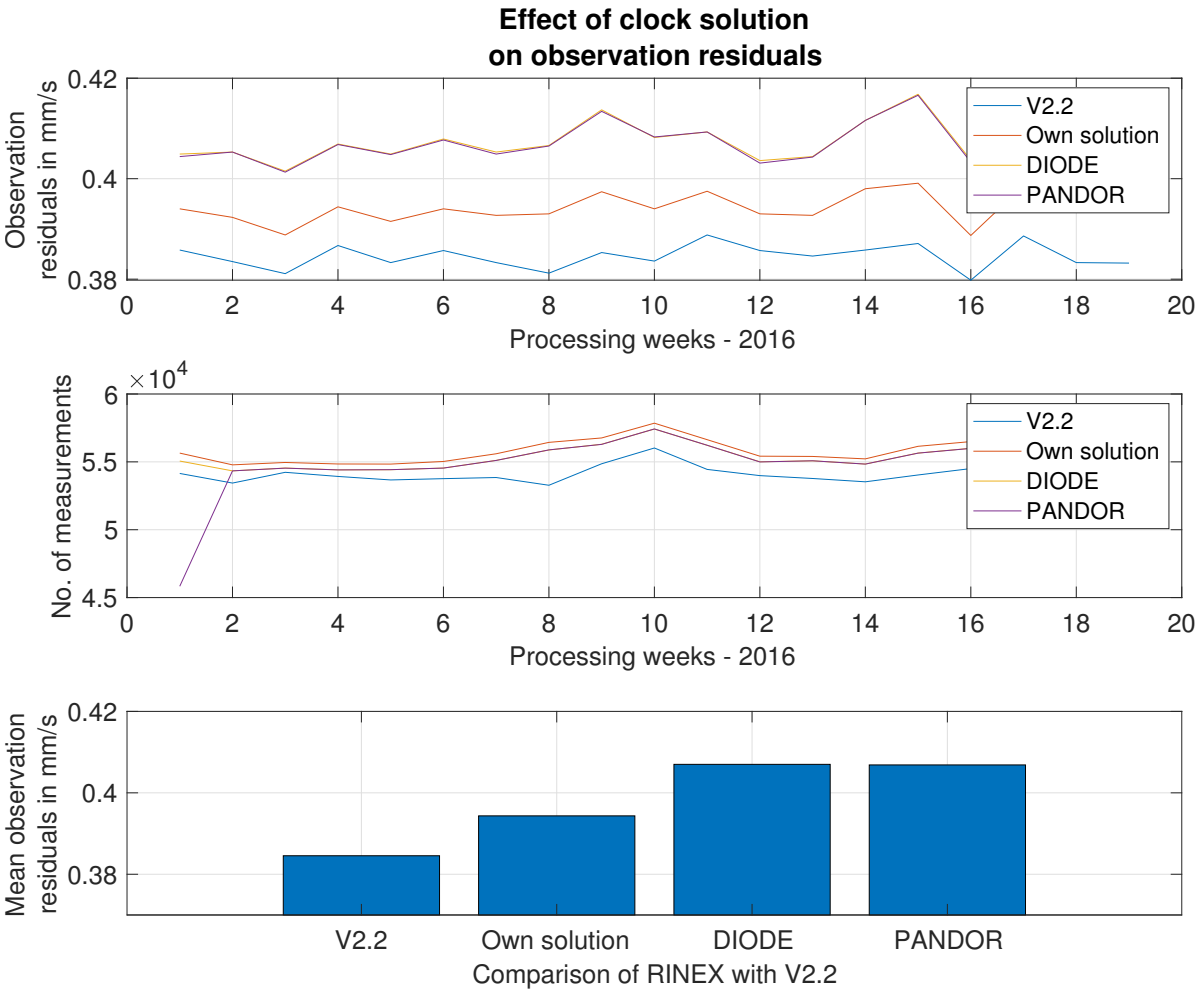

Figure 6.11

6.1.7 Test T07 - Comparison of Discrete and Empirical troposphere model

The purpose of this test is to compare two different troposphere models implemented in the pre-processor. The first one is empirical model which depends on the partial/complete meteorological data present in RINEX (Landskron and Böhm, 2018) and discrete troposphere model that uses real time weather information at the DORIS station location (VMF, 2019). Three POD runs were performed and compared - (i) V2.2 (ii) RINEX processing with Discrete model and (iii) RINEX processing with Empirical model. The parameters used for RINEX processing are same as preliminary conclusions. This is tested over a year of data to see seasonal effects on troposphere models used. From figure 6.12 we clearly see that both empirical and discrete troposphere models are implemented correctly. A slightly higher residual is observed for empirical troposphere model. This is attributed to the inability of models to accurately capture the wet tropospheric component which has the highest uncertainty in the tropospheric correction. Empirical models are based on climate models of whole earth unlike discrete models which are based on real weather observations. In addition to this, we do not use station meteorological data in RINEX if they are flagged 'unusable'. As a fall back we rely on GPT3 model for pressure and humidity values. Such partial availability of meteorological data contributes to imperfect modelling of tropospheric delay. A trend in seen near the middle of the plot 1 of figure 6.12 for both V2.2 residuals and RINEX residuals. The time at which the bulge occurs is close to summer season of 2016. During summer, the air becomes warm and holds more moisture or in

other words humidity is higher. This increases the overall uncertainty in the estimation of wet tropospheric component compared to other seasons which is shown as a increase in residuals in the middle of the plot. This is applicable for all the stations. In figure 6.13 and 6.14, we plot the mean difference of station residuals between V2.2 and RINEX. It can see that stations near equator show higher mean difference with respect to V2.2 station residuals. This effect is due to the reason that atmosphere (including lower layers such as troposphere, stratosphere, mesosphere) is thicker near the equator where centrifugal force and atmospheric temperature are higher compared to pole where the atmosphere is thinner. Again, since thicker parts of atmosphere near equator are warmer they hold more moisture causing it difficult to model delay correction due to wet component. However it must be kept in mind stations affected by SAA effect also fall near equatorial region (figure 6.14) and two effects (troposphere and SAA) must be distinguished. From this test, we conclude that estimation of troposphere delay is better using discrete model than empirical model.

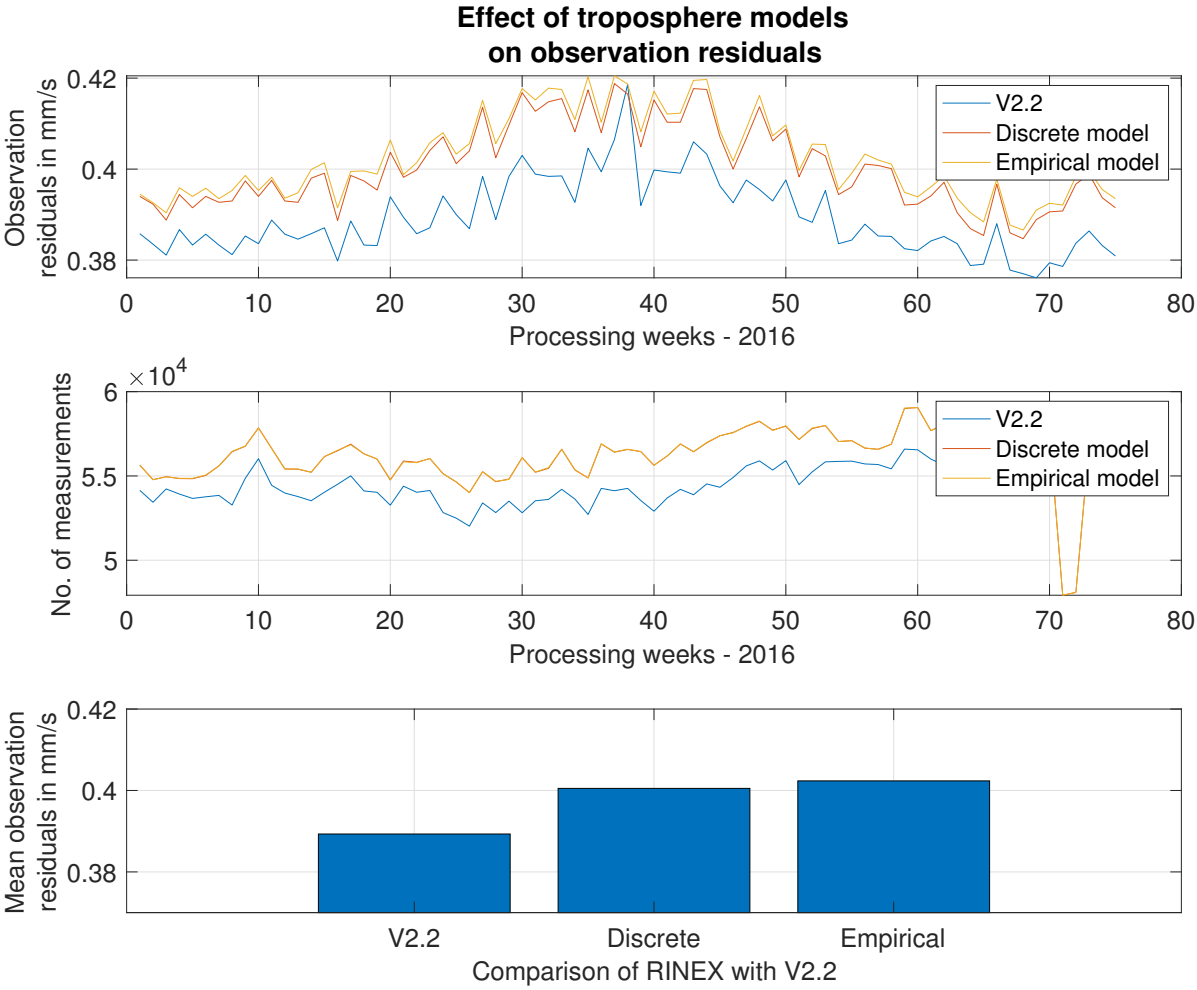

Figure 6.12

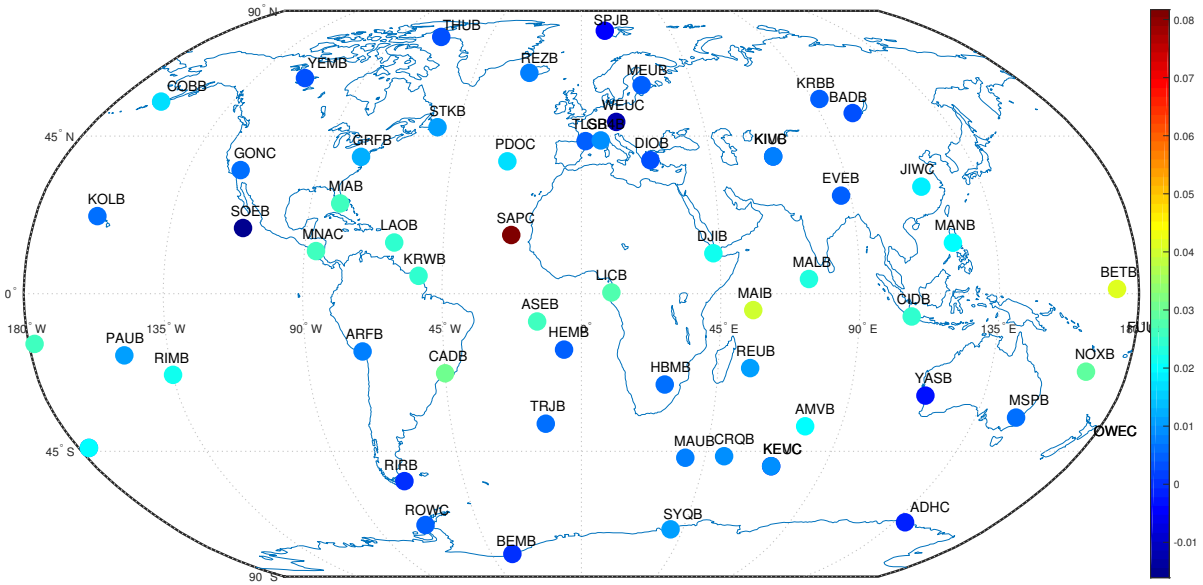

Figure 6.13: World map showing the station specific residual difference between V2.2 and RINEX (Discrete troposphere used)

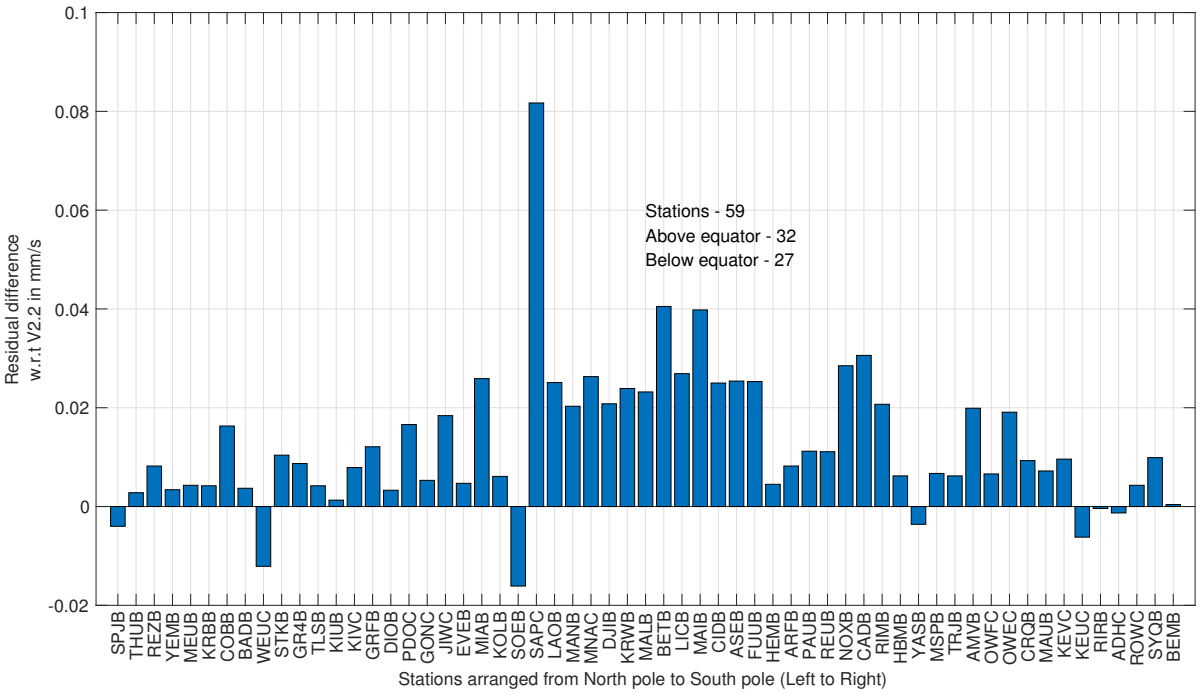

Figure 6.14: X-axis represents the stations arranged based on latitude (Left to Right)

6.1.8 Test T08 - Effect of sigma clipping of range rate data

The purpose of this test is to test the effectiveness of editing strategy implemented in *RX2RR* processor designed to remove outliers in range rate measurements. Three runs are performed and compared - (i) V2.2 (ii) RINEX processing with sigma clipping ON and (iii) RINEX processing with sigma clipping OFF. We observe only a marginal effect in the residuals, indicating our method of editing the data is still not efficient to remove outlier points. Outliers in range rate measurements that lie very close to range rate profile of a pass are challenging to be re-

moved. However, GEODYN has in-built outlier detection algorithm that manages to remove these points. The method used by GEODYN is based on internal residual inspection where the residuals that fall above certain sigma are removed. During the POD runs, 0.4 mm/s filter was maintained. Thus from this study we can conclude that a close cutting of outlier is effective via examination of orbit residuals in GEODYN-II and any a priori external outlier removal algorithm may prove inefficient.

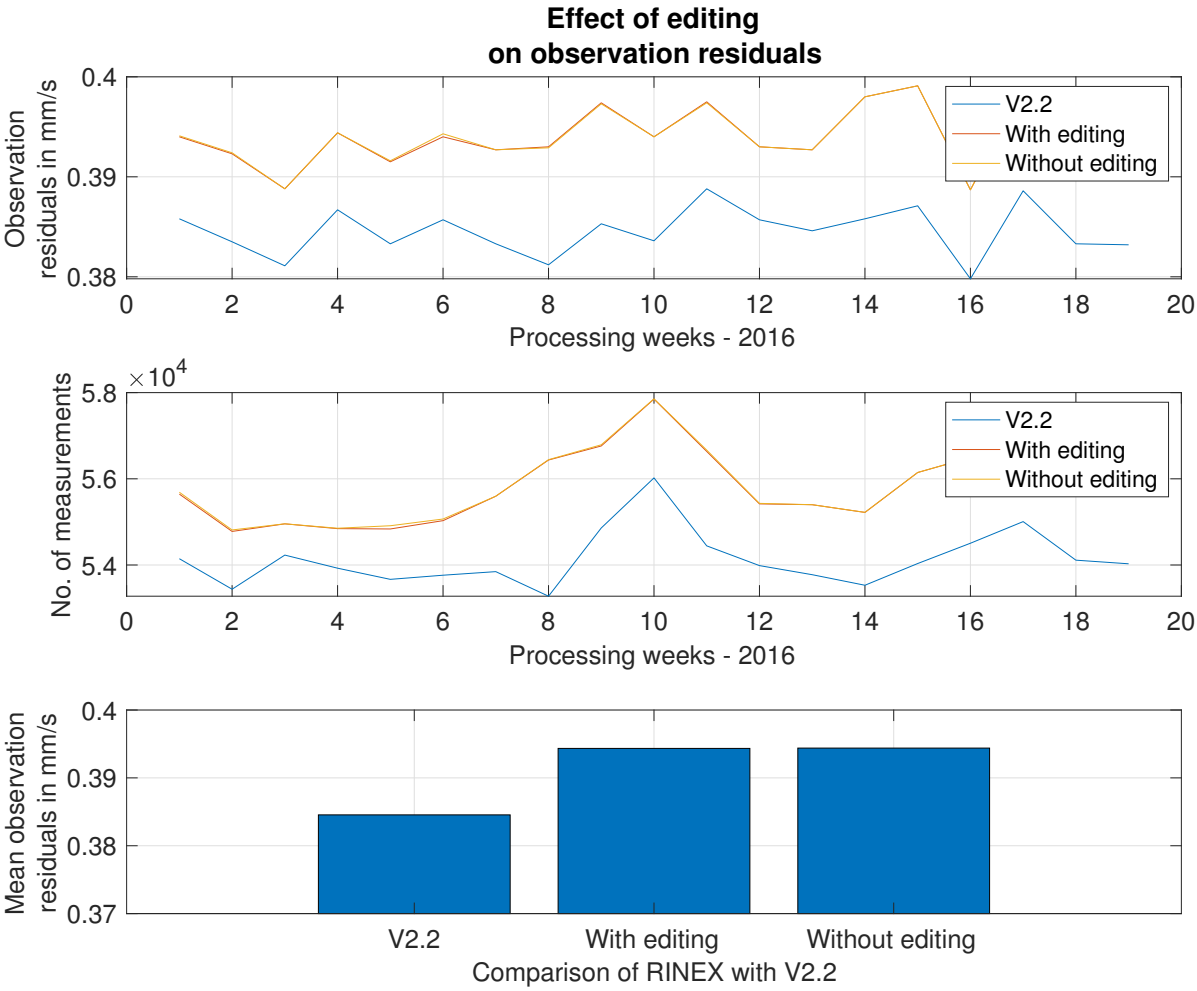

Figure 6.15

6.1.9 Test T09 - Best setting results

Final performance result of the developed RINEX processor *RX2RR* is shown below. Mean difference between the residuals obtained from V2.2 and RINEX for the year 2016 is 0.011 mm/s as shown in figure 6.16. As previously this performance should more or less apply to whole mission period provided taking into tropospheric estimation satellite. We can look at the result in figure 6.16 in two ways - (i) reason why we have close match with V2.2 and (ii) reason why there is a slight difference.

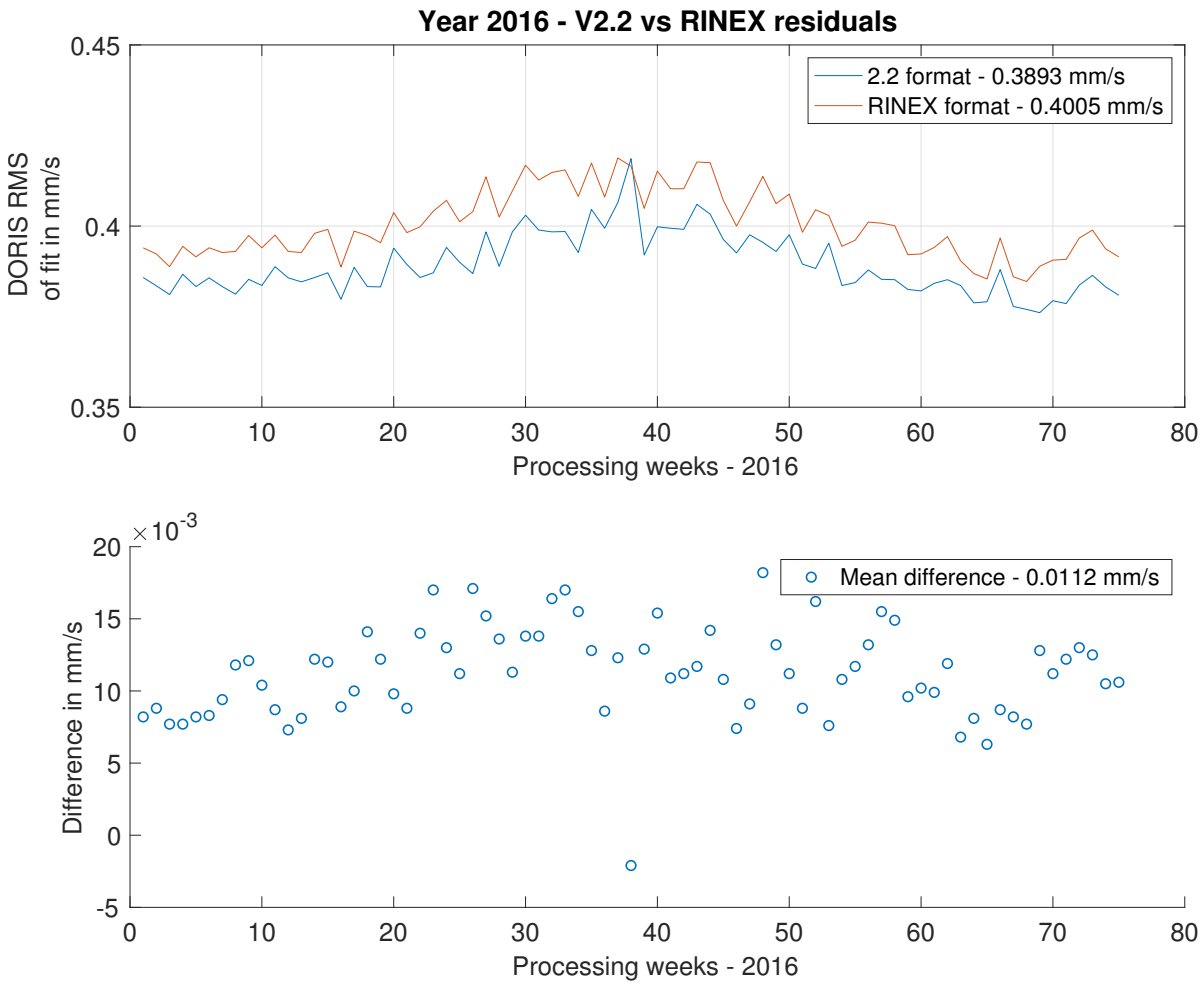

Figure 6.16

Reason for close match of residuals with V2.2

1. Time-tagging accuracy is better than 1 microsecond. This also determines how well we estimate the behaviour of on-board oscillator for frequency correction and hence the range rate. Antenna corrections applied to range rate also depend on this time-tag.

2. Troposphere estimation is performed correctly to a sufficient level and except for stations near equator which are challenging to be modelled.

3. The implementation of antenna phase correction is done correctly. We perform processing with assumption of nominal attitude mode of satellite with no yaw steering mode included in the modelling. This assumption holds good for CryoSat-2 mission. The dates during which nominal attitude law was switched off was checked and no significant change in residuals was observed at these time intervals.

4. Although implementation of ionospheric correction is quite straight forward, a geometrical correction must be made to bring the correction to iono-free phase centres which depend on the antenna phase corrections of two frequencies. Tests prove that this has been implemented correctly.

5. Station beacon changes were observed over the year 2016 and *RX2RR* processor proves to handle such addition/removal of stations.

6. Processing of frequency shifted beacons in Grasse and Wetzell is done correctly.

Reasons for slight difference in the residuals with V2.2

1. Time tagging issue is still present as explained in the Test T01 section. This covers the relativistic frequency offset in clock drift, relativistic periodic terms and modelling of oscillator in the SAA effect.

2. Editing performed in V2.2 by CNES is different from the editing performed by *RX2RR* pre-processor. The number of measurements seen in figure 6.16 is a result of 10 deg elevation cut-off on both RINEX and V2.2. It is interesting to see that we still have 2 percent more data than V2.2. The difference is because of editing strategy employed by CNES. Measurements in V2.2 are flagged if the elevation is less than 10 deg and also the central frequency measurements are flagged. Bringing the quantity of observations close to V2.2 gave us better results than V2.2. The sigma clipping editing strategy only marginally rejects good points although not significantly. Editing strategy still needs to be improved for RINEX format.

3. Discrepancies in troposphere estimation used in GEODYN-II - Although VMF3 has been used for apriori troposphere correction in *RX2RR* pre-processor, the parameter adjustments are performed using Marini/Murray model in GEODYN-II.

4. Antenna phase correction discrepancies - The correction present in the V2.2 data such as ionosphere and antenna corrections relate to 2GHz phase centre. In addition, GEODYN-II dynamic modelling has been set-up for 2Ghz phase centre (both on-ground and on-board). However, the correct implementation to be used for RINEX data processing is to use iono-free phase centres (Lemoine et al., 2016), which has been implemented in *RX2RR* processor. It is suspected that this systematic error is seen in figure 6.16 and could be reason why the difference observed, although minimal, is almost constant throughout the whole year.

Other possible factor that may be affect this difference, but are of negligible magnitude could be due to

1. Fluctuations in the proper time interval - It was noticed that proper time interval sometimes are not a 10 second count interval, but 9.9 seconds. This has been verified to be not a precision issue in the pre-processor, but the effect is present in RINEX on-board time itself.

2. Higher order ionospheric corrections

3. Phase wind-up effects

4. Possible electronic delays in the on-board clocks.

5. Electronic delay between the reception of 2GHz and 400MHz frequencies.

Chapter 7

Conclusions

In this research, we attempt to construct a pre-processor to process DORIS/RINEX measurement files. We start with performing clock synchronisation using polynomial clock model adjusted over the pseudo range data of master beacons. We compare our clock solution to accurate time-tagging solution provided by CNES in PANDOR RINEX version and prove that our clock solution is better. This conclusion has been made by examining the magnitude of tracking residuals which are lower compared to data processing performed using PANDOR RINEX clock solution. We adapt Doppler like processing by converting the phase data to range rate measurement between satellite and station. Antenna phase corrections are implemented using iono-free phase centres assuming nominal attitude for CryoSat-2. The iono free phase centres are used for on-board and ground correction along with phase laws implemented for ground antennas. We implement two troposphere models - empirical and discrete (real time weather data at DORIS stations) for computing tropospheric delay. A new approach has been developed to estimate troposphere delay using only valid meteorological data from RINEX with the help of empirical models. This proves to be comparatively equal to Discrete troposphere model with mean difference of 0.0020 mm/s over the year 2016 with discrete troposphere model being superior. Ionospheric correction has been computed considering the iono-free phase centre geometry correction. A new editing strategy was implemented and tested to remove outliers in range rate observations based on sigma clipping. We don't observe any significant effect in the residuals, indicating our method of editing the data is still not efficient to remove outlier points.

RX2RR pre-processor/converter has been successfully built that includes the corrections and facilitates conversion to a format similar to V2.2. Its performance has been studied and validated on CryoSat-2 mission for the year 2016 using multiple tests in GEODYN-II. Investigating the mean difference between Doppler residuals from RINEX and V2.2 for year 2016, we obtain a value of 0.011 mm/s which has negligible effect on POD. From this we can conclude and answer the main research question of this thesis that - a preprocessor has been built and it successively demonstrates centimetre level radial orbit accuracy using the DORIS/RINEX data. This tool in principle should work for any satellite carrying DORIS/DGXX receiver provided inputs with respect to satellite attitude are supplied, which are required to account for phase centre correction. *RX2RR* very well adapts to changes in beacon and antenna type. Since the 2.2 format has been brought back using the RINEX data, any orbit computation software that has been previously using 2.2 format can now process RINEX measurements. This tool would be particularly helpful for missions from and after Sentinal-3A and Jason-3 mission where only RINEX data are available.

Chapter 8

Recommendations

The following recommendations are proposed for further improvements of the developed *RX2RR* processor.

1. **Improved clock modelling** - It is necessary to include relativistic frequency offset in the clock drift and relativisitic periodic effects in clock modelling. Furthermore, residuals for stations in the vicinity of South Atlantic Anomaly could be reduced by modelling the impact of SAA effect on the oscillator. This has been already studied in literature and correction models are available (Lemoine and Capdeville, 2006), (Štěpánek et al., 2013), (Capdeville et al., 2016)

2. **Data editing strategy needs improvement** - Possibly implement a robust outlier detection algorithm that accounts for close cutting of points that fall outside of range rate profile of a pass. In addition, with respect to ground beacon, only the station that have reached stable warming period could be taken into account for RINEX processing. With repsect to troposphere correction, down weighting law could be implemented to assign weight on individual measurements to make use of enormous amount of lower elevation measurements.

3. **Attitude law implementation** - *RX2RR* processor developed for this thesis uses nominal mode of satellite and this assumption holds good for CryoSat-2 mission for the period tested. In case this pre-processor is used for processing RINEX date of other satellite in the DORIS network, this may induce systematics in the tracking residuals. Thus attitude law must be implemented for proper construction of phase centre correction and possible phase wind-up effects.

Bibliography

Hugues Capdeville, Petr Štěpánek, Louis Hecker, and Jean-Michel Lemoine. Update of the corrective model for Jason-1 DORIS data in relation to the South Atlantic Anomaly and a corrective model for SPOT-5. *Advances in Space Research*, 58(12):2628–2650, dec 2016. ISSN 0273-1177. doi: 10.1016/J.ASR.2016.02.009. URL https://www.sciencedirect.com/science/article/pii/S0273117716000909?via{%}3Dihub.

Chalmers. Chalmers university website ocean loading calculator. 2017. URL http://holt.oso.chalmers.se/loading/.

CNES. Private communication. 2018.

CNES and IDS. DORIS SYSTEM GROUND SEGMENT MODELS. Technical report, 2019. URL ftp://ftp.ids-doris.org/pub/ids/stations/DORIS{_}System{_}Ground{_}Segment{_}Models.pdf.

J L Davis, T A Herring, I I Shapiro, A E E Rogers, and G Elgered. Geodesy by radio interferometry: Effects of atmospheric modeling errors on estimates of baseline length. *Radio Science*, 20(6):1593–1607, 1985. doi: 10.1029/RS020i006p01593. URL https://agupubs.onlinelibrary.wiley.com/doi/abs/10.1029/RS020i006p01593.

Gunnar Elgered. Tropospheric radio-path delay from ground-based microwave radiometry. *Atmospheric remote sensing by microwave radiometry*, pages 215–258, 1993.

ESA. CAL/VAL server for CryoSat-2 mission. *ESA CAL/VAL server*, 2017.

Ch Förste, F Flechtner, R Schmidt, R Stubenvoll, M Rothacher, J Kusche, H Neumayer, R Biancale, J M Lemoine, F Barthelmes, and Others. EIGEN-GL05C-A new global combined high-resolution GRACE-based gravity field model of the GFZ-GRGS cooperation. In *Geophysical research abstracts*, volume 10, pages EGU2008—-A. EGU2008-A-03426, 2008.

Toshio Fukushima. Transformation from Cartesian to geodetic coordinates accelerated by Halley's method. *Journal of Geodesy*, 79(12):689–693, 2006.

GFZ. Geomagnetic field constants Ap and Kp. 2017.

W Gurtner. RINEX: The Receiver-Independent Exchange Format. *GPS World,*, 5(7), 1994.

Alan E Hedin. MSIS-86 thermospheric model. *Journal of Geophysical Research: Space Physics*, 92(A5):4649–4662, 1987.

ICAO. World Geodetic System — 1984 (WGS-84) Manual. Technical report, 2002.

IDS. DORIS satellites models implemented in POE processing. Technical report, 2015. URL ftp://ftp.ids-doris.org/pub/ids/satellites/archives/SatelliteModels{_}Ed1Rev7.pdf.

IDS. IDS Workshop document, 2016. URL https://ids-doris.org/images/documents/report/ids{_}workshop{_}2016/IDS16{_}s2{_}LemoineJM-WhichDatationMethodForDORISRINEXdata.pdf.

IDS. DORIS Antenna types, 2019a. URL ftp://ftp.ids-doris.org/pub/ids/stations/antennas.pdf.

IDS. INTRODUCTION TO DORIS RINEX. Technical report, 2019b.

IERS. EOP 14 C04 series, 2017. URL https://www.iers.org/IERS/EN/DataProducts/EarthOrientationData/eop.html.

ILRS. International Laser Ranging Service Website, SLR data. 2017. URL https://ilrs.cddis.eosdis.nasa.gov/data{_}and{_}products/products/index.html.

Christian Jayles, Jean-Pierre Chauveau, and Albert Auriol. DORIS/DIODE: Real-time orbit determination performance on board SARAL/Altika. *Marine Geodesy*, 38(sup1):233–248, 2015.

Philip Knocke, J Ries, and B Tapley. Earth radiation pressure effects on satellites. In *Astrodynamics Conference*, page 4292, 1988.

Daniel Landskron and Johannes Böhm. VMF3/GPT3: refined discrete and empirical troposphere mapping functions. *Journal of Geodesy*, 92(4):349–360, apr 2018. ISSN 1432-1394. doi: 10.1007/s00190-017-1066-2. URL https://doi.org/10.1007/s00190-017-1066-2.

Daniel Landskron, Gregor Möller, Armin Hofmeister, Johannes Böhm, and Robert Weber. Site-Augmentation of Empirical Tropospheric Delay Models in GNSS. *Österreichische Zeitschrift für Vermessung und Geoinformation (VGI)*, 3:128–135, 2016. URL https://publik.tuwien.ac.at/files/publik{_}258346.pdf.

J.-M. Lemoine and H Capdeville. A corrective model for Jason-1 DORIS Doppler data in relation to the South Atlantic Anomaly. *Journal of Geodesy*, 80(8):507–523, nov 2006. ISSN 1432-1394. doi: 10.1007/s00190-006-0068-2. URL https://doi.org/10.1007/s00190-006-0068-2.

Jean-Michel Lemoine, Hugues Capdeville, and Laurent Soudarin. Precise orbit determination and station position estimation using DORIS RINEX data. *Advances in Space Research*, 58(12):2677–2690, dec 2016. ISSN 0273-1177. doi: 10.1016/J.ASR.2016.06.024. URL https://www.sciencedirect.com/science/article/pii/S0273117716303398.

Flavien Mercier, Luca Cerri, and Jean-Paul Berthias. Jason-2 DORIS phase measurement processing. *Advances in Space Research*, 45(12):1441–1454, jun 2010. ISSN 0273-1177. doi: 10.1016/J.ASR.2009.12.002. URL https://www.sciencedirect.com/science/article/pii/S0273117709007480.

NOAA. Repository with space weather daily average solar flux estimates. 2017.

Gérard Petit and Brian Luzum. IERS conventions (2010). Technical report, BUREAU INTERNATIONAL DES POIDS ET MESURES SEVRES (FRANCE), 2010.

Barend Root. *Validating and improving the orbit determination of Cryosat-2*. {MSc} dissertation, Delft University of Technology, 2012.

D D Rowlands, J A Marshall, J McCarthy, D Moore, D Pavlis, S Rowton, S Luthcke, and L Tsaoussi. GEODYN II system description. *Hughes-STX Contractor Report*, 1993.

J. Saastamoinen. *Atmospheric Correction for the Troposphere and Stratosphere in Radio Ranging Satellites*, pages 247–251. American Geophysical Union (AGU), 1972. ISBN 0-87590-015-1. doi: 10.1029/GM015p0247. URL http://doi.wiley.com/10.1029/GM015p0247.

Ernst Schrama. Precision orbit determination performance for CryoSat-2. *Advances in Space Research*, 61(1):235–247, jan 2018. ISSN 0273-1177. doi: 10.1016/J.ASR.2017.11.001. URL https://www.sciencedirect.com/science/article/pii/S0273117717307962.

Ernst J O Schrama, Bert Wouters, and Roelof Rietbroek. A mascon approach to assess ice sheet and glacier mass balances and their uncertainties from GRACE data. *Journal of Geophysical Research: Solid Earth*, 119(7):6048–6066, 2014.

Torben Schüler. *On Ground-Based GPS Tropospheric Delay Estimation eingereicht*. PhD thesis, Studiengang Geodsie und Geoinformation, Universitt der Buundeswehr Munchen, 2001. URL https://athene-forschung.unibw.de/doc/85240/85240.pdf.

E M Standish Jr. Orientation of the JPL Ephemerides, DE 200/LE 200, to the dynamical equinox of J 2000. *Astronomy and Astrophysics*, 114:297–302, 1982.

Petr Štěpánek, Jan Douša, and Vratislav Filler. SPOT-5 DORIS oscillator instability due to South Atlantic Anomaly: Mapping the effect and application of data corrective model. *Advances in Space Research*, 52(7):1355–1365, oct 2013. ISSN 0273-1177. doi: 10.1016/J.ASR.2013.07.010. URL https://www.sciencedirect.com/science/article/pii/S0273117713004225?via{%}3Dihub.

C. Tourain, G. Moreaux, A. Auriol, and J. Saunier. DORIS Starec ground antenna characterization and impact on positioning. *Advances in Space Research*, 58(12):2707–2716, dec 2016. ISSN 0273-1177. doi: 10.1016/J.ASR.2016.05.013. URL https://www.sciencedirect.com/science/article/pii/S0273117716301995?via{%}3Dihub.

VMF. Vienna Mapping Functions Open Access Data. 2019. URL http://vmf.geo.tuwien.ac.at/.

Pascal Willis, Hervé Fagard, Pascale Ferrage, Frank G Lemoine, Carey E Noll, Ron Noomen, Michiel Otten, John C Ries, Markus Rothacher, Laurent Soudarin, Gilles Tavernier, and Jean-Jacques Valette. The International DORIS Service (IDS): Toward maturity. *Advances in Space Research*, 45(12):1408–1420, 2010. ISSN 0273-1177. doi: https://doi.org/10.1016/j.asr.2009.11.018. URL http://www.sciencedirect.com/science/article/pii/S0273117709007212.

Nikita P Zelensky, Jean-Paul Berthias, and Frank G Lemoine. DORIS time bias estimated using Jason-1, TOPEX/Poseidon and ENVISAT orbits. *Journal of Geodesy*, 80(8):497–506, nov 2006. ISSN 1432-1394. doi: 10.1007/s00190-006-0075-3. URL https://doi.org/10.1007/s00190-006-0075-3.